Microwave Technology for Detecting Torso Injuries

A pilot study on porcine models

Master's thesis in Biomedical Engineering

Linh Nguyen

Microwave Technology for Detecting Torso Injuries

A pilot study on porcine models

Linh Nguyen

Microwave Technology for Detecting Torso Injuries
A pilot study on porcine models

Linh Nguyen

Cover: The left figure is an illustration of the difference between the microwave data of healthy (BLAS) and abdominal bleeding (AB500/AB1000) subjects. The right figure is abdominal bleeding detection result.

Abstract

Blunt trauma (injury without skin broken) is the major fatal incident among traumatic injuries, which accounts for 10 % of global deaths. The torso region (thorax and abdomen) is a sensitive area where serious blunt trauma can lead to death. Despite the importance and difficulty of torso blunt trauma diagnosis in the prehospital setting, the only available on scene diagnostic device is ultrasound, which is operator dependent and requires well trained paramedics. For this reason, microwave technology has been investigated for detecting torso trauma automatically.

S. Candefjord, N.P. Oveland, and colleagues designed a prototype wearable microwave detector to do experiments on ten porcine models. Each subject was tested with four types of torso trauma including hemoperitoneum (abdominal bleeding), pneumothorax (air in the pleural space), hemothorax (blood in the pleural space), and polytrauma (both pneumothorax and hemothorax). Based on these already available data, the main purpose of this master's thesis was to analyze the difference between healthy and trauma states as well as to evaluate whether trauma can be differentiated from baseline (healthy state) using statistical and classification approaches.

There are three main analysis sections in this thesis work. Firstly, for each subject, the subtraction of baseline (i.e. healthy state) from trauma states was derived to explore the consistent signal changes caused by trauma among all subjects. The difference to baseline was interpreted as the mean and standard deviation value among all subject's data. Secondly, these changes were further examined with statistical tests such as the Kruskal–Wallis Test and the Wilcoxon rank-sum Test to identify the statistically significant difference between healthy and trauma states. Finally, a linear kernel support vector machine (a machine learning algorithm) was employed to classify the healthy state and the largest sizes of trauma.

The results showed that for all trauma types, compared to the healthy state, a drop in the signal magnitude and an increase in the phase were observed. These trends were typically clear at antennas placed around the midaxillary line, where ultrasound examination indicated the accumulation of blood or air. Although the change was relatively consistent among subjects, the detection of trauma was a challenge due to the large difference in baseline between subjects (compared to the change caused by traumatic injuries). The statistic tests confirmed the difference between healthy and trauma states with statistical significance (i.e. p-value < 0.05). The classification algorithm was capable of detecting the largest size of abdomen bleeding and thorax trauma at 95 % and 90 % accuracy, respectively. Although these results are promising, further research is needed. The prototype microwave detector could be improved to decrease the high variance potentially due to a variation in antenna-skin contact before performing more experiments. With more data acquired, the machine learning algorithm has the potential to be developed to improve the detection accuracy for smaller trauma levels.

Keywords: *microwave technology, trauma, hemoperitoneum, pneumothorax, hemothorax, statistical test, machine learning, support vector machine.*

Acknowledgements

Contents

1
Introduction

Traumatic injury is defined as severe physical injuries caused by sudden onset. Trauma causes approximately 5.8 million deaths a year around the world, accounting for 10 % of global deaths [1]. Traumatic injuries can be divided into three main groups consisting of blunt, penetrating and burn mechanisms. Penetrating trauma occurs when an object pierces the skin and damages tissues inside the body. This type of trauma along with burn injuries can be easily recognized by a paramedic. On the other hand, blunt trauma without skin broken is usually difficult to identify and requires diagnostic devices to make final conclusions. A 9-year study in Stavanger, Norway (with 290,000 inhabitants) indicated that fatal trauma incidence was 10 per 100,000 inhabitants and 87 % of this was blunt trauma [2].

There are six body regions in traumatic injuries including head/neck, face, thorax, abdomen/pelvis, extremities and external [3]. The torso, which is the central part of the body containing thorax and abdomen, should be considered as a single unit in traumatic study [4]. Three common injuries in the torso trauma are hemoperitoneum (abdominal bleeding), pneumothorax (air in the pleural space between the lung and the chest wall), and hemothorax (blood in the pleural space).

The "Golden hour" or the first 60 minutes after the incident of a major multi-system trauma is found to be critical in blunt trauma [5]. Another study indicated that for multiple-injury patients, the main reason of death in the first twenty-four hours after trauma is often the combination of abdominal trauma and pelvic injuries [6]. Early recognition of abdominal trauma that requires surgical intervention is essential to prevent death [7]. For every 3 minutes waiting for intra-abdominal bleeding, the probability of death increases by 1% [8].

The ultrasound technique and physical examination are the main methods currently utilized to detect trauma in the prehospital setting. However, these methods are operator dependent and require well-trained paramedics. There is a need for complementary methods for objective detection of hemoperitoneum. Recently, some research indicates the potential of microwave technology for torso and brain trauma diagnosis [9–11] but there has not been any comprehensive commercial microwave detector for torso trauma. S.Candefjord, N.P.Oveland and colleagues designed a prototype wearable microwave detector to conduct experiments on porcine models of hemoperitoneum, pneumothorax and hemothorax. Based on the already available data collected from these experiments, the aim of this master's thesis is to:

1. Study incidence and treatments of trauma in general and trauma to the torso in particular. Document current state-of-art and promising work for the detection of traumatic torso injuries, including both measurement setup and data processing.

2. Analyze the microwave signal characteristics, including the variation between repeated measurements, coefficient magnitude/phase and the changes in signal caused by torso trauma.

3. Extract features from the original high dimension data to interpret them in a proper simple way. This process should reduce the data dimension without losing the key features that can help differentiate normal and torso trauma subjects.

4. Assess the difference between baseline (healthy state) and injuries of different sizes with statistical tests like Wilcoxon rank-sum Test or Kruskal–Wallis Test.

5. Evaluate support vector machine (a classification algorithm) for detecting hemoperitoneum, pneumothorax and hemothorax.

1.1 Torso trauma

The torso region can be seen as a central part of the body from which neck and limbs extend. Figure 1.1 shows the torso area, where most of the major organs are. For complex torso trauma, both thoracic and abdominal injuries should be considered to ensure that while treating the injuries in one region, the remaining area will not be overlooked [12]. In the following sections, hemoperitoneum (a crucial type of abdominal trauma) and two major types of thoracic trauma including pneumothorax and hemothorax will be explained in detail.
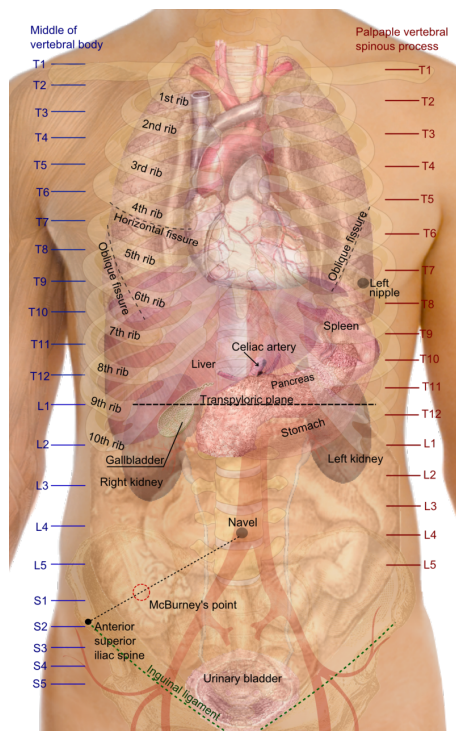
Figure 1.1: The torso region with major organs (source: `https://en.wikipedia.org/wiki/Torso`).

1.1.1   Hemoperitoneum (abdominal bleeding)

Hemoperitoneum is the accumulation of blood in the cavity between the organs in the abdomen and the inner lining of the abdominal wall (Figure 1.2). With the ability for distension, the abdominal space can hold more than five liters of blood or maybe even more than the entire volume of circulating blood. The quick blood loss in the abdominal area could lead to hemorrhagic shock or death if not treated properly [13].
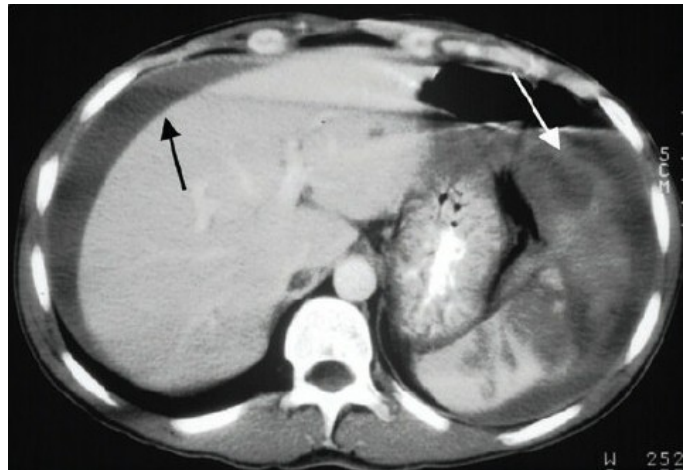
Figure 1.2: CT image of hemoperitoneum. The black arrow points to space where blood accumulates and white arrow indicates injured spleen (source: `https://step2.medbullets.com/gastrointestinal/120194/hemoperitoneum`).

Both blunt and penetrating trauma can be the reason for hemoperitoneum but blunt abdominal trauma is more frequent in emergency departments [14]. Motor vehicle collision accounts for 75 % of blunt trauma, and the remaining causes are falls, assaults, etc [15].

There are three current main diagnostic methods for hemoperitoneum: focused assessment with sonography for trauma (abbreviated FAST), computed tomography (abbreviated CT), and diagnostic peritoneal lavage [7]. The two first methods (FAST and CT) are noninvasive, using the obtained image of the abdomen (Figure 1.2, 1.3). Meanwhile, diagnostic peritoneal lavage requires a surgical procedure to take fluid samples from the abdominal cavity. This method is often applied when patients are unstable or uncooperative [16]. All of these methods require carefully trained doctors, nurses, physicians or paramedics.

After hemoperitoneum is diagnosed, if the patient gets a hemorrhagic shock, blood transfusion is required as the first step. Then, surgery may be needed to locate the source of bleeding. If the spilled blood is not contaminated, it could be reused for blood transfusion. Depending on the blood loss source, different methods are applied to stop the bleeding. For example, if blood comes from a broken blood vessel, the offending vessel will be clamped and ligated. Bleeding from the liver might be controlled by utilizing hemostatic sponges or thrombin [7].
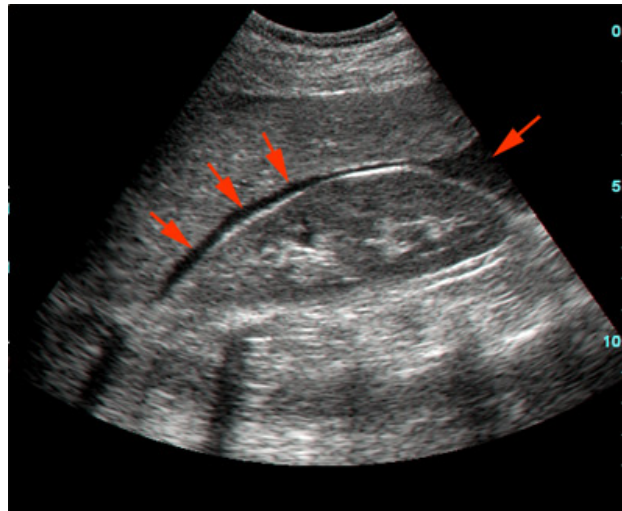
Figure 1.3: Ultrasound image of hemoperitoneum. The black stripe indicated by the red arrows is the space where fluid accumulates (source: `https://en.wikipedia.org/wiki/Focused_assessment_with_sonography_for_trauma`).

1.1.2 Pneumothorax

A pneumothorax is a collapsed lung caused by the appearance of air in the pleural space between the lung and the chest wall. The reasons for pneumothorax can be lung disease or trauma. In this report, only traumatic pneumothorax is investigated. Traumatic pneumothorax can be further divided into penetrating trauma and blunt trauma. As mentioned above, blunt trauma is difficult to detect and can lead to death that could have been prevented. One example of blunt pneumothorax is when sudden chest compression occurs (e.g. in car accidents or falls), causing alveolar rupture. If the visceral pleura is lacerated, air will enter the pleural space [17] (Figure 1.4)
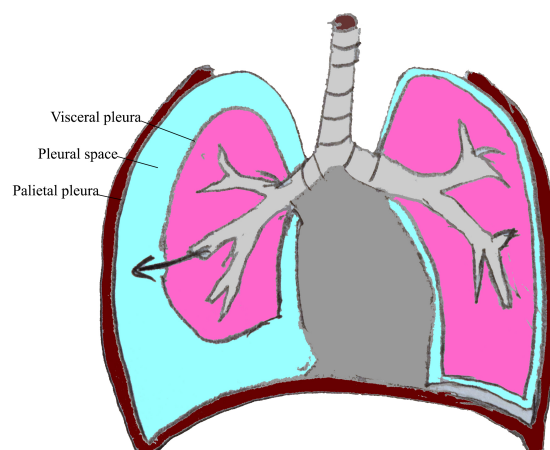
Figure 1.4: Pneumothorax caused by the appearance of air in the pleural space. The black arrow indicates the air flow entering the pleural space when the visceral pleura is lacerated.

Besides clinical examination, there are three imaging techniques to diagnose pneumothorax. The first method is chest radiography or chest X-ray which simply transmits an X-ray beam through the patient to an X-ray film where the two-dimensional image of the chest is recorded. However, this method requires patients to be stable, awake, and not in stages of tension [17]. A more sensitive method is chest CT scanning which generates the chest image by taking a series of X-ray beams around a patient. This is the gold standard to detect traumatic pneumothorax, especially with the blunt trauma [17]. However, these two methods are not usually used on the scene or in the ambulance because of their big size. Bedside ultrasonography is the last common imaging method. With a compact size, this method could be installed in the ambulance, but it requires carefully trained paramedics [18].

Pneumothorax treatment depends on the injury size (i.e. how much of the lung is collapsed). A small pneumothorax can resolve itself or with oxygen administration and monitoring of the chest with X-ray [17]. If the lung cannot re-expand itself, a needle may be inserted through the chest wall to remove the air. Another method is to insert a chest tube with its tip in the intrapleural space and the other tip into a water seal bottle. This method can prevent the air from re-entering the pleural cavity. After 72 hours, if none of these methods works, surgery may be required [17].

1.1.3 Hemothorax

Hemothorax happens when there is blood accumulating between the chest wall and the lung (pleural space). The most common reason of hemothorax is blunt trauma [19], where the chest suffers from a sudden and intense pressure such as in a car accident or fall. Hemothorax can also be associated with pneumothorax when the high pressure from the air in the pleural space causes a part of the lung to collapse. The appearance of blood can prevent the normal movement of the lung, causing poor ventilation or abnormal breathing. The amount of blood in the pleural space may be massive with more than 25 % of the total blood volume or about 1.5 L in an average adult [7].

The diagnosis tools for hemothorax are the same as pneumothorax with chest X-ray, CT, and ultrasound. If the patient is stable without any symptom requiring emergency treatments, chest X-ray is the preferred diagnosis that may reveal the blood accumulation. CT can detect much smaller blood volume than chest X-ray, but it is time consuming and normally not the primary method [20]. Meanwhile, ultrasound is quick but its disadvantage is being operator dependent [18]. To treat hemothorax, a chest tube is inserted into the pleural space to drain fluid, blood and air, which is similar to pneumothorax management. This tube could be attached for a few days until the lung returns to normal state. If the bleeding does not stop, patients may need surgery [20].

1.2 Prehospital torso trauma diagnosis

As mentioned above, the early diagnosis of severe torso trauma that demands surgical intervention is crucial to decrease preventable death. At present, CT is the gold standard to detect traumatic injuries. However, this technique cannot easily be

installed in the ambulance for prehospital diagnosis. The common on-scene trauma assessment is based on clinical parameters and physical examination. However, this method did not show a high accuracy and reliability for internal bleeding trauma (e.g. 87 % with blunt abdominal trauma [21]). The only current standardized diagnosis technique that can be applied at the trauma scene is ultrasonography.

An ultrasound examination called focused assessment with sonography in trauma (abbreviated FAST) is developed for evaluating prehospital abdominal trauma. The extended focused assessment with sonography in trauma (abbreviated eFast) is proposed to determine whether a patient has pneumothorax or hemothorax. The advantage of ultrasound technique is its cheap price, noninvasive nature, safety as a radiation free method, and most importantly its portability for use at trauma scenes [22]. However, there are drawbacks that should be considered for the ultrasound method. The short penetration of sonographic waves by gross obesity and skin emphysema (air in the skin) could cause an incorrect diagnosis [22]. In addition, this technique is operator dependent [18]. Physicians and paramedics have to be trained and certificated to be able to perform an ultrasound examination [22].

Due to the mentioned disadvantages of the current ultrasonography, novel torso trauma diagnosis techniques using microwave waves are being developed [9, 10]. The following section provides more detail about the microwave technique in the torso bleeding diagnosis.

1.3 Microwave technology in torso injury diagnosis

Early research on the application of microwave for pulmonary diagnosis is performed. Pedersen and his colleagues measure both transmission and reflection coefficient (see section 2.1 for the details about microwave technology) in the frequency range from 800 MHz to 950 MHz in a three-layered body model [23]. The results show the difference in the coefficient magnitude between normal, edema (excess fluid trapped in body's tissues) and emphysema (shortness of breath due to over-inflation of air sacs in the lung) patients. Another study evaluates microwave technique on dogs and showed that the phase shift in the transmission coefficient is correlated with changes in the arterial pressure which related to edema [24].

The potential of microwave diagnosis for pneumothorax is indicated by a current research conducted by Christopoulou and colleagues [25]. This research implements two planar patch microwave antennas with the size $1.44 \times 1.44 \, \text{cm}^2$ and places them in the vertical direction on the chest surface. The transmission coefficient between the two antennas is measured. The frequency range 1–4 GHz is evaluated with three simulated rectangular and anatomical models. The first model named THORAX is in rectangular shape with muscle thickness, fat thickness and bone thickness varying in the range 0–25 mm, 0–30 mm and 0–15 mm respectively. The largest difference in mean coefficient magnitudes between the normal state and 1 cm air pneumothorax is at 1.5–2 GHz with around 18 dB. The other two models are anatomical models built from the MRI (magnetic resonance imaging) data of one male and one female volunteer. Pneumothorax in these models are 1.5–2 cm

air thickness. The maximum difference between healthy and pneumothorax signal magnitude is 7 dB at 2.3 GHz for the male model and 19 dB at 1.7 GHz for the female model.

Besides the above research, there is a more general research field called microwave tomography (MWT) [26], which aims to build anatomy images of the human body based on microwaves. From the microwave imaging, paramedics or physicians can diagnose torso injuries. However, the diagnosis using biomedical imaging modality is not the interest of this master's thesis because it is operator dependence (similar to ultrasound technique). Therefore, the details about MWT research are out of scope and only one example of MWT developed by a research team at Queensland University for detecting thoracic fluid accumulation is provided [10]. The team designs a torso scanner with the outer layer in semi-doughnut chamber shape and the inner cavity in an elliptical shape. The outer layer, containing two antenna arrays with twelve antennas in each can scan the upper and lower torso regions at the same time. The antennas are organized around the chest region and run in the frequency range 0.5–2 GHz. Before each measurement, the system is calibrated by operating without patients/phantom inside. The changes of images due to the presence of fluid are magnified by subtracting the scattering profiles of upper and lower regions. The system shows the ability to localize fluid volumes as small as 3 mL in a torso model. However, this method requires the use of healthy subject data as reference for locating the trauma area.

2

Theory

2.1 Microwaves and dielectric properties of materials

Microwaves are known as one form of electromagnetic waves with the frequency range from 300 MHz to 300 GHz (i.e. wavelengths in the range 100–0.1 cm). The propagation of microwaves in the material can be expressed by Maxwell's equations [27]:

$$\nabla \cdot D = \rho \tag{2.1a}$$

$$\nabla \cdot B = 0 \tag{2.1b}$$

$$\nabla \times E = -\frac{\partial B}{\partial t} \tag{2.1c}$$

$$\nabla \times H = J + \frac{\partial D}{\partial t} \tag{2.1d}$$

Where:

- E [V/m]: electric field.

- H [A/m]: magnetic field.

- B [Wb/m^2]: magnetic flux density.

- D [C/m^2]: electric flux density.

- J [A/m^2]: electric current density.

- ρ [C/m^3]: electric charge density.

The magnetic density, electric current and the electric density are the sources of the electromagnetic field. When the field penetrates in a dielectric material, the relationship between the electric current density, electric flux density, and electric field can be expressed as [27]:

$$J = \sigma E$$
$$D = \epsilon E = (\epsilon' - j\epsilon'')E \tag{2.2}$$

where σ (S/m) is the total conductivity of the material, ϵ' (F/m) is the relative permittivity and ϵ'' is the out-of-phase loss factor which can be calculated as:

$$\epsilon'' = \frac{\sigma}{\epsilon_0 \omega} \tag{2.3}$$

where ϵ_0 is the permittivity of free space (8.854^{-12} F/m) and ω is the angular frequency of the microwave field. From these equations, the propagation of microwave field in a media clearly depends on the dielectric properties and the frequency utilized. Since there are differences in the dielectric properties of biological tissues [28], the propagation pattern of the microwave electromagnetic field changes according to the change inside the human body. For instance, the blood appearance in the abdominal cavity of hemoperitoneum patients may create a difference in the propagation and attenuation of the microwave signal in comparison with a healthy person.

The common measured microwave data are scattering parameters (symbolized S-parameters) [27]. S-parameters represent the relationship between the incident waves on the ports to those reflected from the ports, and can be measured with a vector network analyzer. For a N-port network, the scattering matrix is defined as:

$$\begin{bmatrix} V_1^- \\ V_2^- \\ \vdots \\ V_N^- \end{bmatrix} = \begin{bmatrix} S_{1,1} & S_{1,2} & \ldots & S_{1,N} \\ S_{2,1} & S_{2,2} & \ldots & S_{2,N} \\ \vdots & \vdots & \ddots & \vdots \\ S_{N,1} & S_{N,2} & \ldots & S_{N,N} \end{bmatrix} \begin{bmatrix} V_1^+ \\ V_2^+ \\ \vdots \\ V_N^+ \end{bmatrix} \tag{2.4}$$

where V_k^- is the amplitude of the voltage wave reflected from port k, and V_k^+ is the amplitude of the voltage wave incident on port k. A particular S-parameter can be found by:

$$S_{ij} = \frac{V_i^-}{V_j^+}\bigg|_{V_k^+=0 \text{ for } k \neq j}. \tag{2.5}$$

Equation 2.5 indicates that S_{ij} is calculated as the division of wave amplitude V_i^- coming out of port i by incident wave amplitude V_j^+ at port j. To avoid reflections, the incident wave in all ports except the port j should be set to zero when calculating S_{ij} [27]. S_{ij} can be called reflection coefficient if i equals j or called transmission coefficient between antenna i and j if i is not equal j. The measured S-parameters are complex numbers (i.e. $a + bi$) so they can be analyzed in magnitude (i.e. $\sqrt{a^2 + b^2}$) and phase (i.e. $\arctan(b/a)$) separately. The magnitude of S-parameters (e.g. S_{ij}) can be expressed in raw value (i.e. $||S_{ij}||$) or in dB unit, which is calculated by Equation 2.6.

$$S_{ij}(dB) = 10 \log ||S_{ij}(raw)|| \tag{2.6}$$

2.2 Statistic examination

Statistic examination is a procedure analyzing the statistical characteristic of collected data. In this master's thesis, the statistic examination is mainly to test whether defined classes (e.g. healthy subjects and bleeding subjects) are actually distinguishable. This procedure is commonly conducted after collecting all data and before developing classification algorithms. This step may help identify potential features to be used for classification algorithms, and be a connection between classification results and signal characteristics.

2.2.1 Null hypothesis

The *null hypothesis* is one type of conjectures utilized in statistic examination to test conclusions or make decisions based on a set of data. The statement or conclusion tested in an examination is named the null hypothesis and commonly symbolized as H_0. A statistic test is designed to evaluate evidence against the null hypothesis. The statement defining the opposite conclusion with the null hypothesis is called the *alternative hypothesis*, which usually symbolized as H_1. If there is any sample data which is inconsistent with the null hypothesis, the null hypothesis is rejected and the alternative hypothesis is accepted. In contrast, if all data cannot show any evidence against the null hypothesis, then the null hypothesis cannot be rejected.

The statistic tests typically have parameters to measure the extent of apparent departure from the null hypothesis. One of the most common parameters is p-value (probability value) which represents the probability of observing a result given that the null hypothesis is true. A small p-value indicates that the null hypothesis may not adequately consistent with the observed data. If the p-value is smaller than a pre-defined level, which is referred to as the level of significance, the null hypothesis is rejected. The level of significance is commonly 0.05 or 0.01, meaning that there is less than $5\,\%$ or $1\,\%$ probability that the alternative hypothesis is true by chance.

2.2.2 Anderson-Darling Test for Normality

Some statistic tests (e.g. analysis of variance test) require input data to have a normal distribution. If this requirement is fulfilled, these examinations can provide a strong indication such as to whether the mean values between classes are different or not.

One of the powerful statistic tests to examine for the normality of input data is Anderson-Darling Test. This test measures the distance between the hypothesized distribution and the empirical cumulative distribution function to test the null hypothesis that the data set follows a specific distribution. For the normality test of a data set, the procedure is as follows:

1. Arrange all data in ascending order.

2. Calculate the mean and standard deviation of the data set as in Equation 2.7.

$$\hat{\mu} = \frac{1}{n}\sum_{i=1}^{i=n} X_i, \tag{2.7a}$$

$$\hat{\sigma}^2 = \frac{1}{n-1}\sum_{i=1}^{i=n}(X_i - \hat{\mu}^2)^2, \tag{2.7b}$$

where X_i, for i = 1,2,..., n is n data points in the sorted order $X_1 < X_2 < ... < X_n$. $\hat{\mu}$ and $\hat{\sigma}$ are the estimated mean and standard deviation respectively.

3. Standardize each X_i value to create a new Y_i value as follows:

$$Y_i = \frac{X_i - \hat{\mu}}{\hat{\sigma}}. \tag{2.8}$$

4. Calculate the Anderson-Darling parameter A, where A^2 is given by:

$$A^2 = -n - \frac{1}{n} \sum_{i=1}^{i=n} (2i-1)[\ln \Phi(Y_i) + \ln(1 - \Phi(Y_{n+1-i}))], \qquad (2.9)$$

where Φ is the standard normal cumulative distribution function.

If A^2 less than a defined threshold at a given significance level, the null hypothesis of the normal distribution is rejected. The threshold values at different significance levels (e.g. 0.05) are generally given in a form of a table.

Normality test can be visualized with the Quantile-Quantile plot (abbreviated Q-Q plot) for the normal distribution. After sorting data in ascending order, the theoretical quantile value for the ith sample is calculated as:

$$q_i = \Phi^{-1}\left(\frac{i-0.5}{n}\right), \qquad (2.10)$$

where Φ^{-1} is the standard normal quantile function and n is the number of data points. The input data are plotted along the y-axis while the theoretical quantile values appear along the x-axis. If the plot is linear, the data set is likely from a normal distribution (Figure 2.1).
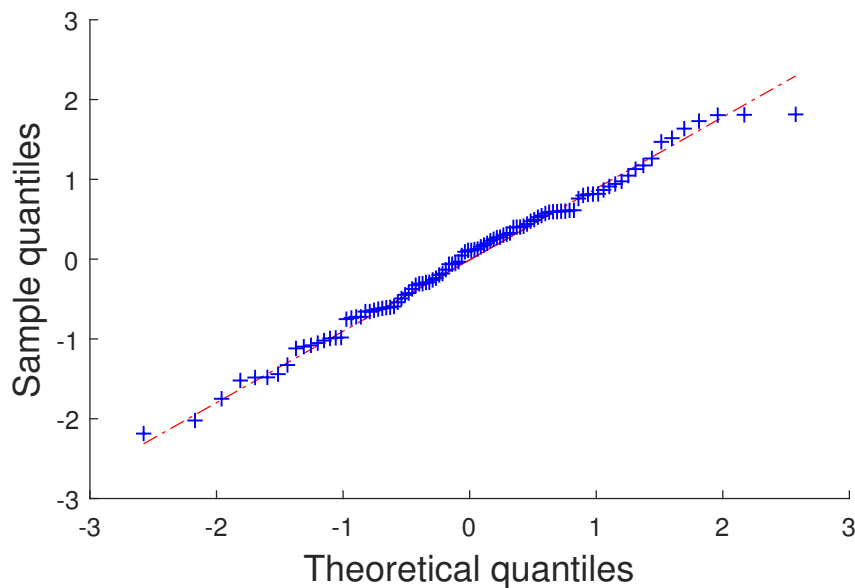
Figure 2.1: Q-Q plot for 100 data points (blue cross) generated from a normal distribution with the mean value being 0 and the standard deviation being 1. The red straight line represents the theoretical normal distribution.

2.2.3 Wilcoxon rank-sum Test

The Wilcoxon rank-sum Test (also called the Mann–Whitney U test) is a statistical examination of the null hypothesis H_0 that the distributions of two populations (i.e. classes) are equal. The alternative hypothesis H_1 is that the distribution is not equal.

The advantage of the Wilcoxon rank-sum Test is that it does not require data sample to have a normal distribution. There are two assumptions of the Wilcoxon rank-sum Test, including:

1. All the observations from both classes are independent of each other, meaning that one observation has no effect on the appearance of the others.

2. The responses are ordinal (i.e. data can be sorted).

The independent observation assumption depends on how the study test is designed or how the researcher believes it is possible to consider the observations are independent. If all assumptions are fulfilled, the Wilcoxon rank-sum Test calculates the W parameter as follows:

1. Combine data from both classes, sort them in the ascending order and give numeric ranks for them with the smallest rank being 1. If there are tied values, the mean of rankings (before adjusting) are assigned for these values. For example, the ranks of data set (3,5,5,5,9) are (1,3,3,3,5).

2. Sum up the ranks for data points from class 1 (symbolized as W_1) and class 2 (symbolized as W_2) separately.

3. If the sample size is small, select the smaller value of W_1 and W_2 to get the p-value from the Wilcoxon rank-sum probability table according to the number of data points of class 1 and 2.

4. If the sample size is large, W_1 and W_2 are standardized as follows:

$$\mu_k = \frac{n_k(n_1 + n_2 + 1)}{2}, \tag{2.11a}$$

$$\sigma_k = \sqrt{\frac{n_1 n_2(n_1 + n_2 + 1)}{12}}, \tag{2.11b}$$

$$z_k = \frac{W_k - \mu_k}{\sigma_k}, \tag{2.11c}$$

where $k=(1,2)$; n_1, n_2 are the number of data points from class 1 and 2 respectively; z_k is the standardized parameter which follows the standard normal distribution.

The p-value is the probability value calculated from the standard normal distribution according to the z_k value. If the p-value less than a level of significance (e.g. 0.05), the null hypothesis is rejected at that level and the alternative hypothesis is accepted (i.e. two populations come from different distribution).

2.2.4 Kruskal–Wallis Test

The Kruskal–Wallis Test is the extension of the Wilcoxon rank-sum Test, which can only examine two classes. It can compare data from two or more groups but often being used for three or more classes. The Kruskal–Wallis Test with a significant

result indicates that at least one population stochastically dominates one other (i.e. there are differences in the mean ranks between the populations). However, this test cannot identify which population pairs are different. To test the relationship between each population pair, the Wilcoxon rank-sum Test may be utilized.

The assumptions of the Kruskal–Wallis Test are the same as the Wilcoxon rank-sum Test, which does not require normality in the data set. The null hypothesis H_0 of the Kruskal–Wallis Test can be given that there is not any difference in the mean ranks between the classes. The alternative hypothesis H_1 is that there are differences in the mean ranks between the classes.

The procedure to calculate the p-value of Kruskal–Wallis Test is as follows:

1. Combine data from all classes and give numeric ranks for them with the smallest rank is 1. If there are tied values, the mean of rankings (before adjusting) are assigned for these values (the same as the first step of the Wilcoxon rank-sum Test).

2. Calculate the H parameter by:

$$H = (N-1)\frac{\sum_{i=1}^{C} n_i (\bar{r}_i - \bar{r})^2}{\sum_{i=1}^{C} \sum_{j=1}^{n_i} (r_{ij} - \bar{r})^2}, \tag{2.12}$$

   where:

   - N is the total number of data points among all classes
   - C is the number of classes to examine
   - n_i is the number of data points in class i
   - r_{ij} is the rank of the jth observation from class i
   - $\bar{r}_i$ is the average rank of class i
   - $\bar{r}$ is the average rank of all class (i.e. average value of all r_{ij})

3. If the sample size is small (e.g. 10 samples for each class), use the calculated H value to obtain the p-value from a table. Otherwise, the p-value can be estimated by approximating the distribution of H by a chi-squared distribution with $g-1$ degrees of freedom [29].

If the p-value less than a level of significance (e.g. 0.05), the null hypothesis is rejected at that level and the alternative hypothesis is accepted (i.e. there are differences in the mean ranks between the classes). The Wilcoxon rank-sum Test can be used to further test the differences between each pair.

2.3 Data classification with machine learning

Data classification can be approached with statistical models or machine learning. While statistical models require specific mathematical proofs or arguments, machine learning algorithms make predictions without being explicitly programmed. Machine learning may also be helpful for exploring new features that have the potential to

differentiate classes. The basic principle of machine learning is to build a mathematical model based on input sample data (known as training data) and then apply this model to new input data to make decisions.

There are generally four types of machine learning: supervised learning, unsupervised learning, semi-supervised learning, and reinforcement learning. In supervised learning, there are specifically defined classes (also known as labels) and each training data belongs to one of these classes. In contrast, unsupervised learning does not require data being labeled. It associates data with different classes based on the data structure. Semi-Supervised learning is at the middle of supervised learning and unsupervised learning, which has a part of data being labeled. Reinforcement learning is utilized to maximize the performance of a system in a particular situation such as maximizing the score in a computer game. For a data classification problem with defined classes, supervised machine learning is applied.

2.3.1 Machine learning training, validation and test scheme

In machine learning, collected data are usually divided into a training set and a test set. When building the classification model, only training data are utilized. The model after training is evaluated with the test data. If the number of training samples is small while the designed model is too complicated, overfitting can happen. Overfitting is the phenomena that the trained model is too adapted to a particular set of data, making it fail to predict future observations (i.e. unseen data).

One common method to avoid overfitting is k-fold cross-validation, which divides the training set into k equal sized subsamples. Of the k subsamples, $k-1$ subsamples are for training models while the remaining subset is used to validate the models. This process is repeated k times, with each of the k subsamples used once as the validation set. Validation errors are the main factor to select the best model. When k equals the number of training data points (i.e. only one data point in each subsample), this method is named leave-one-out cross-validation.

In the testing process of supervised machine learning, the trained model classifies the test data points into defined classes. The accuracy of a classifier is defined as the number of correctly classified data points divided by the total number of test samples. Besides the accuracy, sensitivity and specificity are also widely utilized factors to evaluate a binary classifier (i.e. classifier of two classes). There are four cases that could occur when testing a binary classifier including true positive, false negative, false positive and true negative. For example, for a classifier between healthy and sick people, these cases are defined as:

- True positive (TP): the classifier correctly detects a true sick person as being from the sick people class.

- False negative (FN): the classifier incorrectly detects a true sick person as a healthy person.

- False positive (FP): the classifier incorrectly detects a true healthy subject as being from the sick people class.

- True negative (TN): the classifier correctly detects a true healthy person as being from the healthy people class.

From these four cases, sensitivity and specificity will be calculated as:

$$Sensitivity = \frac{number\ of\ true\ positives}{number\ of\ true\ positives\ +\ number\ of\ false\ negatives}$$
$$= \frac{TP}{TP + FN} \tag{2.13}$$

$$Specificity = \frac{number\ of\ true\ negatives}{number\ of\ true\ negatives\ +\ number\ of\ false\ positives}$$
$$= \frac{TN}{TN + FP} \tag{2.14}$$

Sensitivity is utilized to estimate the quality of the classification in detecting sick subjects while specificity indicates the ability to avoid false detection of healthy subjects as being sick. From the four cases above, the accuracy can be calculated as:

$$Accuracy = \frac{TN + TP}{TN + TP + FN + FP} \tag{2.15}$$

Some binary classifiers have a discrimination threshold that can vary to adjust sensitivity and specificity. Normally, when sensitivity increases, specificity will drop and vice versa. The receiver operating characteristic curve (abbreviated ROC) is a graph showing the effect of adjusting the threshold with X-axis being specificity and Y-axis being sensitivity (Figure 2.2). The area under the curve (abbreviated AUC), which is the yellow shaded area in Figure 2.2, is another factor to asses the quality of a classifier. A classifier with a higher AUC generally has a better classification accuracy.
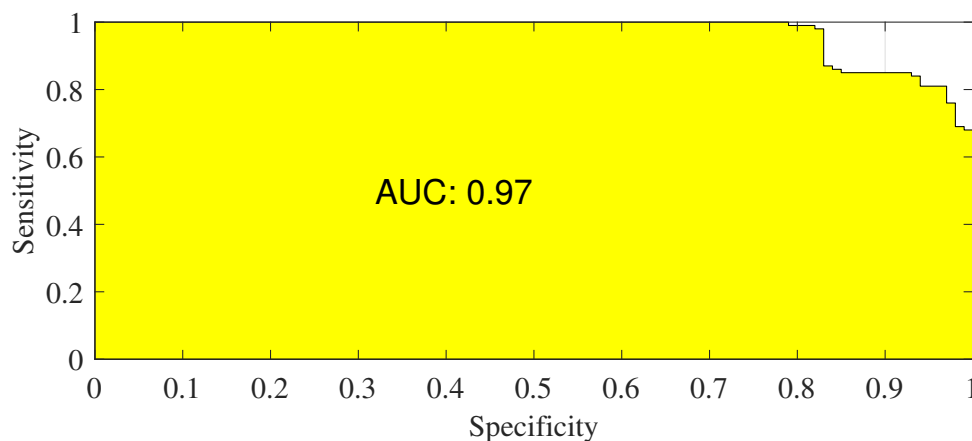
Figure 2.2: A receiver operating characteristic curve (ROC) with the area under the curve (AUC) value being 0.97.

2.3.2 Support vector machine classification

Support vector machine (SVM) is a supervised machine learning technique for data classification. In this section, only SVM for two classes is described. If the two classes are already linearly separable, a hard margin SVM can find the optimal boundary between the two classes. When two classes contain noisy data or mostly separable, a soft margin SVM is applied. For the last case in which two classes are not linearly separable, a kernel SVM will be utilized. The following parts provide the details about these types of SVM.

2.3.2.1 Hard margin support vector machine

The basic principles of SVM may be seen through a simple example of two-dimensional (abbreviated 2D) data in Figure 2.3. In this example, class 1 and 2 are linearly separable, and there are many lines that can differentiate them. The margin is the smallest distance from the closest data points for the two classes to the line. The problem is to find the separating line which generates the largest margin. Basically, SVM is a method to find a hyperplane (or a line for 2D data) to separate two classes with a maximum margin between classes.
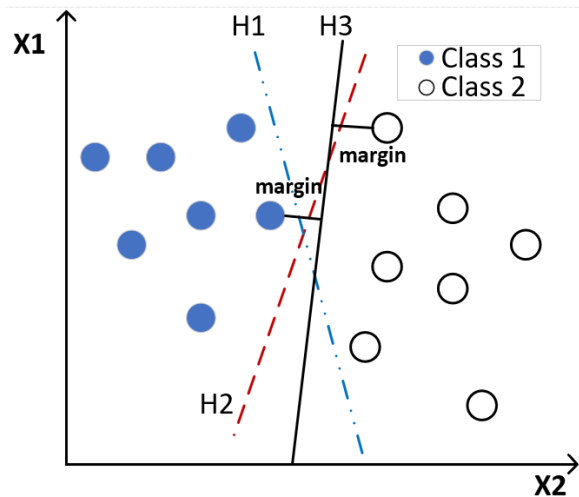
Figure 2.3: An example of SVM on two linearly separable classes. The H1 and H2 lines can separate class 1 and 2 but with a smaller margin than H3, which is calculated by SVM. H3 is also the line that can assure an equal margin for both classes.

Assume that the training set is $(\mathbf{x}_1, y_1)$, $(\mathbf{x}_2, y_2)$,..., $(\mathbf{x}_N, y_N)$ where $\mathbf{x}_i \in \mathbb{R}^d$ is the input data with d-dimensional; y_i is the label of $\mathbf{x}_i$, and N is the total number of training data points. The sought hyper-plane follows the equation $\mathbf{w}^T\mathbf{x} + b = 0$, where $\mathbf{w}$ is the d dimension parameter vector and b is the offset. Assume that after classification, class 1 is on the positive side of the hyper-plane and labeled 1 while class 2 is on the opposite side and labeled -1. The distance h from one data point $(\mathbf{x}_n, y_n)$ to the hyper-plane and the margin are calculated as:

$$h = \frac{y_n(\mathbf{w}^T\mathbf{x}_n + b)}{||\mathbf{w}||} \tag{2.16}$$

$$margin = \min_n \frac{y_n(\mathbf{w}^T\mathbf{x}_n + b)}{||\mathbf{w}||} \tag{2.17}$$

The problem in SVM is to find $\mathbf{w}$ and b so that the margin is maximum or mathematically expressed as:

$$(\mathbf{w}, b) = \arg\max_{\mathbf{w},b} \left\{ \min_n \frac{y_n(\mathbf{w}^T\mathbf{x}_n + b)}{||\mathbf{w}||} \right\} \tag{2.18}$$

It is noticeable that when $\mathbf{w}$ and b are replaced by $k\mathbf{w}$ and kb, the margin is unchanged. Therefore, we can assume that the closest points to the hyper-plane fulfill the condition:

$$y_n(\mathbf{w}^T\mathbf{x}_n + b) = 1 \tag{2.19}$$

Two lines $\mathbf{w}^T\mathbf{x} + b = \pm 1$ are called the support vectors, which have the same distances to the the hyper-plane. The line $\mathbf{w}^T\mathbf{x} + b = 1$ is support vector of class 1 (labeled 1) while $\mathbf{w}^T\mathbf{x} + b = -1$ is the support vector of the class 2 (labeled -1). With this condition, for any k value we have:

$$y_k(\mathbf{w}^T\mathbf{x}_k + b) \geq 1 \tag{2.20}$$

This means that there is no point in the area between two support vectors. The problem (2.18) becomes

$$(\mathbf{w}, b) = \arg\max_{\mathbf{w},b} \frac{1}{||\mathbf{w}||} \tag{2.21}$$

$$\text{Subject to: } 1 - y_n(\mathbf{w}^T\mathbf{x}_n + b) \leq 0, \forall n = 1, 2, ..., N$$

Problem (2.21) can be solved by using the Lagrange function [30], but in this report, the detailed solution is out of scope and will not be provided. The solution, in this case, is called hard margin SVM and only works with linearly separable classes. After finding $\mathbf{w}$ and b or the hyperplane, for a new data $\mathbf{x}$, the classification is:

$$class(\mathbf{x}) = \text{sgn}(\mathbf{w}^T\mathbf{x} + b + \tau) \tag{2.22}$$

Sgn is the sign function which returns -1 if its input is negative and 1 if its input is positive. $\mathbf{w}^T\mathbf{x} + b$ is usually called the score of the test subject with the trained classifier. τ is the added decision value to balance between the sensitivity and specificity.

2.3.2.2 Soft margin support vector machine

Soft margin SVM is developed to replace hard margin SVM when input data contains noise or outliers as on example showed in Figure 2.4a. The line H1 is found by hard margin SVM, which produces a very small margin between two classes. Meanwhile, if the noisy data point is sacrificed (excluded when determining the margin), the separable line H2 derived using soft margin SVM creates a much bigger margin between two classes. If two classes are only mostly linearly separable as in Figure 2.4b, hard margin SVM cannot work. However, if some data points that close to the

(a) Data with noise. **(b)** Almost linearly separable data.
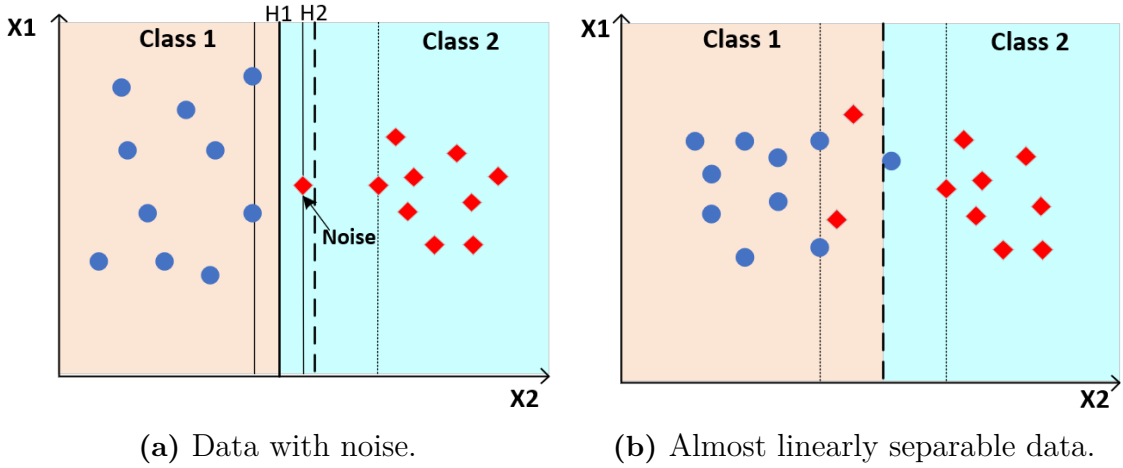
Figure 2.4: Hard SVM margin does not work well with data including noise (or outlier) (a) and data that is almost linearly separable (b). The dark solid line (H1) is found by hard margin SVM method while the dashed dark line is detected by a new method called soft margin SVM.

margin between two classes are sacrificed, a separable line could be found with a quite large margin (the dashed dark line in the Figure 2.4b).

The most different characteristic of soft margin SVM compared to hard margin SVM is the way to balance between the sacrificed points and the margin. With two selected support vectors, the sacrificed points are defined as the points in the area between two support vectors (not situated on the support vectors) or in the wrong class. To solve this problem, a new parameter named ξ_i is introduced. For the points not being sacrificed, ξ_i is 0 while for sacrificed points, ξ_i is their distance to the support vector of their true class. Mathematically, $\xi_i = |\mathbf{w}^T\mathbf{x}_i + b - y_i|$ with $\mathbf{x}_i \in \mathbb{R}^d$ is the input data with dimension d, y_i is its label (-1 or 1 as defined in the hard margin SVM part), and $\mathbf{w}$, b are parameters of the sought hyper-plane. Therefore, the level of sacrifice can be represented by the sum of all ξ_i values, and the new optimization problem is to find the minimum value of:

$$||\mathbf{w}|| + C\sum_{i=1}^{N}\xi_i \tag{2.23}$$

Where C is a positive constant utilized to balance between margin and the number of sacrificed points. The condition also turns in to:

$$y_i(\mathbf{w}^T\mathbf{x}_i + b) \geq 1 - \xi_i \Leftrightarrow 1 - \xi_i - y_i(\mathbf{w}^T\mathbf{x}_i + b) \leq 0, \forall i = 1, 2, ..., N \tag{2.24}$$

To sum up, the final problem is:

$$(\mathbf{w}, b, \xi) = \arg\min_{\mathbf{w}, b, \xi} ||\mathbf{w}|| + C\sum_{i=1}^{N}\xi_i$$
$$\text{Subject to: } 1 - \xi_i - y_i(\mathbf{w}^T\mathbf{x}_i + b) \leq 0, \forall i = 1, 2, ..., N \tag{2.25}$$
$$\xi_i \geq 0, \forall i = 1, 2, ..., N$$

In this report, the detailed solution of soft margin SVM will not be analyzed. However, it is notable that when C is large, the solution will try to reduce $\sum_{i=1}^{N}\xi_i$, making less

sacrifice. In contrast, when C is small, the solution will focus on minimizing $||\mathbf{w}||$ or maximizing the margin. As a result, the sacrifice will be larger.

2.3.2.3 Kernel SVM

When the input data is not linearly separated, kernel SVM may be applied. Kernel SVM utilizes a function Φ to transform input data $\mathbf{x}$ into a new dimension where data become linearly separable or mostly linearly separable. From that, hard or soft SVM may be utilized to classify the data. Briefly, kernel SVM is the solution for the following problem:

$$
\begin{aligned}
(\mathbf{w}, b, \xi) = \arg\min_{\mathbf{w}, b, \xi} ||\mathbf{w}|| + C\sum_{i=1}^{N} \xi_i \\
\text{subject to: } 1 - \xi_i - y_i(\mathbf{w}^T\Phi(\mathbf{x}_i) + b) \leq 0, \forall i = 1, 2, ..., N \\
\xi_i \geq 0, \forall i = 1, 2, ..., N
\end{aligned}
\tag{2.26}
$$

$K(x_i, x_j) = \Phi(x_i)^T\Phi(x_j)$ is called kernel function. There are four basic kernel functions:

- Linear: $K(x_i, x_j) = x_i^T x_j$

- Polynomial: $K(x_i, x_j) = (\gamma x_i^T x_j + r)^d$, $\gamma > 0$

- Radial basis function (RBF): $K(x_i, x_j) = \exp(-\gamma ||x_i - x_j||^2)$, $\gamma > 0$

- Sigmoid: $K(x_i, x_j) = \tanh(\gamma x_i^T x_j + r)$

γ, r, d are kernel parameters which could be adjusted to achieve the best classification result.

3
Method

3.1 Measurement setup

In this experiment, ten porcine models are utilized for testing. A belt with eight microwave antennas named A1, A2, A3, A4, A5, A6, A7, and A8 is wrapped around the abdomen/thorax region of the pigs (Figure 3.1). The even numbered antennas (A2, A4, A6, and A8) are on the left side of the median line while the odd numbered antennas (A1, A3, A5, and A7) are on the right side. Figure 3.2 depicts the approximate location of the antennas around the abdomen/thorax.

Figure 3.1: The microwave belt attached around the thorax of the pig.
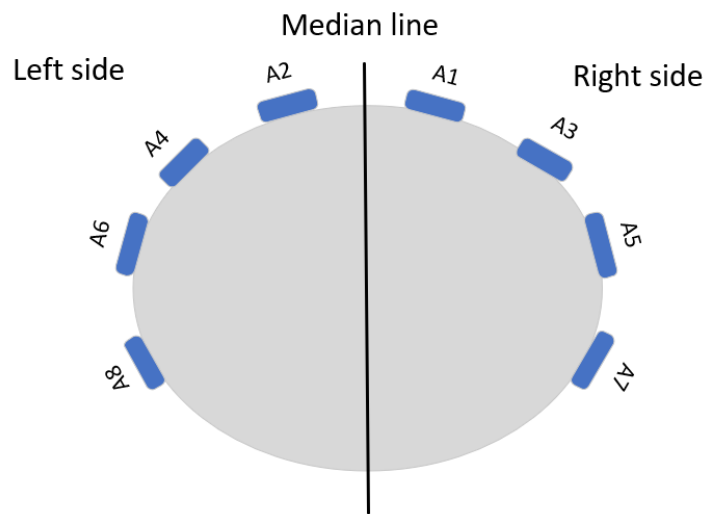
Figure 3.2: The arrangement of eight antennas around the abdominal region with the even and odd numbered antennas being on the left and right side respectively.

Table 3.1 indicates the experiment protocol in chronological order. For hemoperitoneum, the antenna belt is wrapped around the abdomen region, while in thorax trauma (i.e. pneumothorax, hemothorax, and polytrauma) experiments, the antenna belt is around the thorax region. During the experiment of 1000 ml polytrauma (i.e. state L750L1000), pig 10 is not physiologically stable so the state L750L1500 is skipped for this pig. Pig 9 also does not tolerate 1500 ml polytrauma (i.e. state L750L1500) so there are data of only 8 pigs for the state L750L1500.

Table 3.1: Measurement protocol in chronological order.

Type	State	Definition
Pneumothorax	T-BL-BS	Healthy subjects without any surgery (T = Thorax; BL = baseline; BS = before surgery).
	R-BL-AS	Healthy subjects with a catheter attached into the right pleural space to inject air. The left lung is kept healthy (R = right; AS = after surgery).
	R50	50 ml air is injected into the pleural cavity through the attached catheter (named 50 ml pneumothorax).
	R200	200 ml pneumothorax.
	R500	500 ml pneumothorax.
	R1000	1000 ml pneumothorax.
	R1500	1500 ml pneumothorax.
Hemothorax	L-BL-AS	1500 ml air from the previous test is kept in the right pleural space. A catheter is attached into the left pleural space to inject blood (L = left).
	L50	50 ml blood is injected into the left pleural cavity (named 50 ml hemothorax).
	L200	200 ml hemothorax.
	L500	500 ml hemothorax.
	L750	750 ml hemothorax.
Polytrauma	L750L50	750 ml blood from the previous test is kept in the left pleural space and 50 ml air is added into the left pleural cavity (named 50 ml polytrauma).
	L750L200	200 ml polytrauma.
	L750L500	500 ml polytrauma.
	L750L1000	1000 ml polytrauma.
	L750L1500	1500 ml polytrauma.
Hemoperitoneum	AB-BL-BS	Healthy subjects without any surgery (AB = abdominal bleeding).
	BL-AS	Healthy subjects with a catheter attached into the abdominal cavity by surgery to inject porcine blood.
	AB500	500 ml blood is injected into the abdominal cavity (named 500 ml hemoperitoneum).
	AB1000	1000 ml hemoperitoneum.

After setting up one state (e.g. AB1000) for each pig, the antenna belt

is wrapped around the abdomen/thorax area. The microwave measurements are performed with the following procedure:

1. The microwave device automatically chooses one antenna (e.g. A1) to transmit a wide-band wave with the frequency range from 1.6 MHz to 2.0 GHz. The remaining antennas measure the received signal. The reflection is also recorded.

2. Another antenna (e.g. A2) is automatically chosen as a transmitter by the microwave device. The transmitted frequencies are the same as in the step 1. This step is repeated until all eight antennas are chosen as a transmitter.

3. Manually repeat the step 1 and 2 ten times to obtain information about the spread (variance) of data.

There are eight antennas, 630 frequency steps (from 1.6 MHz to 2.0 GHz) and 10 repeated measurements (step 3). Therefore, for 10 pigs at one state, the data dimension is $8 \times 8 \times 630 \times 100$, which represents *"sending $\times$ receiving $\times$ frequency $\times$ measurement index"*. For each frequency f, the S-parameters are calculated and stated as $S_{ij}(f)$ where i is the transmitting antenna and j is the receiving antenna. Due to the symmetry of the measurement system, $S_{ij}(f) = S_{ji}(f)$.

3.2 Data analysis

Data of four torso trauma types including hemoperitoneum, pneumothorax, hemothorax and polytrauma are analyzed separately, but the analysis steps are similar. Firstly, the division and combination of S-parameters are proposed. Secondly, the variance between repeated measurements is evaluated. Then, the changes in trauma data compared to the normal state are explored to derive consistent trends. For each coefficient, statistic tests are applied to test the significant difference between normal and trauma states. Finally, classification methods are tested with different S-parameters combinations.

3.2.1 Coefficient division and combination

A further distance between sending and receiving antennas generally yields a lower magnitude. Therefore, to manage a large number of coefficients, S-parameters can be divided into different levels based on the distance between transmitting and receiving antennas in the belt. Based on the antenna arrangement in the belt (Figure 3.2), there are eight S-parameter levels in total. Level 1 is the first nearby antennas, level 2 being the second nearby antennas and so on. Specific S-parameters of each antenna level are as follows:

- Level 0: S_{77}, S_{55}, S_{33}, S_{11}, S_{22}, S_{44}, S_{66} and S_{88}.

- Level 1: S_{75}, S_{53}, S_{31}, S_{12}, S_{24}, S_{64} and S_{86}.

- Level 2: S_{73}, S_{51}, S_{32}, S_{14}, S_{26}, and S_{48}.

- Level 3: S_{71}, S_{52}, S_{34}, S_{16}, and S_{28}.

- Level 4: S_{72}, S_{54}, S_{36}, and S_{18}.

- Level 5: S_{74}, S_{56}, and S_{83}.

- Level 6: S_{76}, and S_{85}.

- Level 7: S_{78}.

For hemoperitoneum, the examination by ultrasound shows that in bleeding cases, blood is usually predominant around either left or right midaxillary line. Therefore, instead of testing S-parameters on the left and right separately, the average magnitude/phase of symmetric S-parameters between the left and right side (e.g. S_{75} and S_{86}) are utilized. If S_{ij} and S_{mn} are symmetric S-parameters, the average value of S_{ij} and S_{mn} is denoted as S_{ij+mn}. The magnitude and phase of S_{ij+mn} are calculated as follow:

$$
\begin{aligned}
|S_{ij+mn}|(magnitude) &= \frac{|S_{ij}| + |S_{mn}|}{2} \\
\angle S_{ij+mn}(phase) &= \frac{\angle S_{ij} + \angle S_{mn}}{2}
\end{aligned}
\tag{3.1}
$$

The remaining number of coefficients after this process are 12 for transmission coefficients and four for reflection coefficients, including:

- Level 0: S_{77+88}, S_{55+66}, S_{33+44} and S_{11+22}.

- Level 1: S_{75+86}, S_{53+64}, and S_{31+42}.

- Level 2: S_{73+84}, S_{51+62}, and S_{32+41}.

- Level 3: S_{71+82}, and S_{52+61}.

- Level 4: S_{72+81}, and S_{54+63}.

- Level 5: S_{74+83}.

- Level 6: S_{76+85}.

Regarding pneumothorax and hemothorax, since the trauma occurs in either the right or left lung, S-parameters are divided into the left and right side. This process leads to 12 included S-parameters:

- Level 0 right: S_{77}, S_{55}, S_{33} and S_{11}.

- Level 0 left: S_{22}, S_{44}, S_{66} and S_{88}.

- Level 1 right: S_{75}, S_{53}, and S_{31}.

- Level 1 left: S_{24}, S_{64} and S_{86}.

- Level 2 right: S_{73} and S_{51}.

- Level 2 left: S_{26} and S_{48}.

- Level 3 right: S_{71}.

- Level 3 left: S_{82}.

It should be noted that in general, a higher level S-parameters/coefficients refers to a longer distance between transmitting and receiving antennas in the belt and vice versa.

3.2.2 The magnitude variance of repeated measurements

As mentioned in the measurement procedure (section 3.1), for one subject, at a specific state (e.g. BL-AS state), there are ten repeated measurements. By examining the variance of these repeated measurements, the stability of the measurement system as well as the effect of pig's movement, blood circulation and breathing can be assessed. With limited time for the master's thesis, we only examine the variance in magnitude.

The variance in percentage unit can be calculated as standard deviation divided by the average value:

$$v_{ij}(f) = \sqrt{\frac{\sum_{k=1}^{10} ||\log(|S_{ij}^k(f)|) - \log(Savg_{ij}(f))||^2}{10}} \frac{100}{||\log(Savg_{ij}(f))||} \tag{3.2}$$

where k is the measurement index; i and j are the transmitting and receiving antennas respectively; f is the frequency; $Savg_{ij}(f)$ is the average magnitude of $S_{ij}^k(f)$ for k from 1 to 10 (ten repeated measurements). The logarithm scale is applied to avoid unexpected high variances when $Savg_{ij}(f)$ is close to zero, i.e. the received signal is mostly noise. Only measurements having too high variance (e.g. 30 %) across a large frequency range (e.g. 1 GHz) are removed from the analysis.

3.2.3 Data pre-processing

To reduce the effect of signal interference and make data interpretation clear, especially between antenna pairs at a far distance, a smoother developed by Eilers is applied [31]. This smoother is fast and gives continuous control over smoothness. In this master's thesis, the details about this smoother are out of scope. For the magnitude, although data are interpreted in logarithm unit, the statistical tests and classification use the raw data. Meanwhile, for the coefficient phase, the raw data in radian are utilized.

3.2.4 Analysis of the change caused by trauma

The data analysis results indicate that the insertion of a catheter affects the measured signal. Therefore, only data after the catheter insertion are compared. The analysis is divided into four separate parts with respect to four types of torso trauma: hemoperitoneum, pneumothorax, hemothorax, and polytrauma. The normal states (also called baseline) for four trauma types are different. For pneumothorax and polytrauma, the baseline (abbreviated BL) is R-BL-AS state (i.e. healthy subjects after surgery on the right lung). Meanwhile, to examine solely hemothorax, L-BL-AS

state (i.e. 1500 ml air in the right pleural space along with a catheter attached into the left pleural space) is considered the baseline for hemothorax. The baseline for hemoperitoneum is BL-AS state, (i.e. healthy subjects with a catheter attached into the abdominal cavity).

To explore the trend caused by trauma, baselines are subtracted from trauma states (data from the same pig, S-parameter and frequency are subtracted). For each S-parameter, the mean and standard deviation value of 100 measurements (10 pigs × 10 repeated measurements) are showed. If there is a common trend among ten pigs, it should appear in the average data. The standard deviation helps indicate how consistent the trend is.

Transmission and reflection coefficients are analyzed in both phase and magnitude. If there is any similar trend among coefficients, the next step is to test if the sought trends are consistent within ten pigs for each coefficient. A trend is considered consistent if it appears in all pigs for a similar frequency range.

3.3 Statistic examination

The statistic tests examine each coefficient and trauma type separately. The mean magnitude and phase across the frequency range 0.1–2 GHz are calculated for each coefficient. The reason data at frequency below 0.1 GHz being excluded is shown in section 4.1.2. For hemoperitoneum, pneumothorax and hemothorax, each class (i.e. state) has 100 data points (10 pigs × 10 repeated measurements). Meanwhile, for polytrauma, since pig 10 did not tolerate 1000 ml and 1500 ml air (i.e. L750L1000 and L750L1500 state), only 80 data points are used for these classes.

The first examination is to test the normal distribution for the data of each class with the Anderson-Darling Test. The level of significance chosen for all statistic tests in this master's thesis is 0.05. The second test is the Kruskal–Wallis Test with the data subtraction of baseline from trauma classes (Table 3.2). With an assumption that measurements are independent of each other, the Kruskal–Wallis Test can be utilized (see 2.2.4).

By subtracting baseline, the second test removes the effect of baseline difference among 10 pigs from the data set. The third statistic test compares classes without baseline subtraction (Table 3.2). The Kruskal–Wallis Test is first applied for all classes. Then, coefficients showing statistically significant results are further analyzed with the Wilcoxon rank-sum Test to examine the difference between baseline and each trauma size.

3.4 Classification with support vector machine

In this master's thesis, a linear kernel support vector machine (SVM) is tested to detect different types of torso trauma. SVM has advantages over other machine learning methods such as direct geometric interpretation, mathematical tractability and feasibility for a small number of training data sets without the overfitting issues [32]. The results from "Data analysis" (section 4.1 and 4.2) indicates that both the phase and magnitude of reflection coefficients have the potential to differentiate

Table 3.2: The tested classes for each type of trauma. BL stands for the baseline of each trauma type and "-BL" symbol indicates the subtraction of baseline.

Trauma type	Second test's classes		Third test's classes	
Hemoperitoneum	AB500-BL,	AB1000-BL	BL, AB1000	AB500,
Pneumothorax	R50-BL, R500-BL, R1500-BL	R200-BL, R1000-BL,	BL R200, R1000,	R50, R500, R1500
Hemothorax	L50-BL, L500-BL,	L200-BL, L750-BL	BL, L200, L750	L50, L500,
Polytrauma	L750L50-BL, L750L500-BL, L750L1500-BL	L750L200-BL, L750L1000-BL,	BL, L750L200, L750L1000,	L750L50, L750L500, L750L1500

trauma states and baseline. Therefore, for each reflection coefficient, both phase and magnitude are utilized as two dimensions of SVM input data. Meanwhile, for transmission coefficients, only the magnitude is used.

Besides testing each coefficient (see the list of coefficients in section 3.1), other coefficient combinations are tested (Table 3.3).

Table 3.3: Some data combinations for testing with SVM.

Index	Test	Definition
1	All coefficients	This test utilizes all coefficients as different dimensions of SVM input data.
2	All transmission	This test utilizes only transmission coefficients.
3	All reflection	Only reflection coefficients are utilized for SVM.
4	Sum coefficients	This test calculates the sum of all transmission coefficients and all reflection coefficients separately and utilizes them as different dimensions of input data.
5	Sum transmission	Similar to test 4 but utilize transmission coefficients only.
6	Sum reflection	Similar to test 5 but utilize summation of reflection coefficients instead. It should be noted that for reflection coefficients, magnitude and phase are treated as separate dimensions.

Due to the limited time for the master's thesis, only the largest size of each trauma type are tested with SVM. For example, the classification for hemoperitoneum is between AB1000 and baseline while for polytrauma, classification is between L750L1500 and baseline. Pig 9 and 10 could not tolerate L750L1500, so L750L1000 of pig 9 and L750L500 of pig 10 (i.e. the largest available trauma size of these pigs) are utilized. The leave one out (LOO) method is applied to avoid overfitting for the SVM method. The detailed steps are as below:

1. *Remove one subject (i.e. pig) for testing and build training set:*
   One out of 10 subjects (e.g. pig 1) is selected to be removed from the SVM training and saved for testing. All 90 measurements from the nine remaining subjects are utilized for training.

2. *Train the SVM classifier on the training set.*

3. *Validate the trained SVM on the testing subject:*
   All 20 measurements (two classes $\times$ 10 repeated measurements) from the test subject are validated with the trained SVM. If one data point (i.e. measurement data) is correctly classified, its score is 1. In contrast, the incorrect classification leads to score 0. The average score of 20 classifications is then calculated.

4. *Repeat and calculate the final accuracy:*
   Select another subject (e.g. pig 2) for the testing and repeat three above steps. Repeat this step until all subjects are selected one time as the testing subject (the total number of iterations including the first loop is ten). The average accuracy of 10 iterations is the final accuracy of the designed SVM.

Classification accuracy is utilized to select the best coefficient combination. The chosen method is further analyzed with the receiver operating characteristic curve (ROC), which is achieved by adjusting the decision values of the SVM classifier. From the ROC, the area under the curve (AUC) as well as specificity and sensitivity are calculated.

4

Results

4.1 Data analysis for abdominal data

In this section, the microwave abdominal data characteristics are analyzed. Firstly, the effect of the smoother on the signal is shown. Then, the stability of the measurement device as well as the variance caused by the pig (e.g. breathing and blood circulation) are examined by deriving the variation of repeated measurements. The coefficient magnitude at the normal state is also analyzed. Finally, the difference between baseline and hemoperitoneum states are explored.

4.1.1 Data pre-processing with the smoother

The applied smoother adjusts the smoothing degree of the output data by changing a parameter named λ in a way that a bigger λ leads to a higher smooth level [31]. The smoothing effect of different λ values can be seen in Figure 4.1a. Based on our experience, we believe that $\lambda = 1000$ is a good choice for removing much noise without hiding data that is valuable for our study. The effect of the smoother can be clearly seen with coefficients of far-distance antenna pairs (i.e. high level S-parameters) where the signal to noise ratio is large (Figure 4.1b). In this master's thesis, the smoother with $\lambda = 1000$ is utilized.

(a) S_{86} (level 1 coefficient). **(b)** S_{81} (level 4 coefficient).
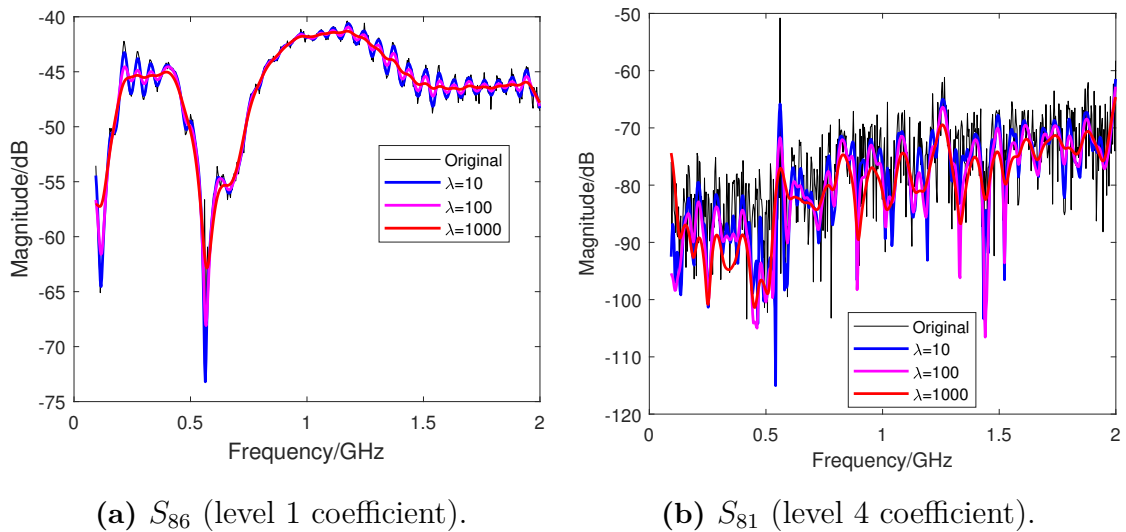
Figure 4.1: The original coefficient magnitude and the smoothed data with different λ value for level 1 S-parameter S_{86}(4.1a) and level 4 coefficient S_{81}(4.1b).

The applied smoother also helps remove abnormal peaks at the frequency around $0.56\,\mathrm{GHz}$ for some coefficients (Figure 4.2). These peaks are considered abnormal and should be removed because there is a high variance at these peaks between ten repeated measurements. The variance could be up to 40 dB as shown in Figure 4.2 between measurement 1 and 4. There is no clear pattern about which coefficient has this phenomenon so it is likely due to interference from the outside environment.
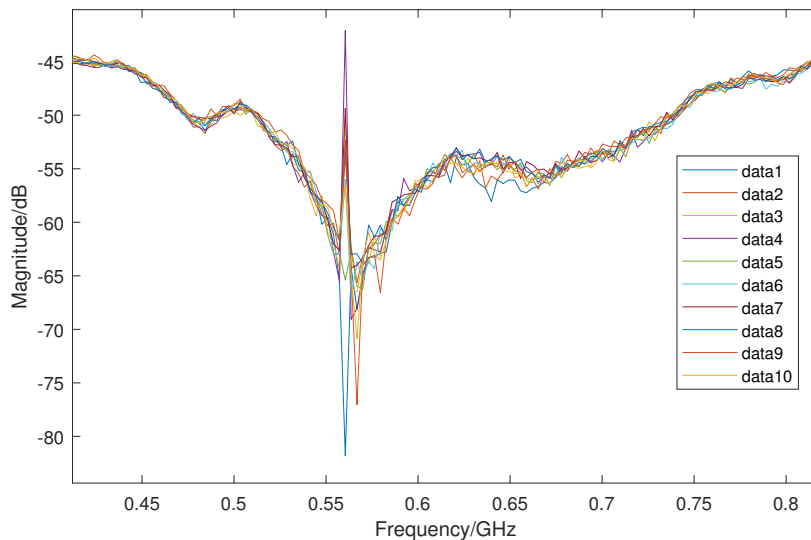

Figure 4.2: S_{86} magnitude of pig 1 at BL-AS state with ten repeated measurements. The abnormal large variance is observed at around $0.56\,\mathrm{GHz}$. Some other pigs and coefficients show the same pattern.

### 4.1.2 The variance of repeated measurements

There is a high variance (around $20\,\%$) between 10 repeated measurements at the lower end of the frequency range (Figure 4.3). This phenomenon can be seen in all S-parameters, so data at frequencies lower than $100\,\mathrm{MHz}$ will not be further analyzed. High variance values are also observed in some other cases. For pig 3 at the state AB500, S_{86} shows one measurement being totally different from the other nine measurements in a large frequency range (Figure 4.4). The same phenomenon is found for S_{55} of pig 1 at the AB1000 state. The reason for this is unknown, and these data should be removed before further analysis.

Besides the two cases above, Table 4.1 indicates the other cases with medium-high variance (around $10\,\%$) within repeated measurements (Figure 4.5). However, since this variation occurs for several repeated measurements, these data are kept for further analysis.

In general, the variance values depend on the magnitude. For low magnitudes (around $-70\,\mathrm{dB}$) like coefficients between far distance antennas (e.g. S_{85}) or measurements at low frequencies, the average variance is about $8\,\%$. This could be understood as for low magnitude signal, the signal to noise ratio is small, causing a
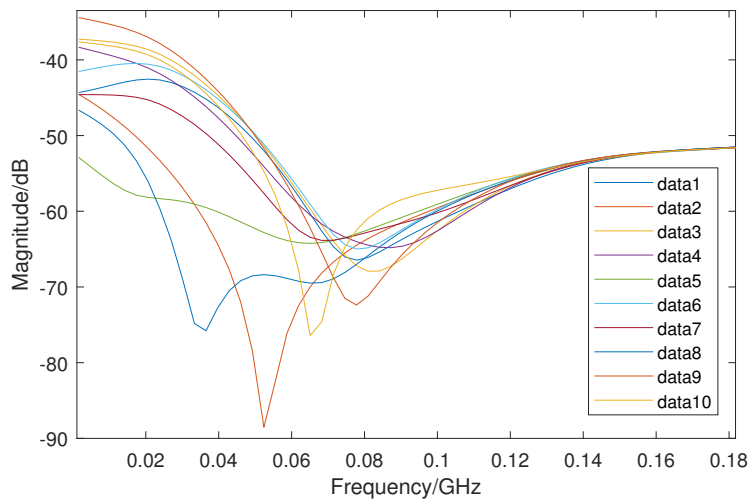
Figure 4.3: A representative example of the high variance between 10 repeated measurements at low frequencies. In this example, S_{75} magnitude of pig 2 at BL-AS state is shown.
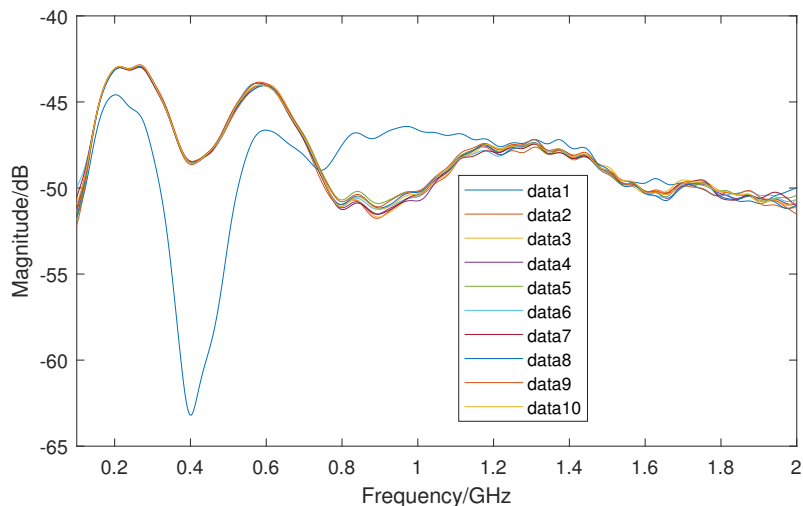
Figure 4.4: The measurement 1 of S_{86} of pig 3 at the state AB500 is completely different from the other repeated measurements.

high variance between repeated measurements. The variance is typically reduced when the signal magnitude increase. For high magnitude (about -40dB) signal such as between sequential antenna pairs (e.g. S_{75}), the mean variance is approximately 1%.

4.1.3 Coefficient magnitude characteristic

Signal magnitude depends on the frequency and the distance between the sending and receiving antennas. Frequency variation leads to the change in the conductivity of tissues, which may change the scattering pattern [33]. Meanwhile, a longer distance

**Table 4.1:** All the cases found with medium-high variance in the collected data.

S-parameter	Frequency	Pig	State
S_{12}	1.54–1.64 GHz	1	AB500
S_{12}	1–1.3 GHz	7	BL-BS
S_{12}	0.5–1.3 GHz	7	BL-AS
S_{12}	0.5–1.4 GHz	7	AB500
S_{12}	1–1.2 GHz	7	AB1000
S_{12}	0.8–1.4 GHz	9	BL-AS
S_{12}	1–1.3 GHz	10	BL-AS
S_{46}	0.9–1.2 GHz	10	BL-AS
S_{68}	0.4–1.1 GHz	10	BL-AS
S_{75}	0.7–1 GHz	10	BL-AS
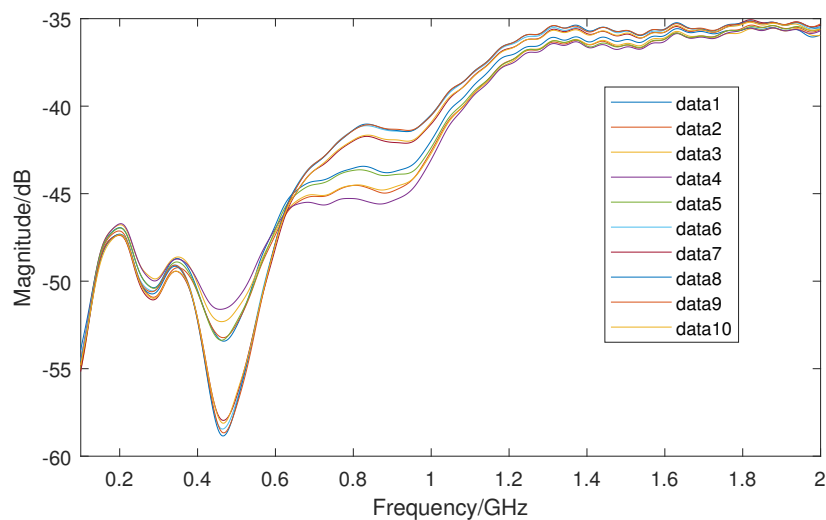
Figure 4.5: One example of medium-high variance among 10 repeated measurements of pig 10 at the BL-AS state with S_{86}.

between transmitting and receiving antennas may cause higher attenuation on the received signal.

Regarding the reflection coefficients, the resonance frequency, where the magnitude is lowest is at 0.75–0.9 GHz. There is a variation in the resonance frequency among different antennas as indicated in Figure 4.6. In a 500 MHz bandwidth around the resonance frequency, the magnitude is typically below -6 dB.

For the transmission coefficients, the maximum magnitude is typically at 0.8–1.2 GHz. The trend that further distance leads to lower signal magnitude can be observed in Figure 4.7. The maximum magnitudes for different coefficient levels (i.e. different distance between antenna pairs) are shown in Table 4.2. More examples of other reflection and transmission coefficients can be found in Figure A.1, A.2, A.3, A.4, and A.5.
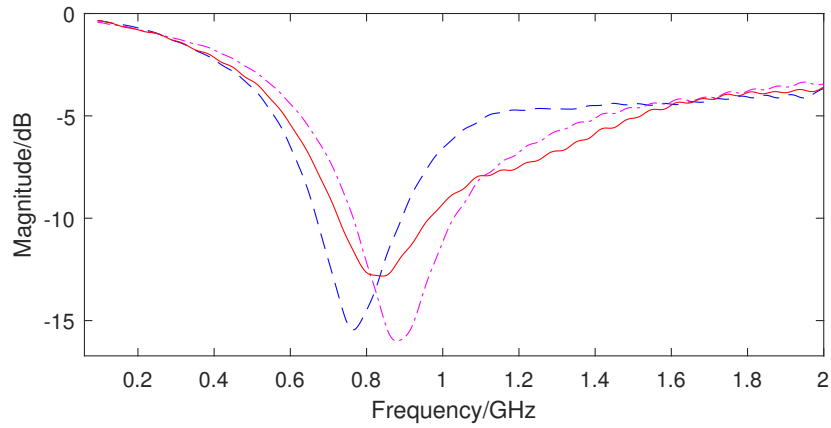
Figure 4.6: A representative example of S_{11}, S_{22}, and S_{33} of pig 10. The other reflection coefficients of pig 10 and other pigs show the same shape with the resonance frequency around $0.8\,\mathrm{GHz}$.

Table 4.2: The maximum magnitude for different coefficient levels (in dB).

Level 1	Level 2	Level 3	Level 4	Level 5	Level 6	Level 7
-20 to -45	-40 to -60	-50 to -70	-55 to -75	-75	-75	-55 to -75
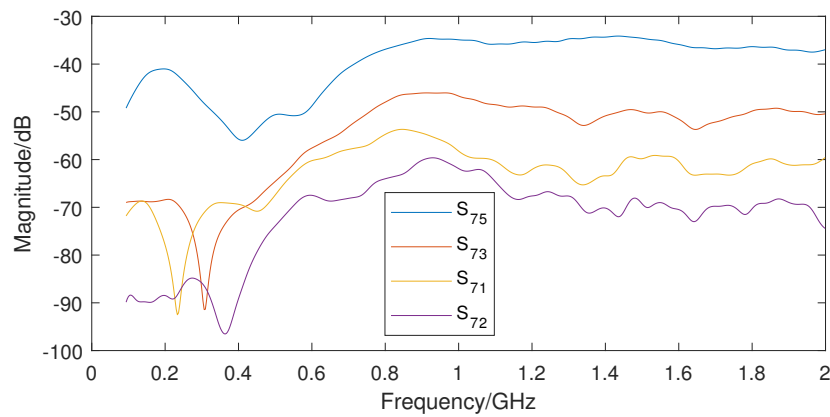
Figure 4.7: An example of transmission coefficients from level 1 (S_{75}), 2 (S_{73}), 3 (S_{71}), and 4 (S_{72}) of one pig at BL-AS state.

4.1.4 Comparison of healthy and hemoperitoneum

In this part, the changes caused by hemoperitoneum (i.e. AB500 and AB1000) in both phase and magnitude are analyzed for transmission and reflection coefficients separately.

4.1.4.1 Transmission coefficient

The average (among ten pigs) subtractions of baseline (BL) from hemoperitoneum states show a trend in all transmission coefficients that at above $0.6\,\mathrm{GHz}$, the magnitude is reduced when more blood accumulates in the abdominal region. Magnitude decrease caused by blood accumulation is more obvious at lower level coefficients (e.g. S_{75+86}) than higher level coefficients (e.g. S_{74+83}) (Figure 4.8; all coefficients are showed in Figure A.6 - Appendix). The standard deviation is also typically smaller at lower level coefficients. The average magnitude differences between BL and AB500 is at about 0.25–$0.75\,\mathrm{dB}$ and between BL and AB1000 is 1–$2.5\,\mathrm{dB}$ (Figure 4.9). At frequencies below $0.6\,\mathrm{GHz}$, although in some cases, magnitude differences are high, there is not a clear trend about the effect of blood accumulation. The trend for each pig can be observed through the mean coefficient magnitude across the frequency range 0.6–$2\,\mathrm{GHz}$ as shown in Figure A.7 - Appendix.
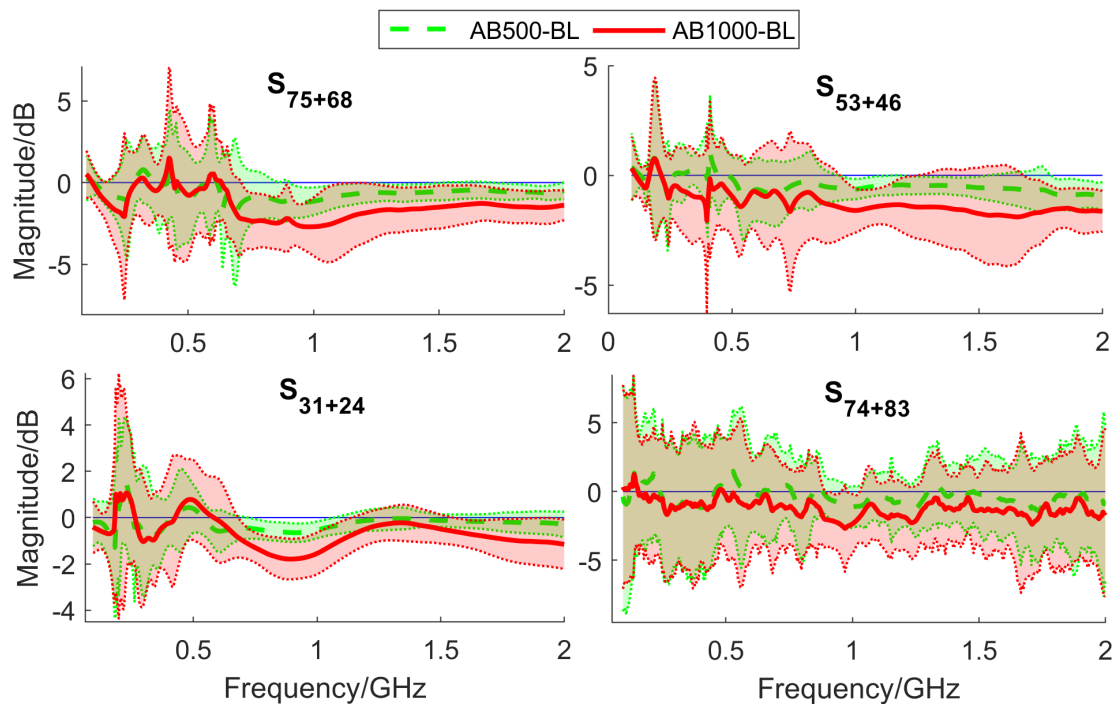

Figure 4.8: An example of the trend that blood accumulation in the abdominal region dampens the signal magnitude at frequencies above $0.6\,\mathrm{GHz}$. The solid lines are the mean among all measurements of 10 pigs while the shaded areas are the standard deviation. Coefficient combinations of level 1 and 5 are shown in this example.

For the transmission coefficient phase, there is a large phase shift (up to 2π) at frequencies below $0.6\,\mathrm{GHz}$. Therefore, to investigate the change in phase, only
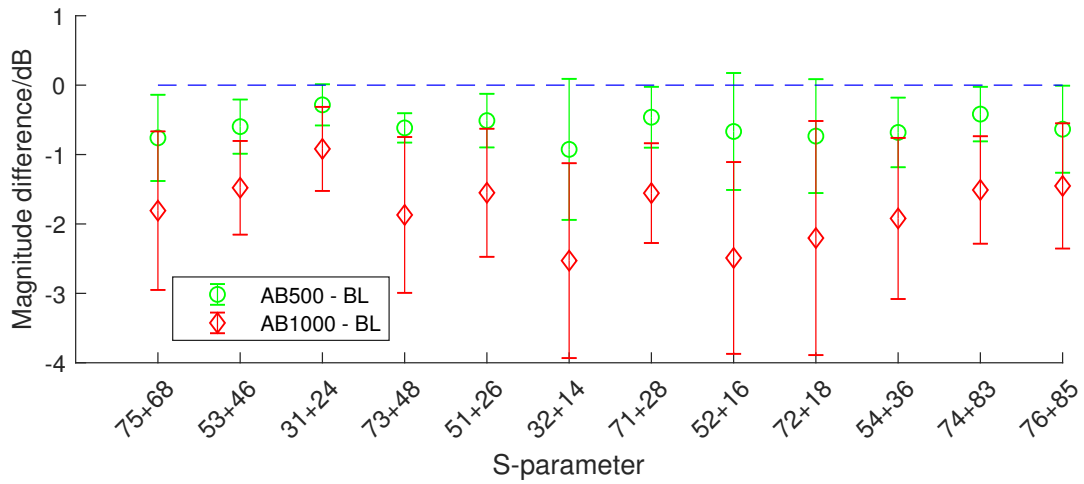
Figure 4.9: The average (across frequencies above 0.6 GHz) magnitude differences between BL and AB500/AB1000 for all transmission coefficient combinations (showed in circle and diamond shape). The vertical line at each coefficient indicates the standard deviation of all measurements. Magnitude drop at trauma states can be seen for all coefficients.

data at frequencies above 0.6 GHz are analyzed. The results do not show any clear pattern between coefficient combinations (Figure 4.10).
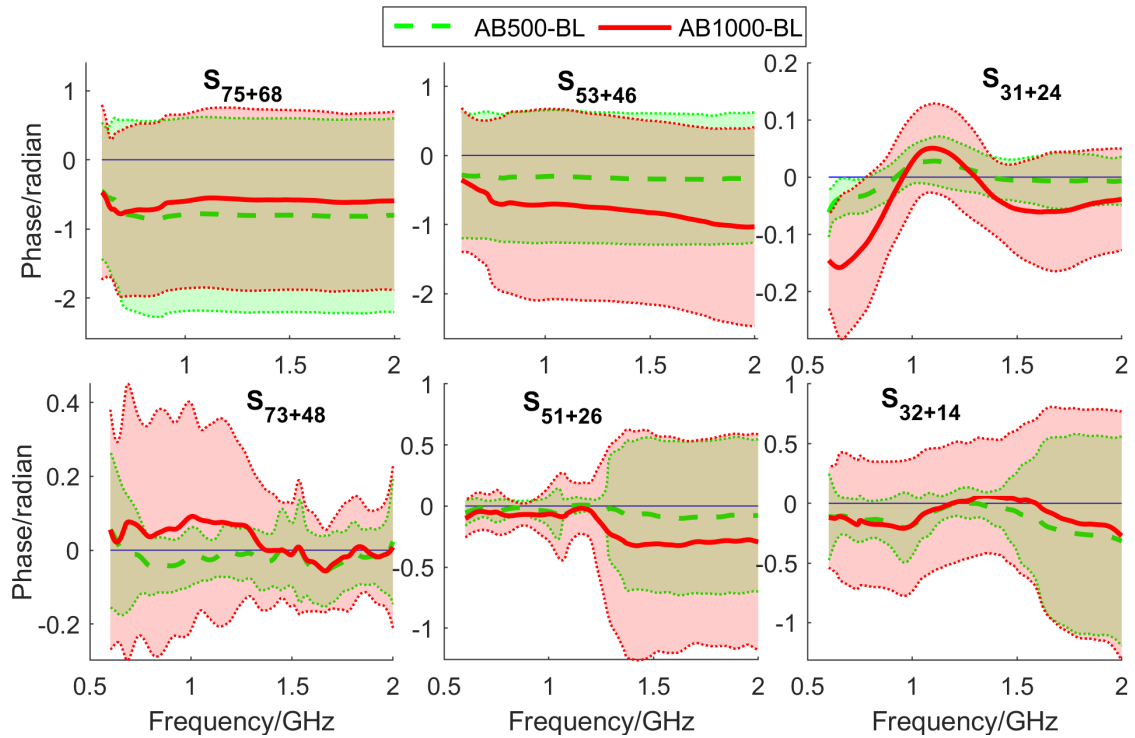
Figure 4.10: The mean (solid lines) and standard deviation (shaded areas) among all measurements for some coefficient phases. Large phase shifts along the frequency range can be seen through the high standard deviation.

4.1.4.2 Reflection coefficient

The reflection coefficients show common trends in both phase and magnitude when more blood is injected into the abdominal cavity. For the magnitude, there are opposite trends between frequencies below and above a frequency threshold (symbolized as $f_{MThreshold}$, Figure 4.12) around 0.8 GHz. Below $f_{MThreshold}$, a larger size of hemoperitoneum has a lower magnitude while above this threshold, magnitude increases are observed (Figure 4.11a). The highest average magnitude difference between baseline and 1000 ml hemoperitoneum is about 1.5 dB.

Regarding the phase, at a frequency range around 0.8 GHz (symbolized as f_{PRange}), a larger size of hemoperitoneum has a higher phase value compared to the baseline (Figure 4.11b). The highest average increase in phase is with 1000 ml bleeding at around 0.2 rad. For both phase and magnitude, the standard deviation of 500 ml bleeding is relatively large compared to the mean difference between AB500 and baseline, which may make the classification become a challenge.

Besides $f_{MThreshold}$ and f_{PRange}, two new parameters named f_{MRange} and f_{PMax} are introduced. f_{MRange} is the frequency range above $f_{MThreshold}$ where hemoperitoneum at a larger size has a higher magnitude. Meanwhile, f_{PMax} is the frequency where the difference in phase between hemoperitoneum and baseline reach the highest value (Figure 4.12). These frequency parameters vary between pigs and coefficients.

The examination of the above trends for each pig indicates that only S_{77+88} has the consistent trends (both phase and magnitude) for both AB500 and AB1000 (Figure A.8, A.9). The other coefficients do not clearly follow the trend for some pigs at AB500 or AB1000 state. Therefore, to estimate the frequency parameters (i.e. $f_{MThreshold}$, f_{MRange}, f_{PRange} and f_{PMax}), the mean and standard deviation of 100 measurements of S_{77+88} are utilized (Figure 4.11). For AB1000, $f_{MThreshold}$ is 0.66–0.88 GHz while the stop frequency of f_{MRange} is 1–2 GHz. Therefore, $f_{MThreshold}$ can be set at 0.66 GHz and f_{MRange} is 0.88–1 GHz. Regarding the phase for AB1000, the inner boundary of standard deviation area (i.e. the *mean − standard deviation* boundary) can be utilized to calculate f_{PRange}. This value as calculated from Figure 4.11b is 0.6–88 GHz.

Although the trend is clear, the classification between baseline and hemoperitoneum (AB500 and AB1000) classes may be difficult due to a large difference in the baseline between pigs. An example is illustrated in Figure 4.13 and shows that for S_{75+86}, the maximum variation in the coefficient magnitudes of ten pigs is about 12 dB, while the largest difference between baseline and AB1000 is only about 4 dB.

4.2 Data analysis for thorax data

In this section, the microwave thorax data (i.e. pneumothorax, hemothorax ,and poly trauma) characteristics are analyzed. A same smoother as for abdominal data is applied for all data. The variance of repeated measurements are examined and the magnitude characteristics are analyzed. The difference between baseline and each thorax trauma type is explored separately.
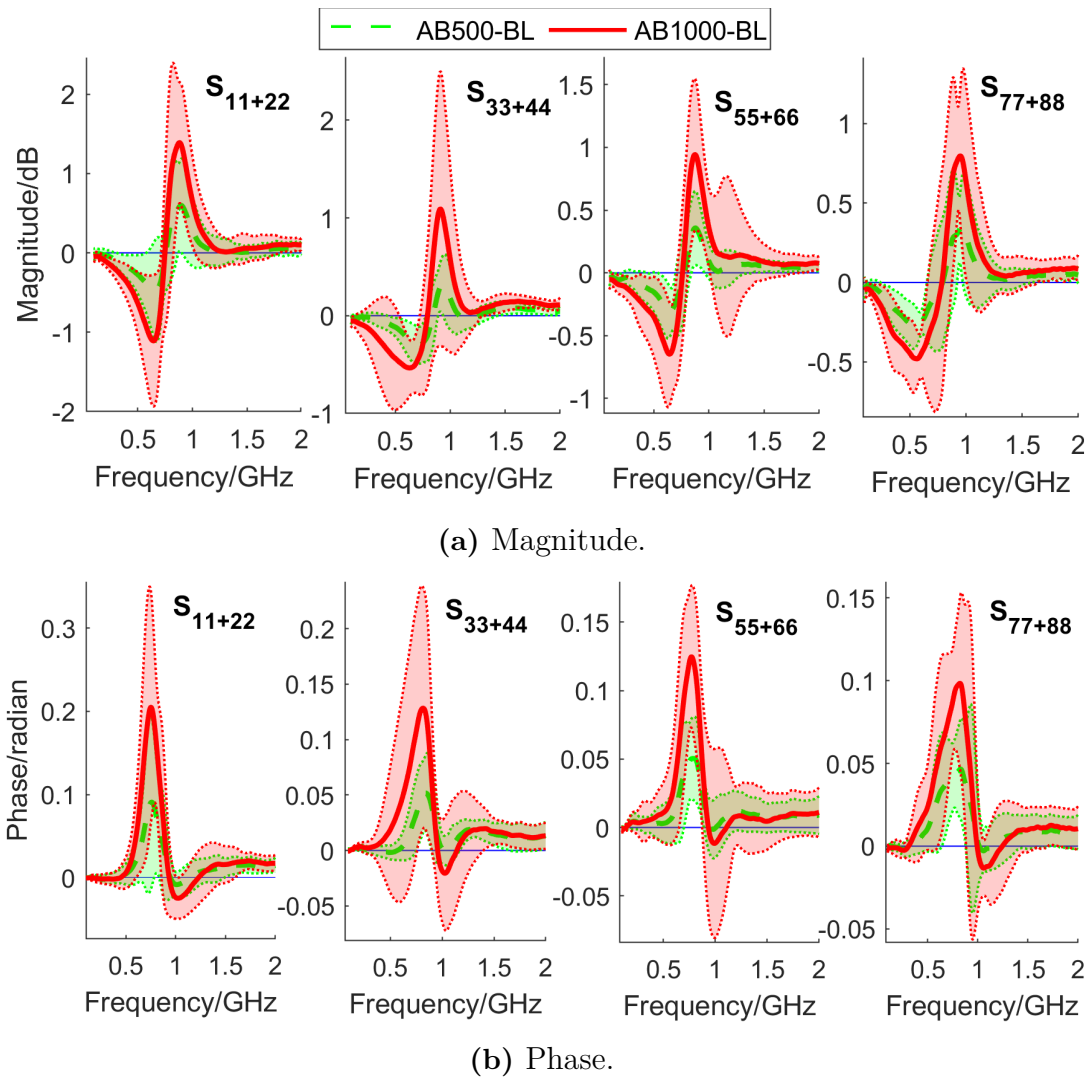
(a) Magnitude.

(b) Phase.

Figure 4.11: The subtraction of baseline from hemoperitoneum states in magnitude (4.11a) and phase (4.11b) for reflection coefficients. The solid lines and shaded areas are respectively the mean and standard deviation among all measurements of ten subjects. Opposite trends for magnitude at below and above $f_{MThreshold}$, and the phase increase can be clearly seen.

4.2.1 The variance of repeated measurements

The high variances between repeated measurements are observed at the lower end of the frequency range, which is similar to the abdominal data (Figure 4.3). Therefore, data at frequencies lower than 100 MHz will be excluded. Unlike abdominal data (Figure 4.4), the thorax data do not have any measurement being significantly different from repeated measurements. Therefore, all measurements are included for analysis. There are cases with the medium-high variance (around 10 %) within repeated measurements (similar as in Figure 4.5), but this phenomenon can be caused by pig's movement or breathing, so these data should be included.
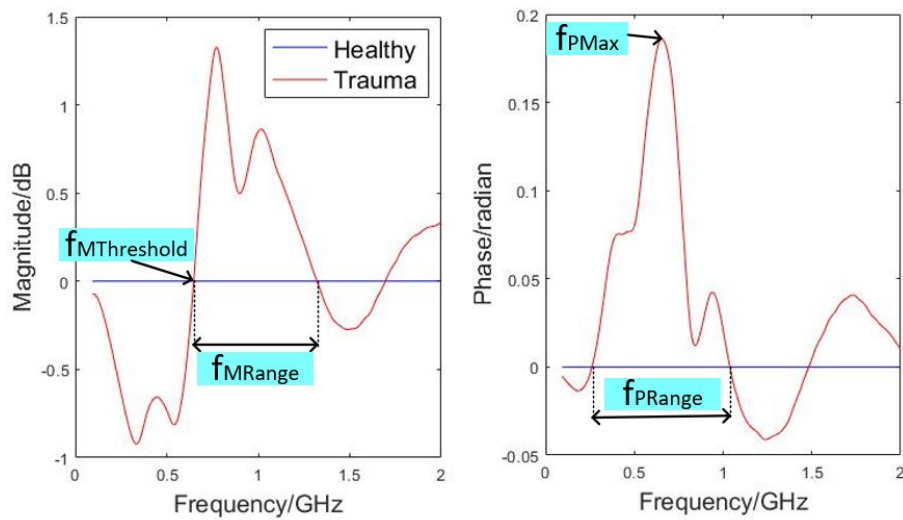
Figure 4.12: $f_{MThreshold}$, f_{MRange}, f_{PRange} and f_{PMax} for the common trends of reflection coefficients. It should be noted that $f_{MThreshold}$ is the start frequency of f_{MRange}.
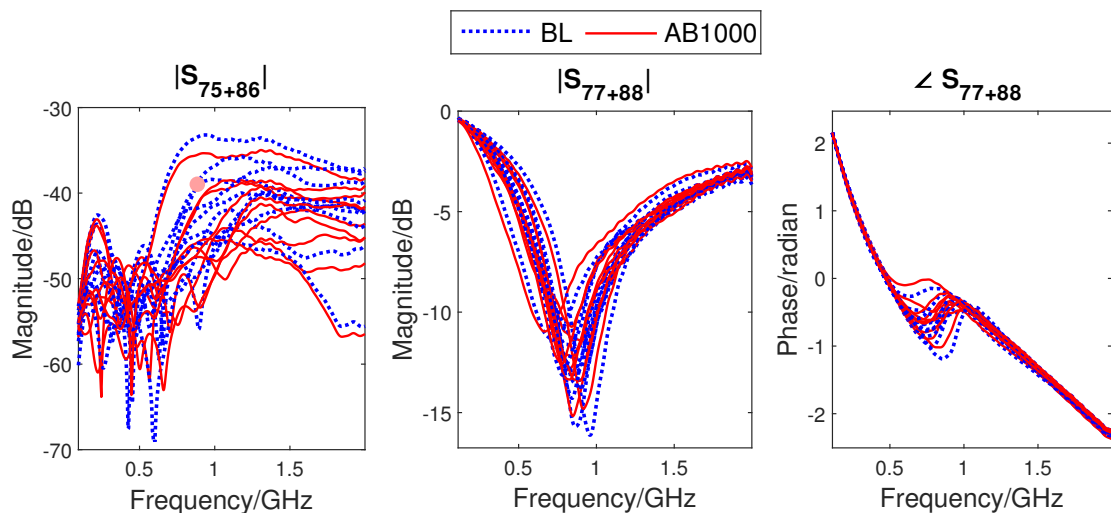
Figure 4.13: The large difference in magnitude and phase among ten pigs at the baseline (blue line) and AB1000 state (red line).

4.2.2 Coefficient magnitude characteristic

The magnitude characteristics are analyzed based on all 100 measurements of ten pigs at T-BL-BS state. Regarding the reflection coefficients, the resonance frequency (where the magnitude is lowest) is at 0.8–1 GHz, and varies among different coefficients or pigs (Figure 4.14a). For the transmission coefficients, data at above 0.8 GHz typically have higher magnitude than at below 0.8 GHz (Figure 4.14b). In addition, coefficients of lower levels (i.e. shorter direct path between transmitting and receiving antennas) has higher magnitude (Figure 4.14b). More examples of other reflection and transmission coefficients can be found in Figure A.10, A.11, A.12, A.13, A.14.

(a) Reflection coefficients. **(b)** Transmission coefficients.
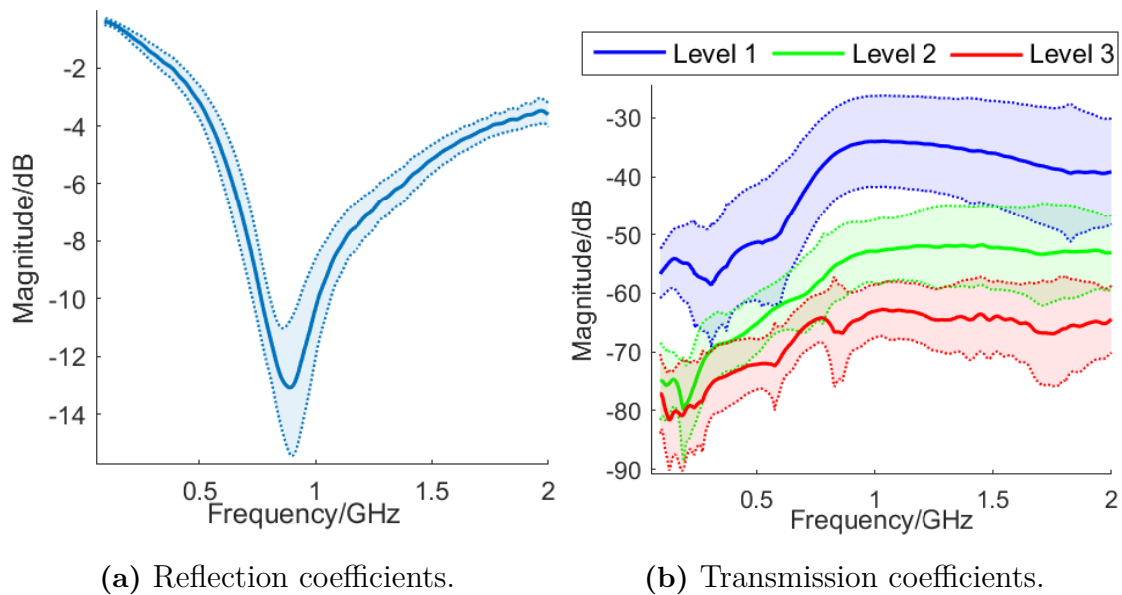
Figure 4.14: The mean (solid line) and standard deviation (shaded area) of all reflection coefficients (4.14a) and transmission coefficients of level 1, 2 and 3 (4.14b). The resonance frequency is at 0.8–1 GHz and lower level coefficients typically have higher magnitude.

4.2.3 The change caused by thorax trauma

In this part, the change in data of pneumothorax, hemothorax and polytrauma compared to the baseline are provided. Transmission and reflection coefficients are analyzed separately in both phase and magnitude.

4.2.3.1 Transmission coefficient

The mean magnitudes of all measurements show a trend in thorax trauma types that above 0.6 GHz, thorax trauma at a larger size has a lower magnitude (Figure 4.15; data for all transmission coefficients are shown in Figure A.15, A.16, A.17 - Appendix). Although in pneumothorax or hemothorax experiments, only one lung was tested with traumatic injuries, both left and right coefficients show this trend. It is noted that the trend is not clear for the level 3 coefficients (i.e. S_{28} and S_{17} - Appendix). In addition, the standard deviation is quite high at some frequencies (e.g. above 1.5 GHz of S_{86} and S_{75}, pneumothorax), indicating that this trend may substantially vary among ten pigs.

The average magnitude over the frequency range 0.6–2 GHz showed a similar trend as mentioned above. For pneumothorax and hemothorax, all examined transmission coefficients have this trend (Figure 4.16a, 4.16b). Meanwhile, for polytrauma, the mean magnitude of L750L500 is lower than L750L1000 at some S-parameters (e.g. S_{57}). The average magnitude drop between 1500 ml pneumothorax (i.e. R1500) and baseline is about 0.25–1.25 dB while this figure between baseline and 750 ml hemothorax (i.e. L750) is 0.25–1.5 dB. The mean magnitude change caused by L750L1500 polytrauma can be up to 5 dB. Regarding the standard deviation, S_{64} and S_{62} show a variation up to 1 dB above the zero line at the largest size of pneumothorax and
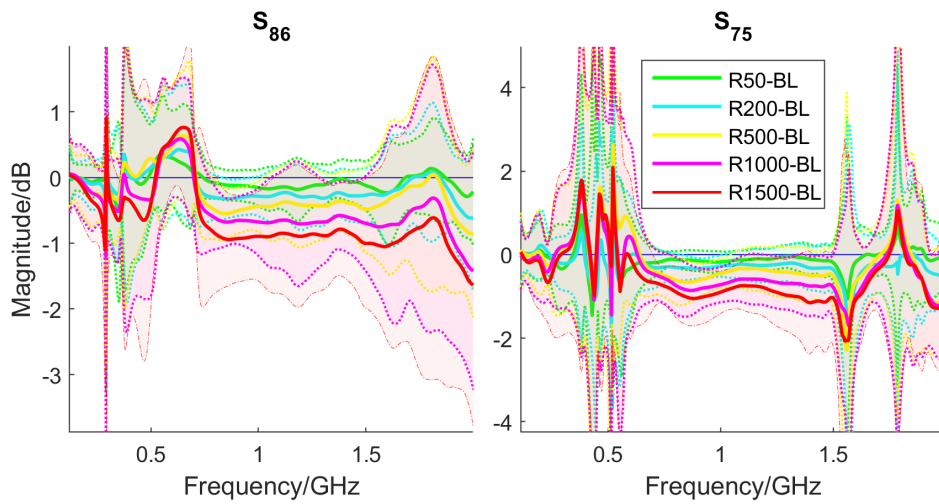
(a) Pneumothorax.
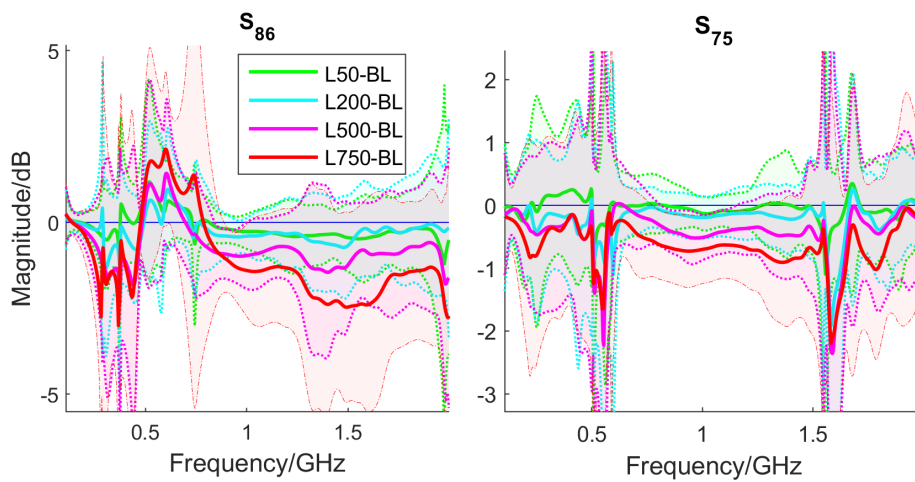
(b) Hemothorax.
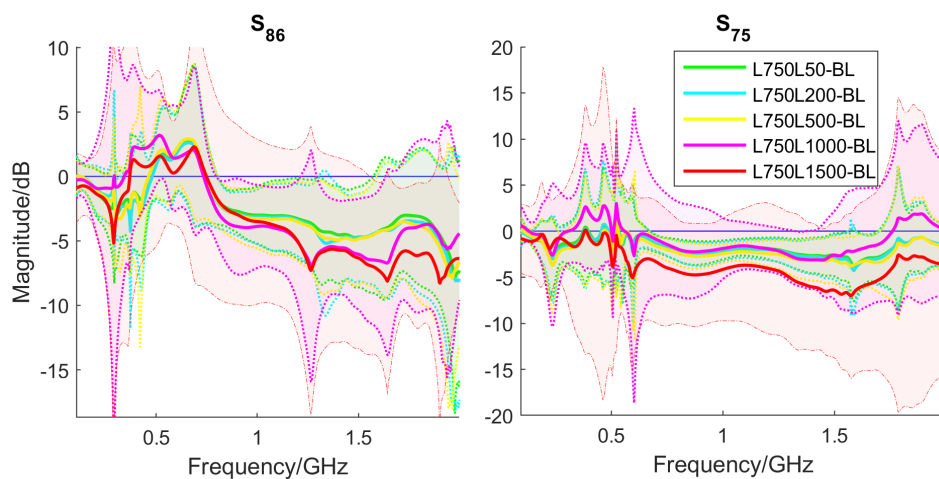
(c) Polytrauma.

Figure 4.15: Some examples of the mean (solid line) and standard deviation (shaded area) of the difference in magnitude between baselines and pneumothorax state (4.15a), hemothorax state (4.15b) and polytrauma state (4.15c). Magnitude drop at trauma states can be seen though the mean values.

hemothorax, meaning that some cases have the magnitude increase in the thorax trauma. Polytrauma shows a high standard deviation up to 4 dB at L750L1000 or 7 dB at L750L1500. The data for each pig and coefficient are shown in Figure A.18, A.19, A.19 - Appendix.

**(a)** Pneumothorax.   **(b)** Hemothorax.   **(c)** Polytrauma.
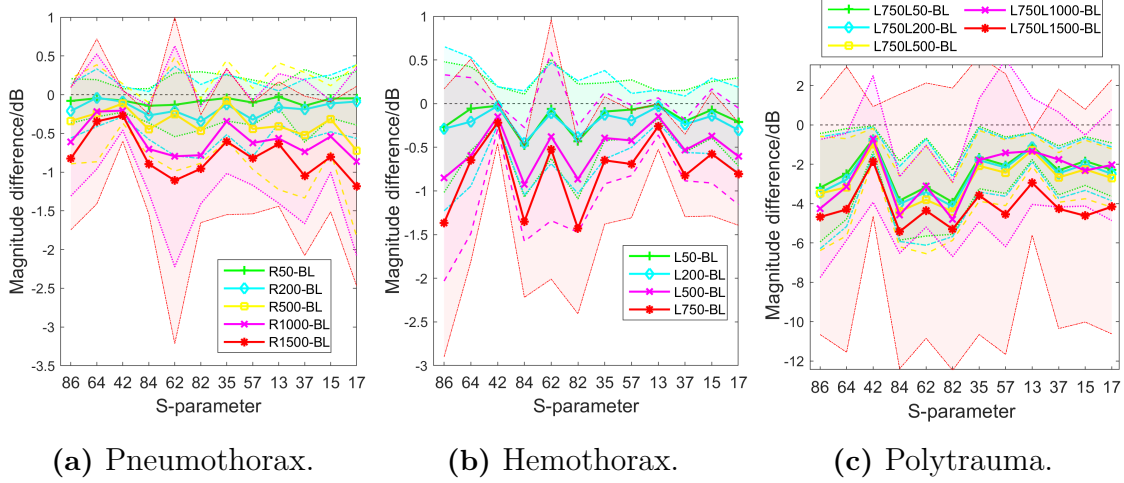
Figure 4.16: The mean (over the frequency range 0.6–2 GHz) magnitude difference between healthy state and thorax trauma types. The solid lines are the average of 100 measurements while shaded areas are standard deviation. Magnitude drop at trauma states and high standard deviation at some coefficients can be observed.

For the transmission coefficient phase, large phase shifts at above 0.6 GHz are observed as similar to abdominal data (Figure 4.10). Therefore, the phase of transmission coefficient is not further analyzed.

4.2.3.2 Reflection coefficient

A similar trend as mentioned in the reflection coefficients of abdominal data is observed in thorax data (Figure 4.17; all data are in Figure A.21, A.22, and A.23 - Appendix). For pneumothorax and hemothorax, the standard deviation indicates that only S_{77} and S_{88} have consistent frequency parameters (i.e. $f_{MThreshold}$, f_{MRange}, and f_{PRange}) among all measurements. The largest change between 1500 ml pneumothorax and baseline is quite similar between S_{77} and S_{88} at about 0.4 dB in magnitude and 0.06 rad in phase. Meanwhile, for hemothorax, the difference between 750 ml hemothorax and baseline is higher for the left side (where hemothorax happens) than the right side. For example, the highest mean differences for S_{88} (left side) are 0.5 dB in magnitude and 0.08 rad in phase while these figures for S_{77} (right side) are 0.25 dB and 0.04 rad. Regarding polytrauma, although the mean difference between L750L1500 and baseline is high, its deviation is also too large that there is not a consistent frequency range for the trend.

Frequency parameters for the trend of S_{77} and S_{88} are estimated based on the standard deviation range of the subtraction between baseline and the highest level of pneumothorax/hemothorax (i.e. R1500-BL or L750-BL). The estimation method is similar to that applied for abdominal data (section 4.1.4.2). For polytrauma, due
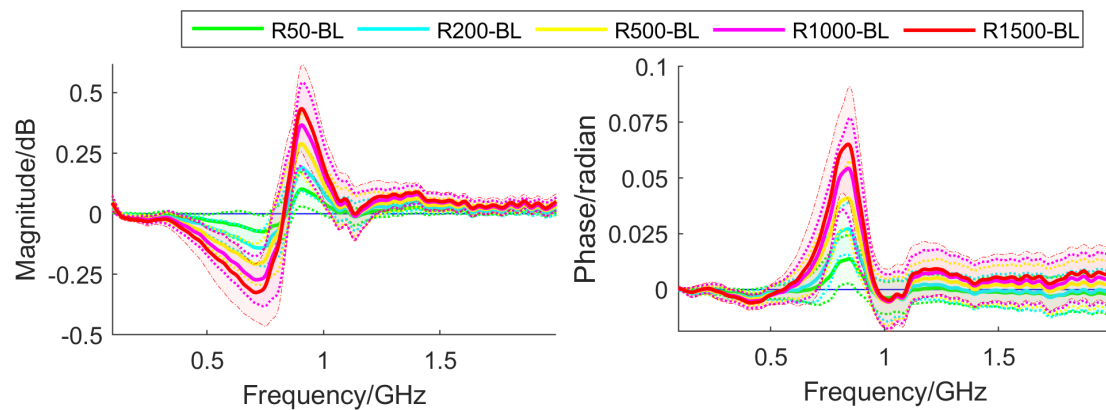
Figure 4.17: An example of the common trend in both magnitude and phase among ten subjects for S_{77} and pneumothorax state. The solid lines are the average values across ten subjects while the shaded areas are the standard deviation.

to the instability of L750L1500 state, these frequency values are derived from the difference between L750L1000 and baseline. The result indicates that the frequency parameters are relatively similar between S_{77} and S_{88} and there is not much difference between three thoracic trauma types (Table 4.3). From this table, $f_{MThreshold}$ can be set to 0.77 GHz; f_{MRange} is 0.88–1 GHz, and f_{PRange} is 0.7–0.95 GHz.

Table 4.3: Frequency parameters (GHz) for three types of thorax trauma.

Trauma	$f_{MThreshold}$		f_{MRange}		f_{PRange}	
	S_{88}	S_{77}	S_{88}	S_{77}	S_{88}	S_{77}
Pneumothorax	0.81	0.77	0.87–1	0.86–1	0.72–0.93	0.72–0.93
Hemothorax	0.77	0.77	0.88–1	0.85–1.3	0.7–0.97	0.7–0.95
Combination	0.8	0.77	0.87–1.1	0.85–1.1	0.7–0.96	0.7–0.94

Although some consistent trends are clearly seen in thorax trauma, there is still the same classification challenge caused by the large baseline variation between pigs as mentioned in abdominal data. The challenge for thorax data may be even more difficult than for abdominal data because compared to the baseline, the magnitude/phase difference is smaller for thorax trauma than for hemoperitoneum. In addition, for thorax trauma, some pigs do not follow the trend of transmission coefficients or reflection coefficients at L750L1500 states.

4.3 Statistic examination

In this section, the results of three statistic tests are provided. The first test is to examine the normality of collected data for each coefficient at one state. The second examination tests the significant change in magnitude or phase between trauma states and baseline. The final examination tests whether it is still distinguishable between baseline and torso trauma when the differences in baseline between subjects are considered. The input data points are the mean magnitudes/phases over the

whole examined frequency range (i.e. 0.1–2 GHz). It should be noted that since transmission coefficient phases do not show any consistent trend as indicated in the data analysis result section, these data are not analyzed with statistical tests.

4.3.1 Normal distribution test

The Anderson-Darling Test for normality is provided by MATLAB as the function *adtest*. This test is applied for the data set of each class (i.e. each state) and each coefficient separately. The input data size for each test is 100 (corresponding to 100 measurements).

All the test results are statistically significant (i.e. p-value < 0.05), meaning that the input data do not come from a normal distribution. For this reason, all statistic tests which require data samples coming from a normal distribution cannot be applied. One example for Q-Q plot of a data set of S_{73+84} at AB-BL-AS state is provided in Figure 4.18, which shows that the data points are not linear and do not approximate the theoretical red line.
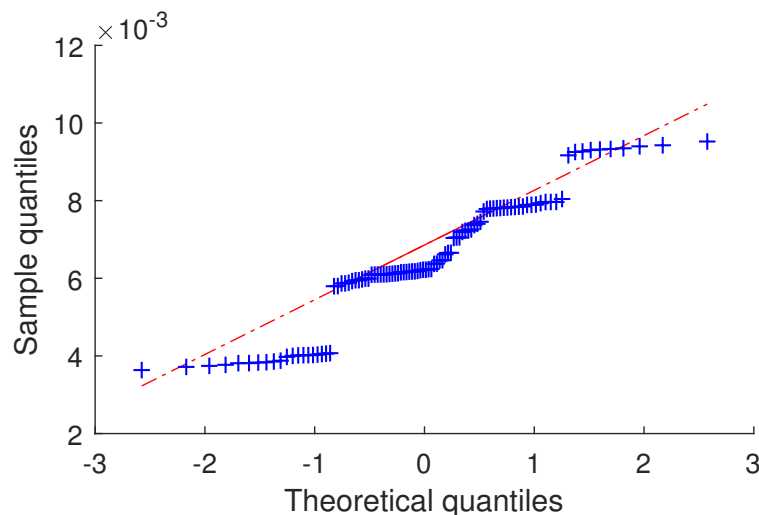
Figure 4.18: Q-Q plot of data set at AB-BL-AS state of S_{73+84}.

### 4.3.2 Examination on the subtraction of baseline

In this section, the Kruskal–Wallis Test is utilized to test if the consistent changes found in the previous section between torso trauma states and baselines are significant. Hemoperitoneum, pneumothorax, hemothorax and polytrauma are tested separately and the subtraction of baseline data is utilized in this test.

#### 4.3.2.1 Coefficient magnitude

For the hemoperitoneum cases, the obtained p-values are almost zero for all coefficients (Figure 4.19a), while for thorax trauma, only S_{66} of polytrauma does not have statistically significant result (Figure 4.19b). Therefore, for almost all coefficients, the null hypothesis is rejected and the alternative hypothesis is true. In other words,

there are significant changes in the obtained signal of torso trauma compared to the normal state.
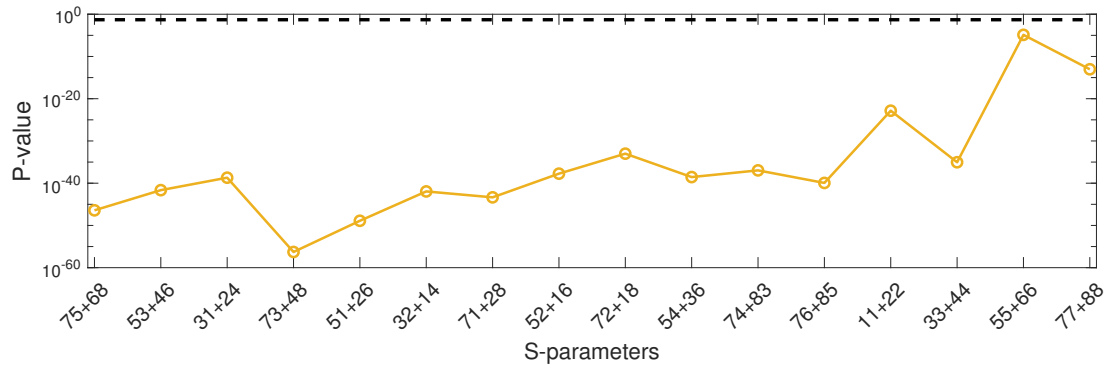

(a) Hemoperitoneum.
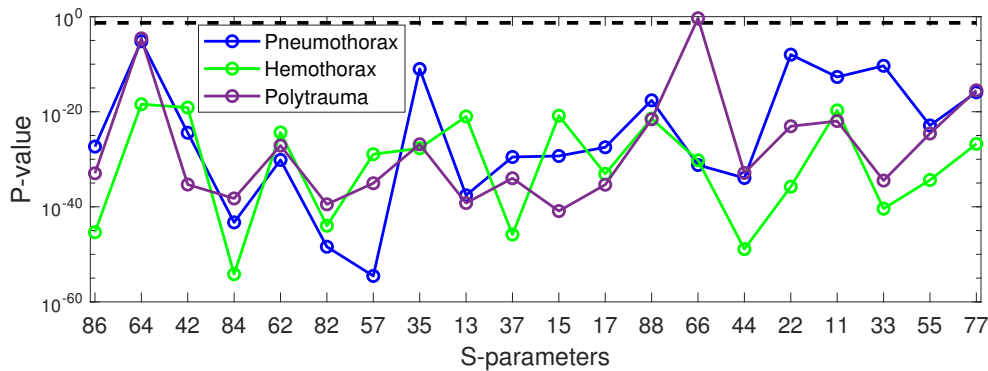
(b) Thorax trauma.

Figure 4.19: The p-value of Kruskal–Wallis Test for different types of trauma using coefficient magnitude. The black dashed line is the statistically significant level at 0.05. Almost all coefficients show statistically significant results.

The coefficient having smallest p-value for hemoperitoneum, pneumothorax, hemothorax and polytrauma are S_{73+84}, S_{75}, S_{84} and S_{15} respectively. Figure 4.20 shows the mean and range of data from examined classes for these four coefficients. For hemoperitoneum, pneumothorax and hemothorax, when the trauma size increases, magnitude drop can be clearly observed. Meanwhile, for polytrauma, the median magnitude drop of L50-, L200-, L500- and L1000- is significantly lower than L1500-. In addition, for L750L1500, the variation of magnitude decrease is also much higher than the other trauma sizes.

4.3.2.2 Coefficient phase

In this part, only reflection coefficients are examined. The results show that all tests are statistically significant (Figure 4.21). S_{11+22} have the smallest p-value for hemoperitoneum while for thorax trauma, the smallest p-value of each trauma type is with S_{11}. Some examples of the mean and range of the difference in phase between baseline and trauma types are shown in Figure B.1.

(a) Hemoperitoneum.

(b) Pneumothorax.

(c) Hemothorax.
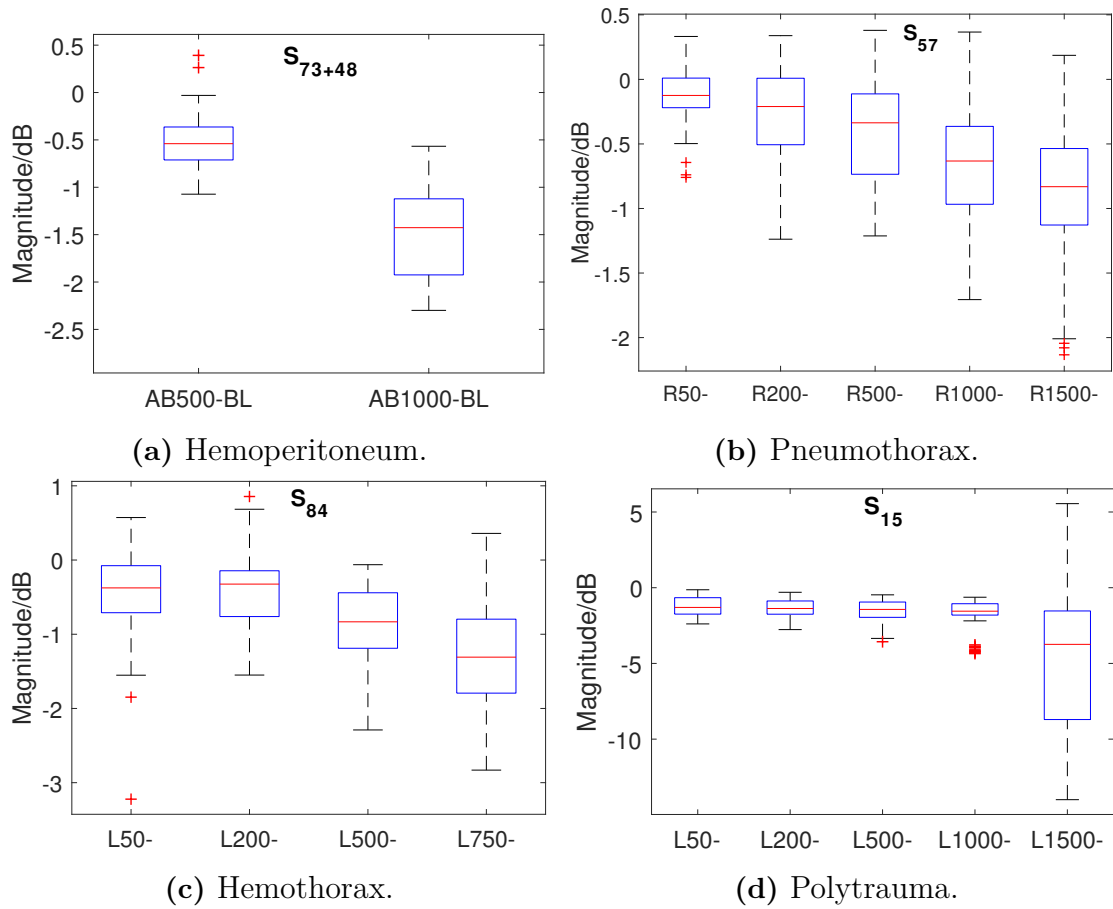
(d) Polytrauma.

Figure 4.20: The magnitude mean (the red line) and range of the difference between the baselines and four types of trauma. The "-" symbol at the end of some x-axis labels indicates the subtraction of baseline. It is noted that for the x-axis of polytrauma, the symbol L750 (represents hemothorax) is skipped for clarity.


(a) Hemoperitoneum.

(b) Thorax trauma.
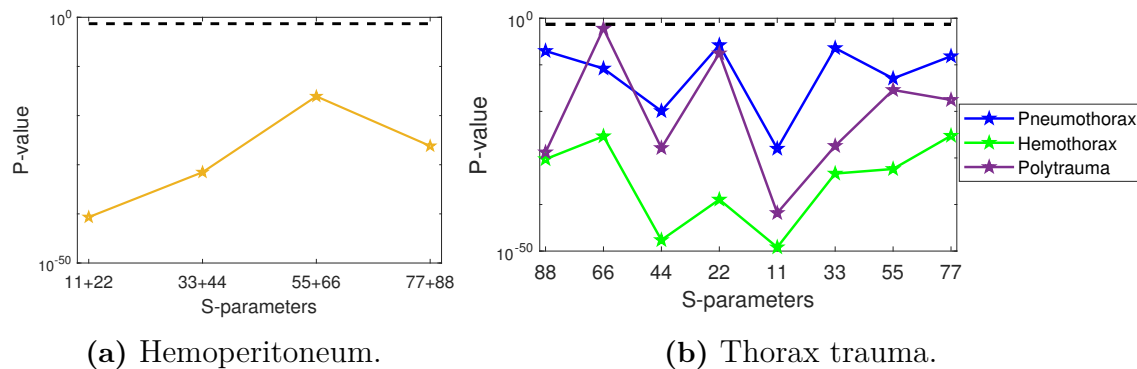
Figure 4.21: The p-value of Kruskal–Wallis Test for different types of trauma using coefficient phase. The black dashed line is the statistically significant level at 0.05. All tests are statistically significant.

### 4.3.3 Examination on the difference between healthy and trauma classes

The third statistic test utilizes the Kruskal–Wallis Test and the Wilcoxon rank-sum Test to examine the difference between healthy and trauma classes without baseline subtraction.

#### 4.3.3.1 Coefficient magnitude

For hemoperitoneum, the results are statistically significant (i.e. p-value <0.05) for all coefficients (Figure 4.22a). Therefore, the null hypothesis is rejected or in other words, there is a significant difference between baseline and hemoperitoneum classes. For pneumothorax and hemothorax, most of the transmission coefficients have p-value above 0.05 while many reflection coefficients (e.g. S_{55}) have statistically significant results (Figure 4.22b). About polytrauma, only S_{66} has p-value higher than the significant level. The difference in data mean and range between healthy and trauma classes from the coefficients generating the smallest p-values can be observed from Figure B.2.

**(a)** Hemoperitoneum.
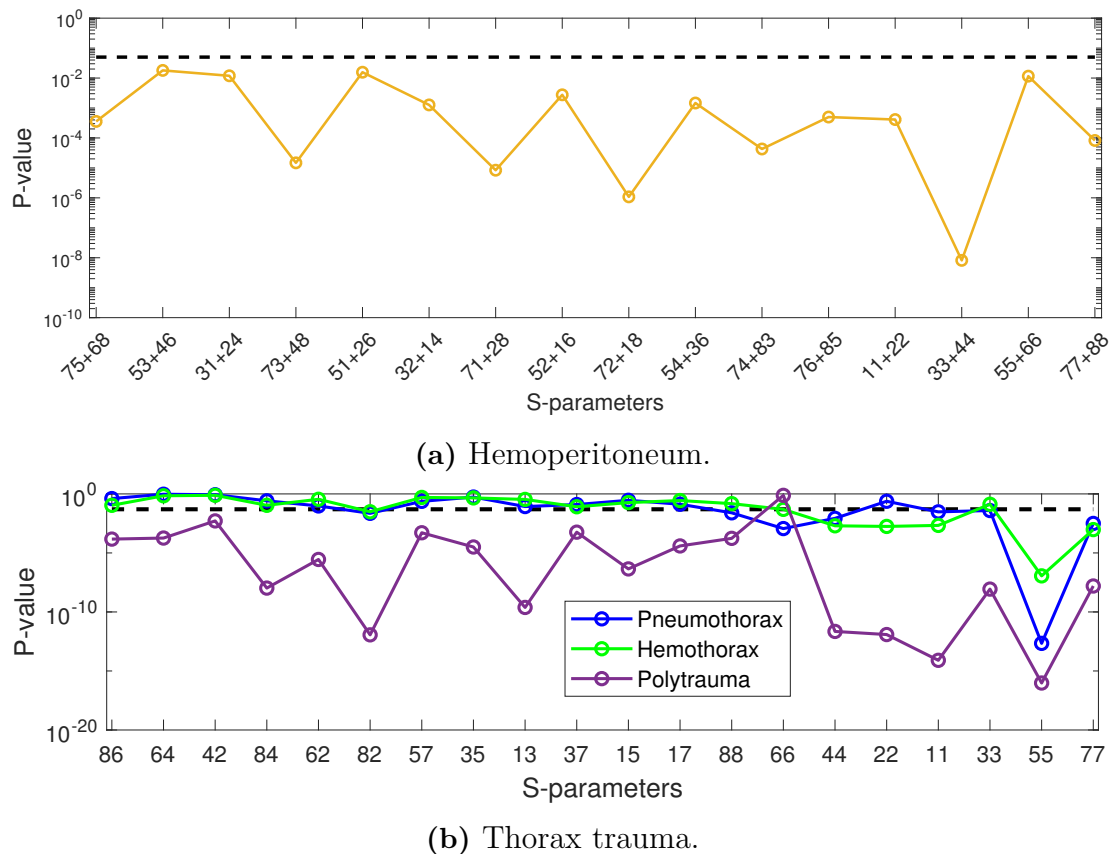
(b) Thorax trauma.

Figure 4.22: The p-value of Kruskal–Wallis Test for different types of trauma using the magnitude of transmission coefficients. The black dashed line is the statistically significant level at 0.05.
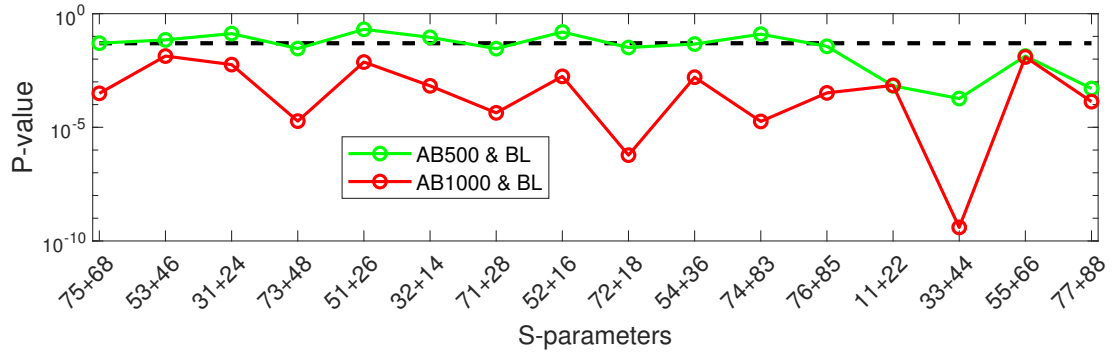
(a) Hemoperitoneum.
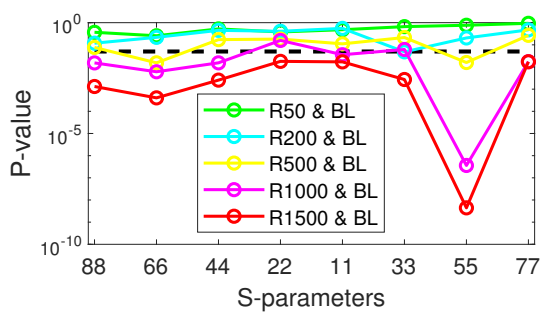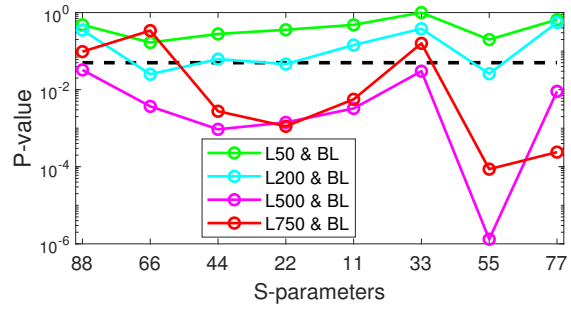
(b) Pneumothorax.
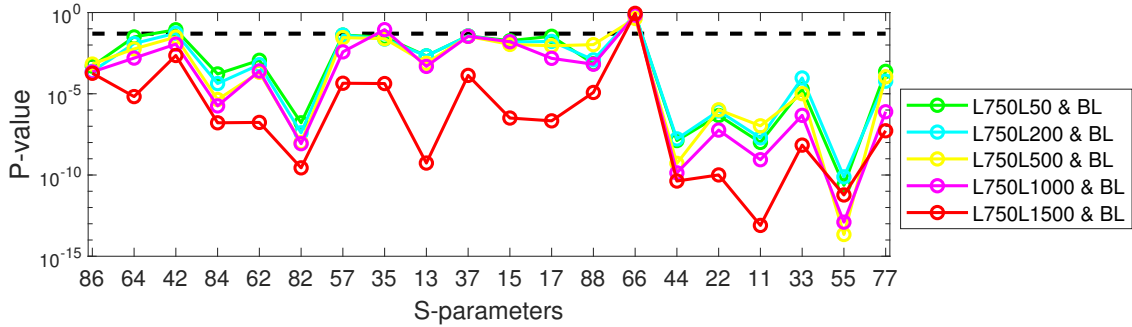

(c) Hemothorax.

(d) Polytrauma.

Figure 4.23: The p-value of Wilcoxon rank-sum Test between baseline and different trauma sizes. The black dashed line is the statistically significant level at 0.05. For pneumothorax and hemothorax, p-values of transmission coefficients are not shown due to their high values as indicated in the Kruskal–Wallis Test.

All trauma types are further analyzed with the Wilcoxon rank-sum Test to examine the relationship between baseline and different trauma sizes. For hemoperitoneum, between AB500 and BL, only few transmission coefficients (e.g. S_{73+48}) have statistically significant results while all p-values of reflection coefficients are below the significant level (Figure 4.23a). All coefficients have significant results for the test between AB1000 and BL.

For the thorax trauma, the general trend is that larger trauma size has lower p-values (Figure 4.23b, 4.23c, 4.23d). For pneumothorax, none of S-parameters has statistically significant result for R50 and R200 level while for R1500, all reflection coefficients have p-value below the significant level. Regarding hemothorax, the result for L50 is not statistically significant while only one S-parameter has p-value slightly smaller than 0.05 for L200. Poly trauma has many coefficients showing p-value below the significant level even for the lowest trauma level (i.e. L750L50).

4.3.3.2 Coefficient phase

All reflection coefficients have statistically significant results for the Kruskal–Wallis Test of hemoperitoneum classes (Figure 4.24a). Regarding thorax trauma, many S-parameters have p-value below the significant level for hemothorax and polytrauma (Figure 4.24b). Meanwhile, for pneumothorax, only a few coefficients have statistically significant results. Some examples of the mean and range of the difference in phase between healthy and trauma types are shown in Figure B.3.

**(a)** Hemoperitoneum. **(b)** Thorax trauma.
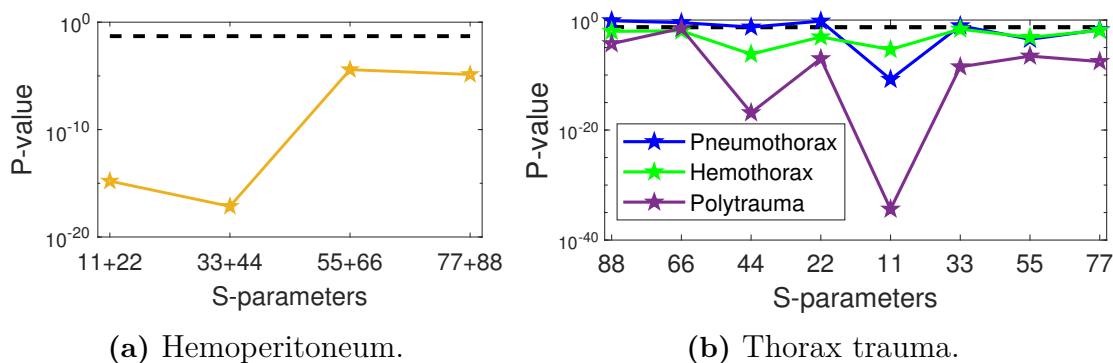
Figure 4.24: The p-value of the Kruskal–Wallis Test with coefficient phase for different types of trauma. The black dashed line is the statistically significant level at 0.05.

The Wilcoxon rank-sum Test is applied to examine the significant difference between baseline and each trauma size. For hemoperitoneum, all tests have statistically significant results while only S_{11} has significant results for all trauma sizes of pneumothorax (Figure 4.25a, 4.25b). Regarding hemothorax, while all tests for the largest trauma size (i.e. L750) are statistically significant, none of the S-parameters has p-value smaller than the significant level for L50 (Figure 4.25c). In contrast, except S_{66}, all other coefficients have statistically significant results for all trauma sizes of polytrauma (Figure 4.25d).

(a) Hemoperitoneum.

(b) Pneumothorax.

(c) Hemothorax.

(d) Polytrauma.
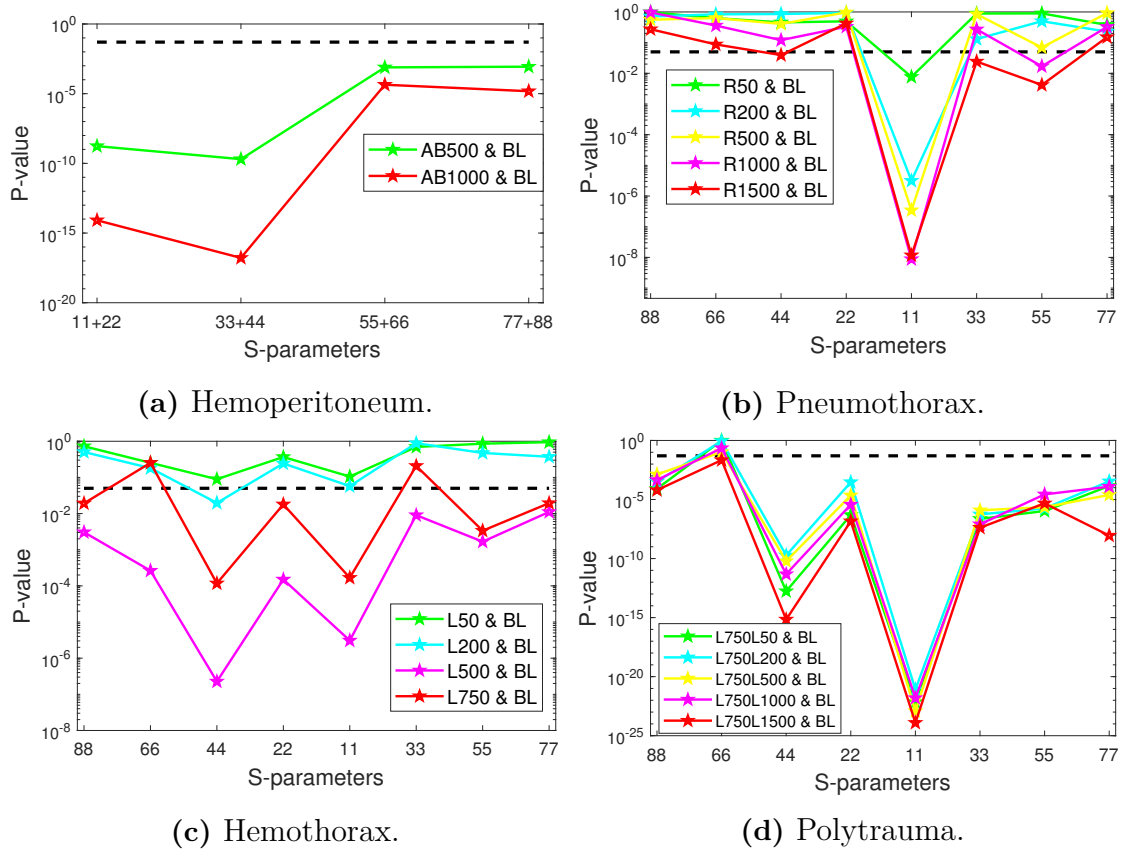
Figure 4.25: The p-value of the Wilcoxon rank-sum Test between healthy state and different trauma sizes. The black dashed line is 0.05 statistically significant level.

4.4 Classification with support vector machine

	Hemoperitoneum
S_{57+86}	52
S_{35+64}	55
S_{13+42}	58
S_{37+84}	70
S_{15+62}	46.5
S_{23+41}	48.5
S_{17+82}	49
S_{25+61}	54
S_{27+81}	54.5
S_{45+63}	54
S_{47+83}	55.5
S_{67+85}	57.5
S_{11+22}	52
S_{33+44}	69
S_{55+66}	60.5
S_{77+88}	71

	Pneumothorax	Hemothorax	Polytrauma
S_{86}	50	48	51.5
S_{64}	53.5	47	71.5
S_{42}	59.5	45	63.5
S_{84}	49.5	65	60.5
S_{62}	54.5	48.5	65
S_{82}	52	65	66
S_{57}	50	50	48.5
S_{35}	50.5	54.5	53
S_{13}	50	51.5	39
S_{37}	59	51.5	34
S_{15}	57	49.5	51
S_{17}	41.5	53	62.5
S_{88}	55	55	60
S_{66}	57	58	70
S_{44}	56.5	51	55
S_{22}	58.5	55.5	66
S_{11}	60.5	61	88
S_{33}	45	50	54.5
S_{55}	55	54.5	62.5
S_{77}	55	49.5	55

(a) Each coefficient.

	Hemoperitoneum	Pneumothorax	Hemothorax	Polytrauma
All coefficients	70	53	70	90
All transmission	62.5	50	57	65
All reflection	72	56	60	85
Sum coefficient	85	50	50.5	70
Sum transmission	55	55	50.5	61
Sum reflection	95	55	55	60

(b) Other combinations.

Figure 4.26: The SVM classification accuracy (in %) between baselines and the largest trauma sizes of four trauma types. Figure 4.26a is the result for each coefficient, while 4.26b is for different combinations of all transmission and/or reflection coefficients.

The *fitcsvm* function from MATLAB is used for testing support vector machine (SVM). Regarding the analysis of each coefficient separately, the highest accuracy is with S_{77+88} for abdominal bleeding, S_{11} for pneumothorax and polytrauma, and S_{84}/S_{82} for hemothorax (Figure 4.26a). For the other combination tests (Figure 4.26b), the use of only transmission coefficients (i.e. "all transmission or "sum transmission") typically does not generate as high accuracy as reflection coefficients (i.e. "all reflection" or "sum reflection"). The highest accuracy for hemoperitoneum is at 95 % for the sum of all reflection combinations. For thorax trauma, the accuracy

of pneumothorax and hemothorax are quite low at equal or below 70 % while for polytrauma, the use of all coefficients generates the highest accuracy at 90 %.

The scatter plot of all measurements and the receiver operating characteristic curve (ROC) of the best SVM model for hemoperitoneum and polytrauma is shown in Figure 4.27 and 4.28. From Figure 4.27b, the classifier between AB1000 and BL-AS can achieve 90 % specificity when the sensitivity is kept 100 %, but to get 100 % specificity, sensitivity is only 30 %. About polytrauma (Figure 4.28), to detect all L750L1500 subjects (i.e. sensitivity = 100 %), none of normal subjects is detected (i.e. specificity = 0 %). If specificity is kept 100 %, the sensitivity can be 50 %.

From these scatter plots, data of pig 3 at abdominal BL-AS or L750L1500 state are misclassified and have quite a far distance to the other measurements on the same class. Another misclassification for polytrauma is with pig 7 at BL-AS state.
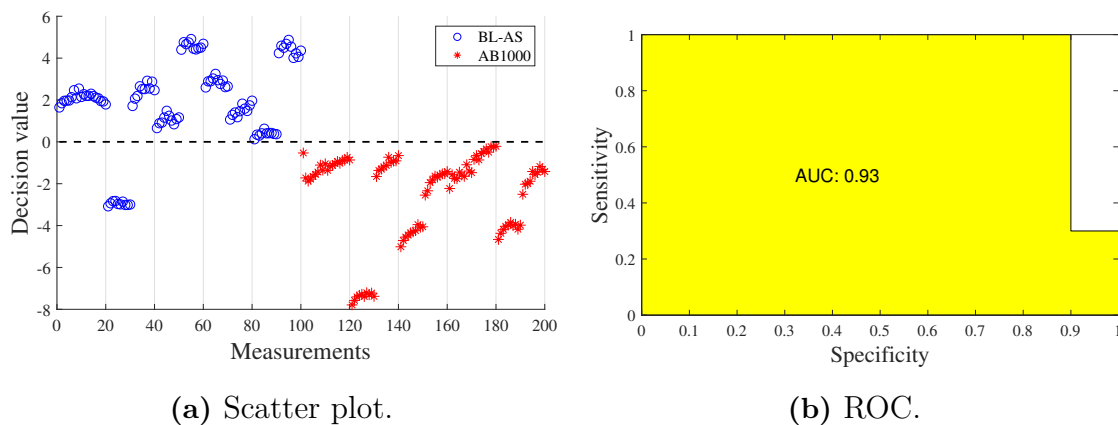
(a) Scatter plot.   **(b)** ROC.

Figure 4.27: Scatter plot (4.27a) and receiver operating characteristic curve (ROC) (4.27b) of the best SVM classifier between AB1000 and BL-AS.
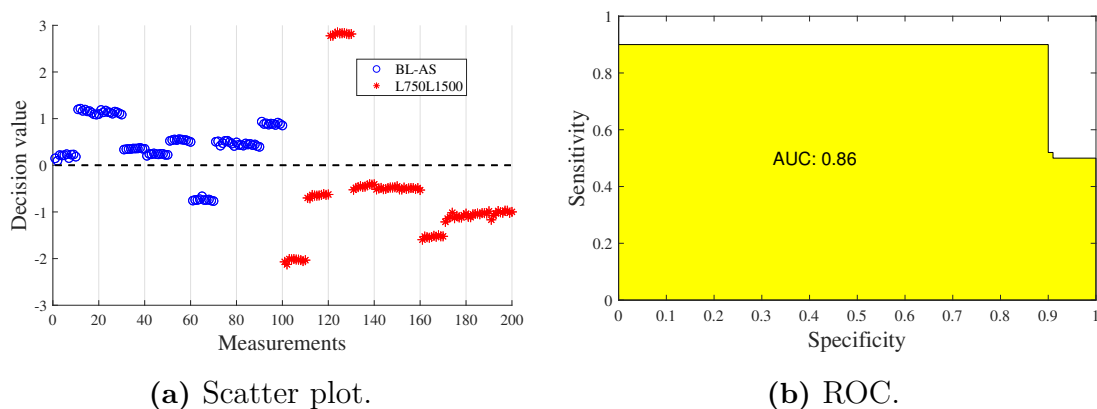
(a) Scatter plot.   **(b)** ROC.

Figure 4.28: Scatter plot (4.28a) and receiver operating characteristic curve (ROC) (4.28b) of the best SVM classifier between L750L1500 and BL-AS.

5

Discussion

The main results of the master's thesis (chapter 4) can be divided into three parts including the signal change caused by traumatic torso injury, statistic tests for the difference between baseline and trauma states, and the classification of baselines and the largest size of each trauma type. Four examined trauma types are hemoperitoneum, pneumothorax, hemothorax and polytrauma. Similar signal changes from baseline are observed among all trauma types, but the trends are different between the magnitude and phase of reflection and transmission coefficients (see Figure 4.8, 4.11 for hemoperitoneum and Figure 4.15, 4.17 for thorax trauma). For statistic tests, in general, almost all coefficient magnitude/phase have statistically significant results for hemoperitoneum and polytrauma while for pneumothorax and hemothorax, the statistically significant results are most common for reflection coefficients (see Figure 4.22, 4.24). Regarding the classification with SVM, the largest size of hemoperitoneum and polytrauma can be detected with 95% and 90% accuracy respectively, but the accuracy for detecting hemothorax and pneumothorax is quite low (see Figure 4.26).

5.1 Data analysis

5.1.1 The variance of repeated measurements

In general, the variation between ten repeated measurements is small when the signal magnitude is above the noise level (approximately $-70\,\mathrm{dB}$), meaning that the measurement system is generally stable. However, there are still several cases with medium-high variance (see Figure 4.5). The reason for this could be related to the measurement object, e.g. the pig's movement, breathing or blood circulation. It could also be related to the measurement system, e.g. antenna-skin contact can vary due to the use of antennas not custom designed for torso measurements. The current device is an experimental prototype, so further developments of the hardware may make the measurement more precise and stable. High variance is also found at frequencies below about $0.1\,\mathrm{GHz}$ (see Figure 4.3). This problem can be explained to be due to the capacity coupling between the cables, antennas, and surroundings. For this reason, the data of frequencies lower than $0.1\,\mathrm{GHz}$ are excluded from the analysis. Only two measurements of two coefficient are removed from the analysis due to high variations compared to other repeated measurements (see Figure 4.4).

5.1.2 Signal characteristic and the change caused by trauma

For transmission coefficients, higher level coefficients generally have a lower magnitude and larger variation between subjects (see Figure 4.14). The reason can be that a longer distance between transmitting and receiving antennas causes more signal loss, noise interference, and complex scattering pattern. When comparing baseline and trauma states, the average data of all measurements show a similar trend among all coefficients that at above around $0.6\,\mathrm{GHz}$, signal magnitude drops in cases that involve trauma (see Figure 4.8, 4.15). This trend is more obvious at lower level coefficients, which may be due to their high signal to noise ratio. The trend for hemoperitoneum seems more consistent along the frequency than for thorax trauma. The explanation for this can be that in the thorax region, the variation on the collected data caused by blood circulation as well as breathing may be more prominent than in the abdomen region. Another noticeable thing is that although traumatic injury is tested in either left or right lung for pneumothorax and hemothorax, antennas on both left and right sides show magnitude drop (see Figure 4.15). Therefore, we can conclude that air/blood accumulation can be detected by antennas that are not right on the injury positions.

Regarding reflection coefficients, all coefficients show the resonance frequency at 0.75–$1\,\mathrm{GHz}$ (see Figure 4.14a). Although the trends caused by trauma are similar among reflection coefficients, the standard deviation is different (see Figure 4.11). The coefficients with the most consistent trend are S_{77} and S_{88}. This result is consistent with the ultrasound examination that blood accumulates mostly around the left or right midaxillary line. The trend in reflection coefficients happens at a specific frequency range (e.g. f_{PRange}, f_{MRange}) which varies between subjects. For f_{PRange}, its consistent range (calculated from ten pigs) is around the resonance frequency while $f_{MThreshold}$ is approximately the resonance frequency (see Table 4.3). The resonance frequency can be easily calculated as the smallest values of reflection coefficients, so the relationship between the resonance frequency and the estimated f_{PRange}, f_{MRange} and $f_{MThreshold}$ may be further analyzed to have a better estimation.

Although the trend is clear, in this master's thesis work, we are unable to identify any method to remove or diminish the large baseline difference between pigs (e.g. Figure 4.13). The subtraction of symmetric coefficients (e.g. S_{75} - S_{86}) is tried to remove the baseline with a prediction that the baseline between left and right symmetric antenna pairs can be similar. However, the results show that the baseline difference between symmetric coefficients is still larger than the magnitude change caused by trauma.

5.2 Statistic tests

5.2.1 Kruskal–Wallis Test

For baseline subtraction data, t he Kruskal–Wallis Test has statistically significant results for almost all coefficients (see Figure 4.19). Without baseline subtraction, some coefficients do not have statistically significant results (see Figure 4.22). This is an indication of challenges caused by the baseline difference between pigs.

For hemothorax and pneumothorax, there are not statistically significant results for transmission coefficients. This is in agreement with the large standard deviation among 10 pigs as indicated in the data analysis section (Figure 4.15). Meanwhile, some reflection coefficients have p-values below 0.05, showing that reflection coefficients may have more potential for detecting hemothorax and pneumothorax than transmission coefficients.

5.2.2 Wilcoxon rank-sum Test

Further tests between baseline and each size of trauma indicate that when more blood/air is injected, the p-values are typically smaller (see Figure 4.23). This result is quite consistent with the trends in "Data analysis" that the deviation from the baseline is larger for a larger trauma size.

The test between BL and AB500 only has significant results with reflection coefficients and two transmission coefficients, meaning that even with 500 mL blood injected, the change from the baseline is not substantial (see Figure 4.23a). This can be explained by the fact that the abdominal cavity is capable of holding a large amount of blood (e.g. five liters), making the appearance of 0.5 L blood difficult to detect. 50–200 mL pneumothorax and hemothorax also have none or only a few coefficients having statistically significant results. However, the statistic tests utilize only the average magnitude/phase across the whole frequency range, so these trauma sizes may still be detected with the use of magnitude/phase at all frequency steps as indicated in the classification section.

5.3 Classification with support vector machine

5.3.1 SVM with each coefficient combination

In general, the use of each coefficient separately can not generate as high accuracy as coefficient combinations of all transmission and/or reflection coefficients (Figure 4.26a). However, the test for each coefficient may carry information about the location of traumatic injuries. For hemoperitoneum, S_{73+84} and S_{77+88} have the highest accuracy among coefficients, which is consistent with the ultrasound examination about the location of blood accumulation. For pneumothorax, although the accuracy is relatively low overall, the highest accuracy is for S_{11}, which is placed on the traumatic lung. Meanwhile, the highest accuracy for hemothorax is with S_{84} and S_{82}, which are placed close to the midaxillary line of the tested lung. Regarding polytrauma, both left and right antennas can achieve above 70 % accuracy.

5.3.2 SVM with all transmission and/or reflection coefficients

For six tested coefficient combinations, the use of all/summation of transmission coefficients typically has lower accuracy than all/summation of reflection coefficients (see Figure 4.26b). This result is in agreement with the statistic tests where the reflection coefficients show more statistically significant results compared to the

transmission coefficients. Another reason for the low accuracy of transmission coefficient combinations may be due to the difference in the magnitude range between coefficient levels (see Figure 4.14b). When taking the summation of all transmission coefficients, the magnitude of level 1 coefficients can dominate other levels, making their contribution to the summation minimal. Normalization method, which equalizes the power (i.e. the magnitude) between coefficients [34], is tested, but it is not successful. The reason could be due to that the normalization transforms both baseline and trauma signal to a same magnitude range, reducing the change caused by trauma.

The highest accuracy for hemoperitoneum is 95 % with the summation of all reflection coefficients, while for polytrauma, the use of all coefficients has the best result with 90 % accuracy (see Figure 4.26b). The incorrect classification includes all measurements of pig 3 at the normal and L750L1500 state, and pig 7 at the normal state (see Figure 4.27, 4.28). The distance of misclassified measurements to other measurements of the same class is quite far, which reduced the AUC value. The data of incorrectly classified subject are investigated, but we have not found any abnormality on the data.

These promising results indicate the potential of microwave technology for detecting traumatic injuries. However, for the classification results, the high accuracy is merely for serious trauma sizes. Therefore, more research is required to further develop this technology. Further developments of the hardware would likely allow us to make more sensitive measurements, and could then probably detect smaller trauma sizes.

5.4 Limitation

Although consistent trends are found and the classification results are promising, there are some limitations that need to be considered. Firstly, the total number of training and testing subjects is small for a machine learning algorithm. This may be one of the reasons for not having high classification accuracy at 1500 ml pneumothorax and 750 ml hemothorax. To achieve a better detection result with a small number of training subjects, further investigation on data pre-processing or feature extraction is needed. Secondly, some repeated measurements show significant variance as compared to the change caused by trauma. This might be due to the subject's movement itself or the variable antenna-skin contact of the prototype instrument. In addition, in this thesis, the variance and signal characteristics in phase are not analyzed even though the statistic tests show the potential of the phase with significant results. Thirdly, the relationship between statistical tests and classification results seems not being sufficiently explored. Further study about the connection between p-value and classification results may be helpful. Finally, although the data analysis section indicates different frequency ranges for different trends caused by trauma, the statistic tests and SVM only test the use of the whole frequency range. Finding a best/useful frequency range for torso trauma detection may require a comprehensive work to avoid being bias.

6
Conclusion

This pilot study indicated promising results for detecting torso trauma with microwave technology. By calculating the mean and standard deviation of all data from ten subjects, consistent trends between healthy and trauma were identified for both transmission coefficients and reflection coefficients. All examined transmission coefficients showed magnitude drop in trauma data. Meanwhile, the phase of reflection coefficients was typically higher for trauma states. The magnitude of the reflection coefficients had a more complex trend with magnitude decrease at frequencies lower than a defined frequency threshold (which was close to the resonance frequency) and magnitude growth above the frequency threshold. The differences between healthy and trauma states were confirmed with the Kruskal–Wallis Test and The Wilcoxon rank-sum Test. The tested SVM was also capable of detecting serious hemoperitoneum and thorax trauma with 95 % and 90 % accuracy, respectively. However, there were still some limitations to this research such as a small number of subjects, low detection accuracy for small sizes trauma and significant variance between repeated measurements.

Torso trauma is a crucial problem and there is a need for new methods to diagnosis blunt torso trauma. This master's thesis indicates that microwave technology is a promising candidate to be used in the prehospital setting.

7

Future work

Based on the promising results as well as limitations of this thesis work, some investigations could be conducted to further develop microwave technology for detecting torso trauma. The first step may be to asses the variability of antenna-skin contact of the current antenna belt to check if the variance of repeated measurements can be reduced. Plastic bags used for containing a matching liquid between antennas and the skin may help to increase signal stability as indicated in the previous work on microwave technology for detecting brain trauma [34]. When an improved antenna belt is designed, more experiments are needed to examine the explored results in this thesis such as the signal magnitude drop at trauma states. More subjects also help improve the quality of machine learning algorithms.

While waiting for the above long term investigations, some further data analysis can be tried. Firstly, instead of utilizing the whole frequency range (i.e. 0.1–2 GHz) as in the current statistic tests and classification, different frequency ranges (bandwidth) may be tested to select the best bandwidth for torso trauma. Secondly, for now, the coefficient combinations generating the highest classification accuracy for abdominal bleeding and thorax trauma is not consistent ("sum of reflection coefficients" for abdominal bleeding and "all coefficients" for thorax trauma). Therefore, it may be more robust to explore a combination that can apply to both trauma types. Finally, we can test other coefficient combinations for the classification algorithms. For example, each level of transmission coefficients can be summed separately to avoid the domination in magnitude of low level coefficients to high level coefficients.

Bibliography

[1] World Health Organization. Injuries and violence: The facts, 2010.

[2] K. Søreide, A. J. Krüger, A. L. Vårdal, C. L. Ellingsen, E. Søreide, and H. M. Lossius. Epidemiology and contemporary patterns of trauma deaths: Changing place, similar pace, older face. *World Journal of Surgery*, 31(11):2092–2103, 2007.

[3] S. M. Sasser, R. C. Hunt, E. E. Sullivent, M. M. Wald, J. Mitchko, G. J. Jurkovich, M. C. Henry, J. P. Salomone, S. C. Wang, R. L. Galli, A. Cooper, L. H. Brown, and R. W. Sattin. Guidelines for field triage of injured patients: Recommendations of the national expert panel on field triage. *Pediatrics*, 123(4):1252–1252, 2009.

[4] D. Trunkey. Torso trauma. *Current Problems in Surgery*, 24(4):215–265, April 1987.

[5] F. B. Rogers, K. J. Rittenhouse, and B. W. Gross. The golden hour in trauma: Dogma or medical folklore? *Injury*, 46(4):525–527, 2015.

[6] D. Nast-Kolb, C. Waydhas, S. Kastl, K. H. Duswald, and L. Schweiberer. The role of an abdominal injury in follow-up of polytrauma patients. *Chirurg*, 64:552–9, 1993.

[7] American College of Surgeons Committee on Trauma. *Advanced Trauma Life Support for Doctors: student course manual.* American College of Surgeons, 2012.

[8] J. R. Clarke, S. Z. Trooskin, P. J. Doshi, L. Greenwald, and C. J. Mode. Time to laparotomy for intra-abdominal bleeding from trauma does affect survival for delays up to 90 minutes. *The Journal of Trauma: Injury, Infection, and Critical Care*, 52(3):420–425, Mar 2002.

[9] M. Christopoulou and S. Koulouridis. Inter-subject variability evaluation towards a robust microwave sensor for pneumothorax diagnosis. *Progress In Electromagnetics Research*, 42:61–70, 2015.

[10] S. A. Rezaeieh, A. Zamani, K. S. Bialkowski, and A. M. Abbosh. Novel microwave torso scanner for thoracic fluid accumulation diagnosis and monitoring. *Scientific Reports*, 7(1), 2017.

[11] J. Ljungqvist, S. Candefjord, M. Persson, L. Jönsson, T. Skoglund, and M. Elam. Clinical evaluation of a microwave-based device for detection of traumatic intracranial hemorrhage. *Journal of Neurotrauma*, 34(13):2176–2182, 2017.

[12] J. B. Hall, G. A. Schmidt, and J. P. Kress. *Torso Trauma*, chapter 95. McGraw-Hill Education, 2015.

[13] T. C. Nunez and B. A. Cotton. Transfusion therapy in hemorrhagic shock. *Curr Opin Crit Care*, 15(6):536–541, 2009.

[14] L. I. Jennifer and M. John. Advances in abdominal trauma. *Emergency Medicine Clinics of North America*, 25(3):713–733, 2007.

[15] . Patel, J. Gadhavi, and H. Parmar. A study of blunt and penetrating abdominal trauma, its various patterns of injuries, and its management. *International Journal of Medical Science and Public Health*, 5(7):1309, Oct 2016.

[16] J. O. Jansen, S. R. Yule, and M. A. Loudon. Investigation of blunt abdominal trauma. *BMJ (Clinical research ed.)*, 336(7650):938–942, April 2008.

[17] A. Sharma and P. Jindal. Principles of diagnosis and management of traumatic pneumothorax. *Journal of Emergencies, Trauma and Shock*, 1(1):34, Jun 2008.

[18] N. Oveland, R. Buendia, B. Sjöqvist, M. Oropeza-Moe, N. Andersen, A. Fhager, M. Persson, M. Elam, and S. Candefjord. A wearable microwave detector for diagnosing thoracic injuries-test on a porcine pneumothorax model. *Scandinavian Journal of Trauma, Resuscitation and Emergency Medicine*, 23(Suppl 2), 2015.

[19] M. H. Chung, C. Y. Hsiao, N. S. Nian, Y. C. Chen, C. Y. Wang, Y. S. Wen, H. C. Shih, and D. H-T. Yen. The benefit of ultrasound in deciding between tube thoracostomy and observative management in hemothorax resulting from blunt chest trauma. *World Journal of Surgery*, 42(7):2054–2060, 2018.

[20] E. Weldon and J. Williams. Pleural disease in the emergency department. *Emergency Medicine Clinics of North America*, 30(2):475–499, 2012.

[21] G.w.h. Schurink, P.j. Bode, P.a. V. Luijt, and A.b.V. Vugt. The value of physical examination in the diagnosis of patients with blunt abdominal trauma: a retrospective study. *Injury*, 28(4):261–265, 1997.

[22] R. Miriam, K. Thomas, B. Raoul, M. Ingo, and W. Felix. Prehospital and emergency department ultrasound in blunt abdominal trauma. *European Journal of Trauma and Emergency Surgery*, 35(4):341, Jul 2009.

[23] P. C. Pedersen, C. C. Johnson, C. H. Durney, and D. G. Bragg. Microwave reflection and transmission measurements for pulmonary diagnosis and monitoring. *IEEE Transactions on Biomedical Engineering*, BME-25(1):40–48, 1978.

[24] M. F. Iskander, C. H. Durney, D. J. Shoff, and D. G. Bragg. Diagnosis of pulmonary edema by a surgically noninvasive microwave technique. *Radio Science*, 14(6S):265–269, 1979.

[25] M. I. Christopoulou and S. D. Koulouridis. Dual patch antenna sensor for pneumothorax diagnosis: Sensitivity and performance study. *2014 36th Annual International Conference of the IEEE Engineering in Medicine and Biology Society*, 2014.

[26] Serguei Semenov. Microwave tomography: review of the progress towards clinical applications. *Philosophical Transactions of the Royal Society A: Mathematical, Physical and Engineering Sciences*, 367(1900):3021–3042, 2009.

[27] D. M. Pozar. *Microwave engineering.* Wiley India, 2017.

[28] C. Gabriel, S. Gabriel, and E. Corthout. The dielectric properties of biological tissues: I. literature survey. *Physics in Medicine and Biology*, 41(11):2231–2249, Jan 1996.

[29] J. H. McDonald. *Handbook of biological statistics.* Sparky House Publishing, 2009.

[30] O. L. Mangasarian and D. R. Musicant. Lagrangian support vector machines. *Journal of Machine Learning Research*, 1:161–177, 01 2001.

[31] P. H. C. Eilers. A perfect smoother. *Analytical Chemistry*, 75(14):3631–3636, 2003.

[32] M. A. Nanda, K. B. Seminar, D. Nandika, and A. Maddu. A comparison study of kernel functions in the support vector machine and its application for termite detection. *Information*, 9(1):5, 2018.

[33] S. Candefjord, J. Winges, A. A. Malik, Y. Yu, T. Rylander, T. Mckelvey, A. Fhager, M. Elam, and M. Persson. Microwave technology for detecting traumatic intracranial bleedings: tests on phantom of subdural hematoma and numerical simulations. *Med Biol Eng Comput*, 55(8):1177–1188, 2016.

[34] M. Persson, A. Fhager, H. D. Trefna, Y. Yu, T. Mckelvey, G. Pegenius, J.E. Karlsson, and M. Elam. Microwave-based stroke diagnosis making global prehospital thrombolytic treatment possible. *IEEE Transactions on Biomedical Engineering*, 61(11):2806–2817, 2014.

A
Data analysis

A.1 Abdominal data
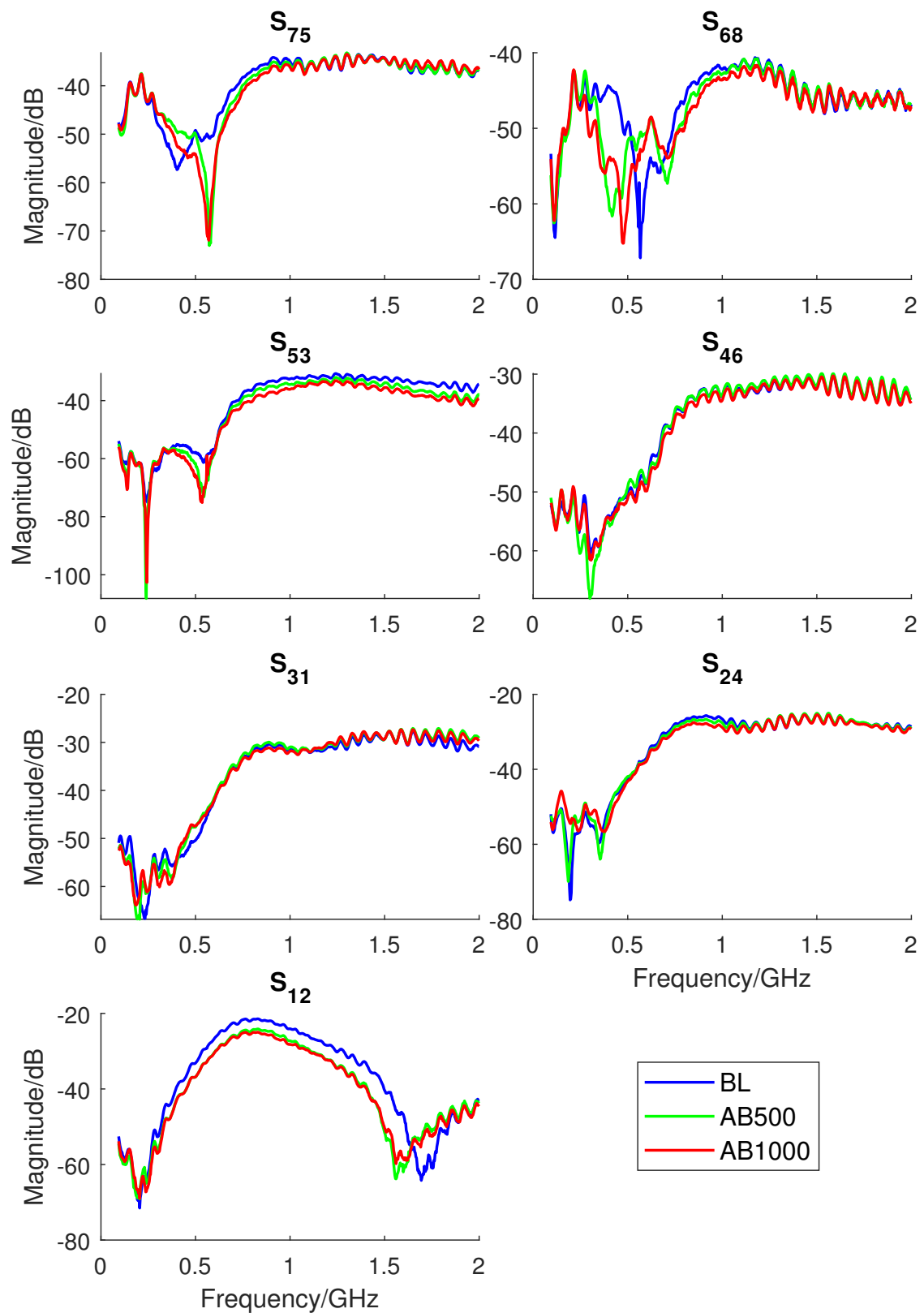
Figure A.1: The raw magnitude of some transmission coefficients of pig 1 in the hemoperitoneum tests.
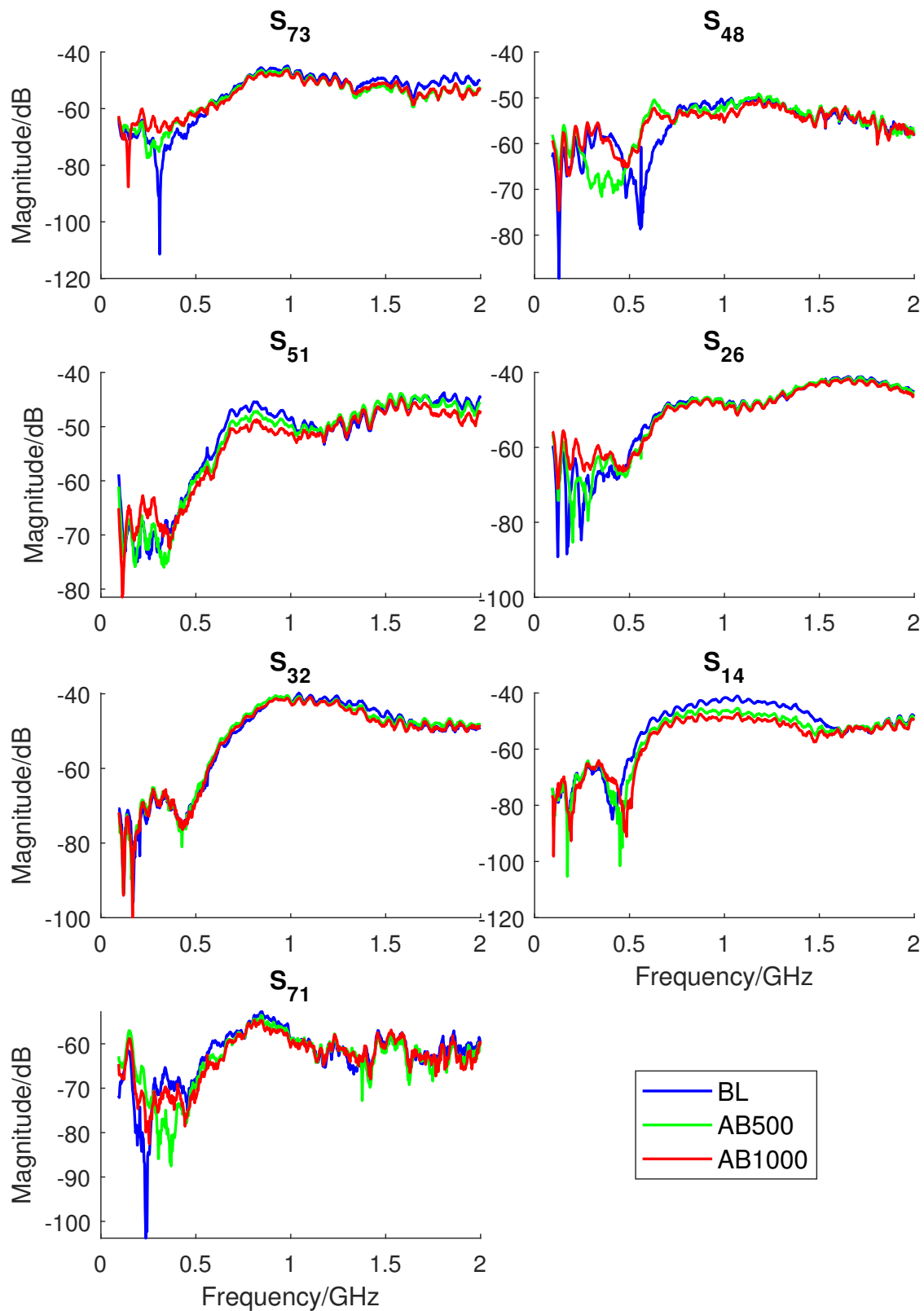
Figure A.2: The raw magnitude of some transmission coefficients of pig 1 in the hemoperitoneum tests.
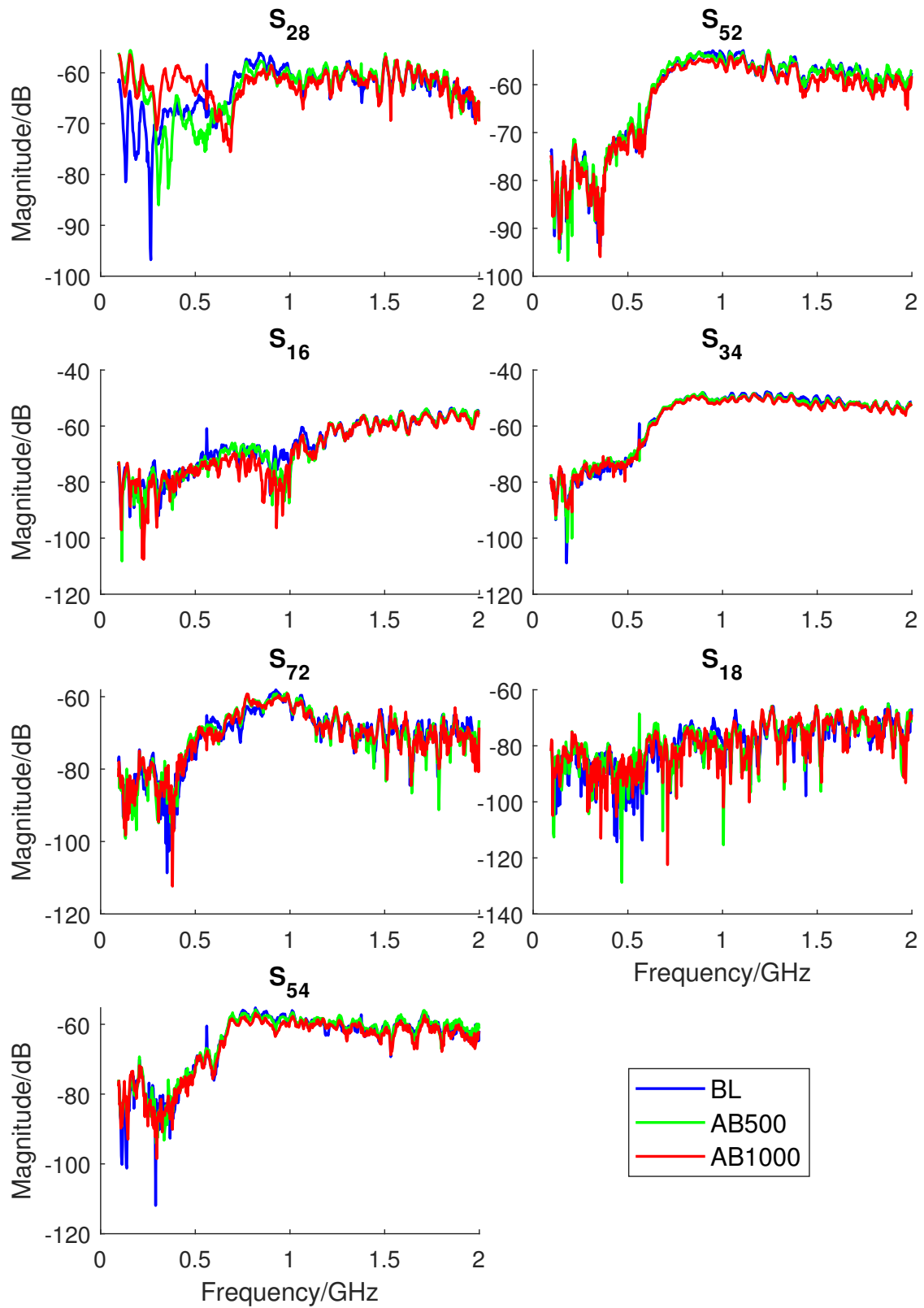
Figure A.3: The raw magnitude of some transmission coefficients of pig 1 in the hemoperitoneum tests.
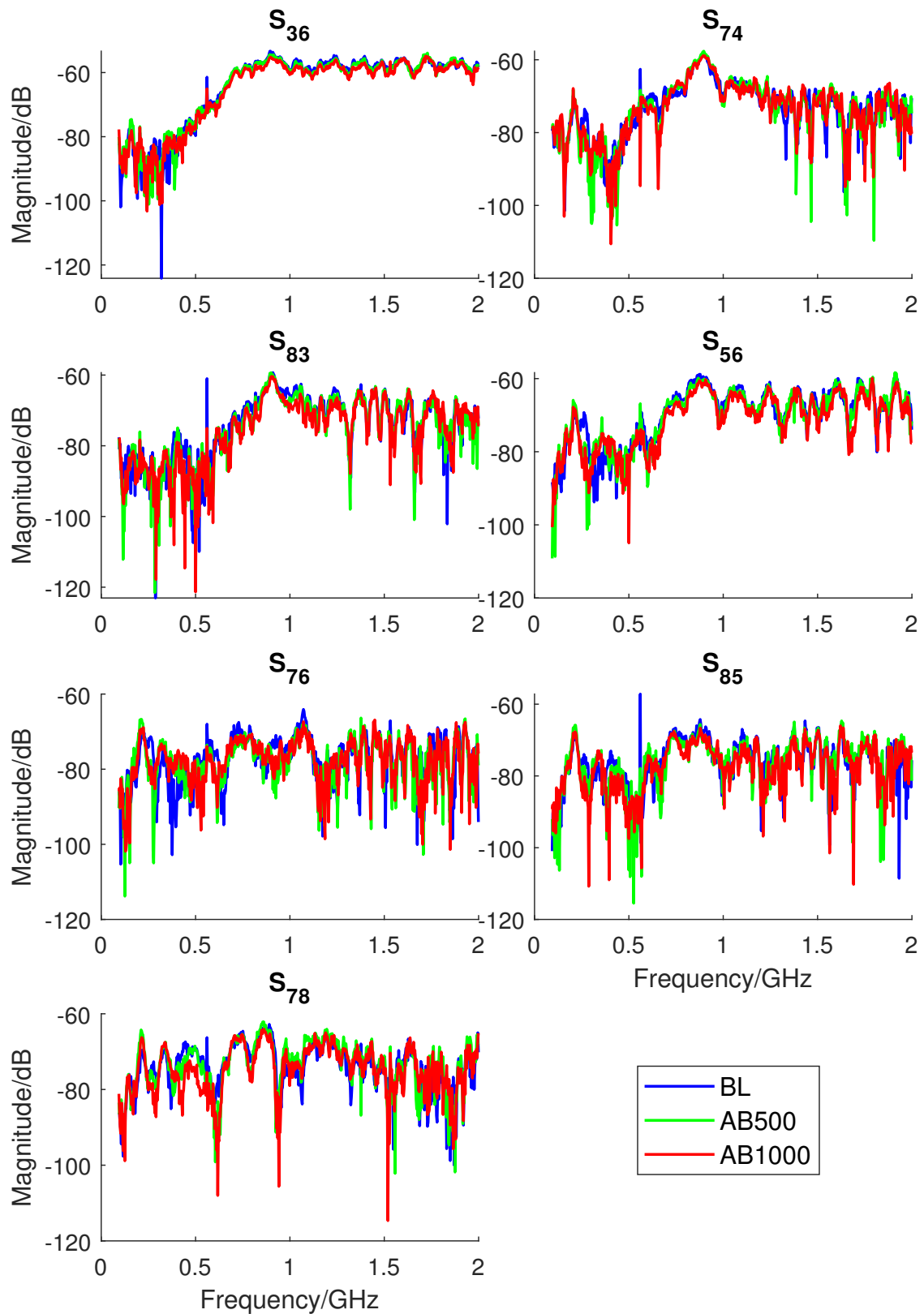
Figure A.4: The raw magnitude of some transmission coefficients of pig 1 in the hemoperitoneum tests.
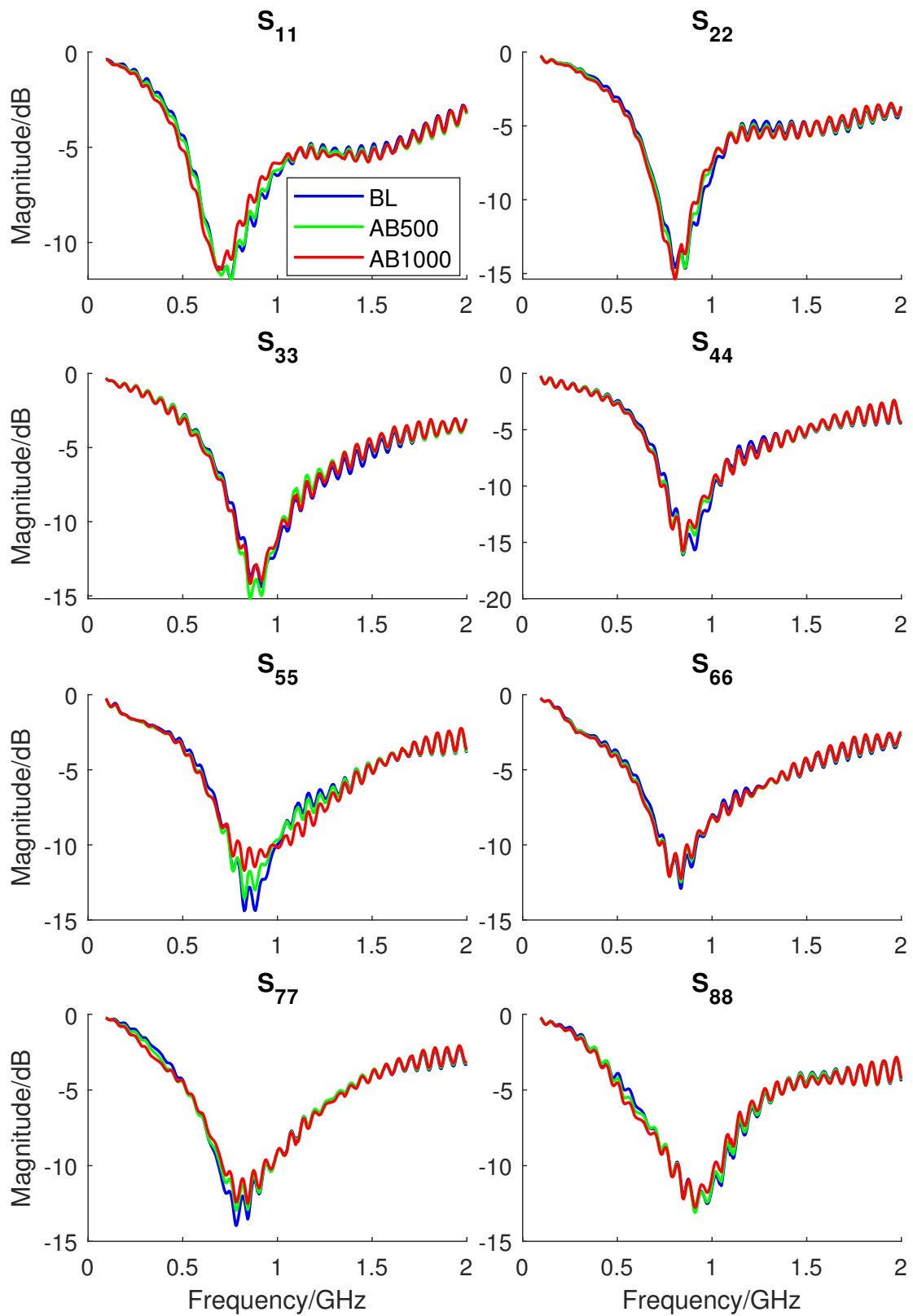
Figure A.5: The raw magnitude of all reflection coefficients of pig 1 in the hemoperitoneum tests.
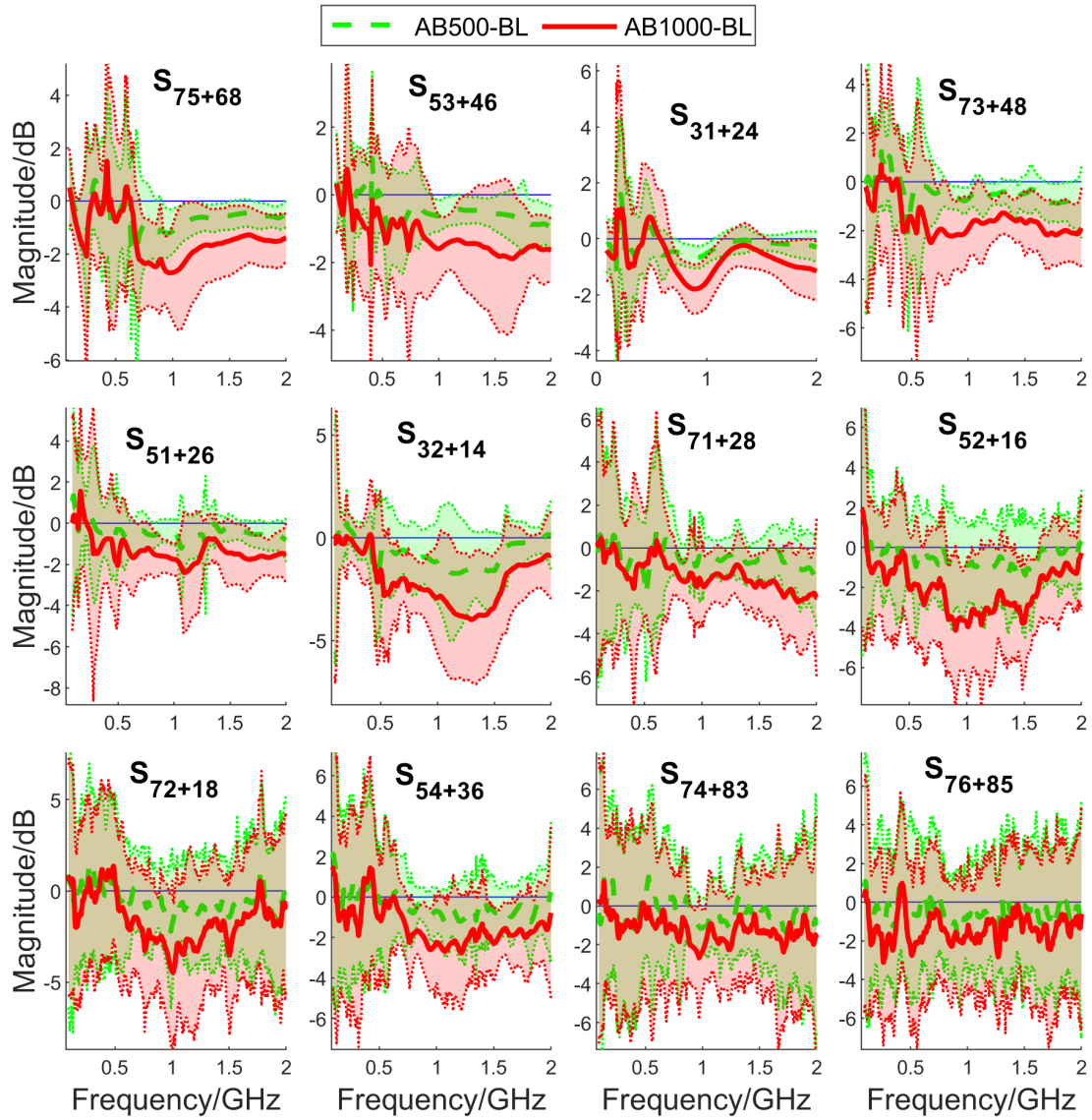
Figure A.6: The mean coefficient magnitude difference (between the baseline and hemoperitoneum) of all measurements from 10 pigs for all transmission coefficient combinations. The shaded areas are the standard deviation of 100 measurements. The magnitude decrease can be clearly seen in hemoperitoneum.
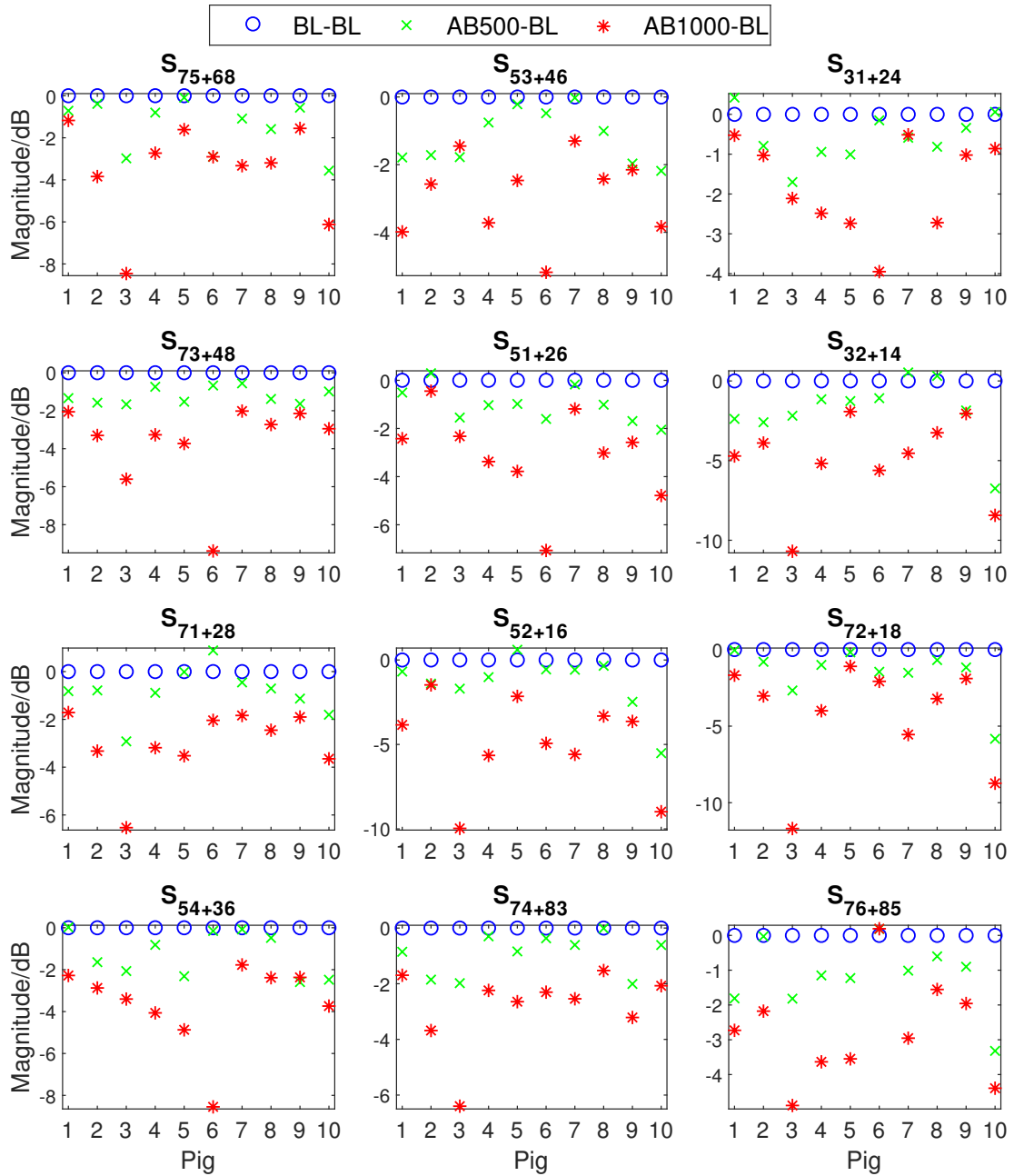
Figure A.7: The mean coefficient magnitude over the frequency range 0.6–2 GHz for all pigs and coefficient combinations.
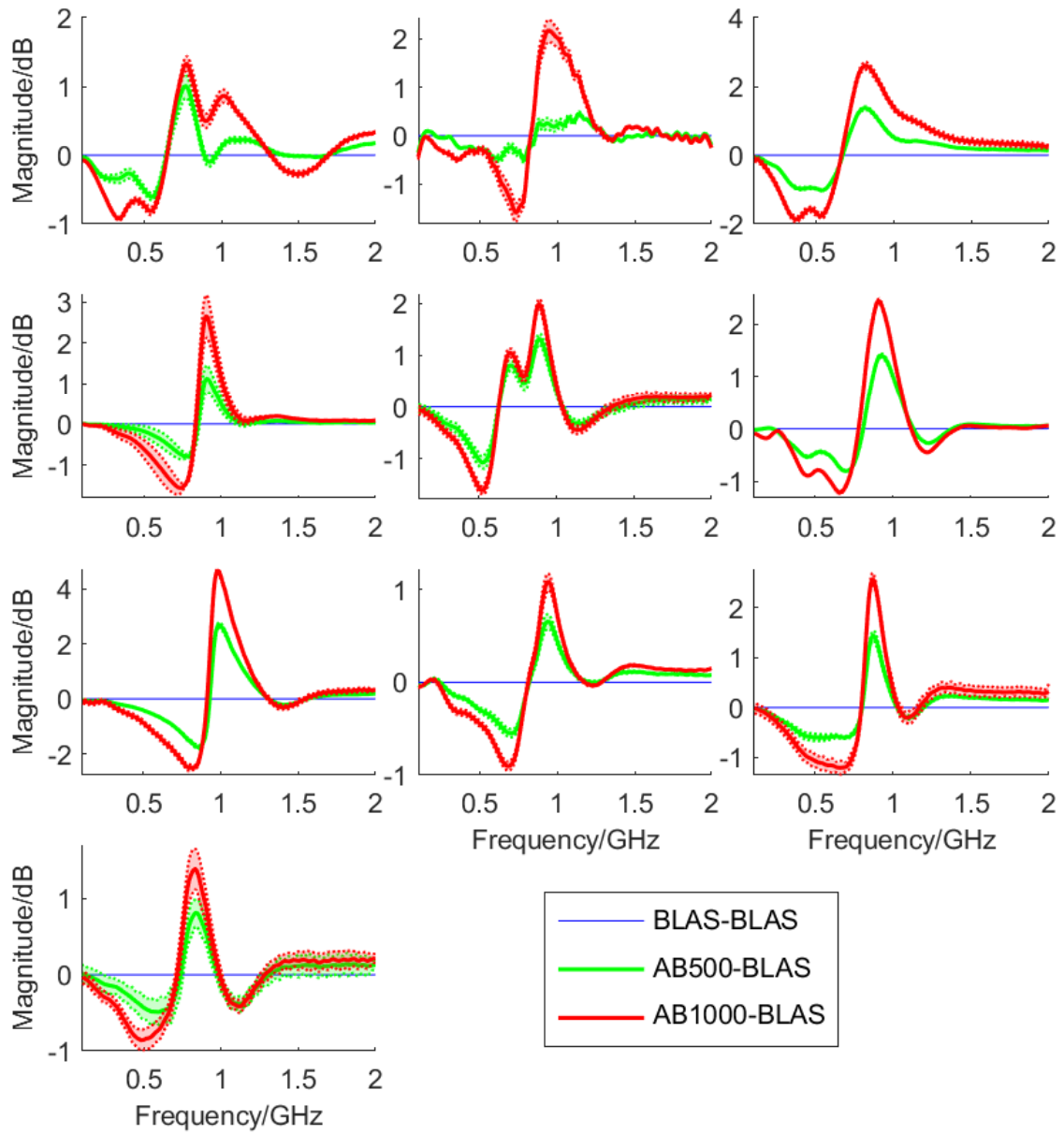
Figure A.8: The magnitude difference (between the baseline and hemoperitoneum) of 10 pigs for coefficient S_{77+88}. The shaded areas are the standard deviation of 10 repeated measurements.
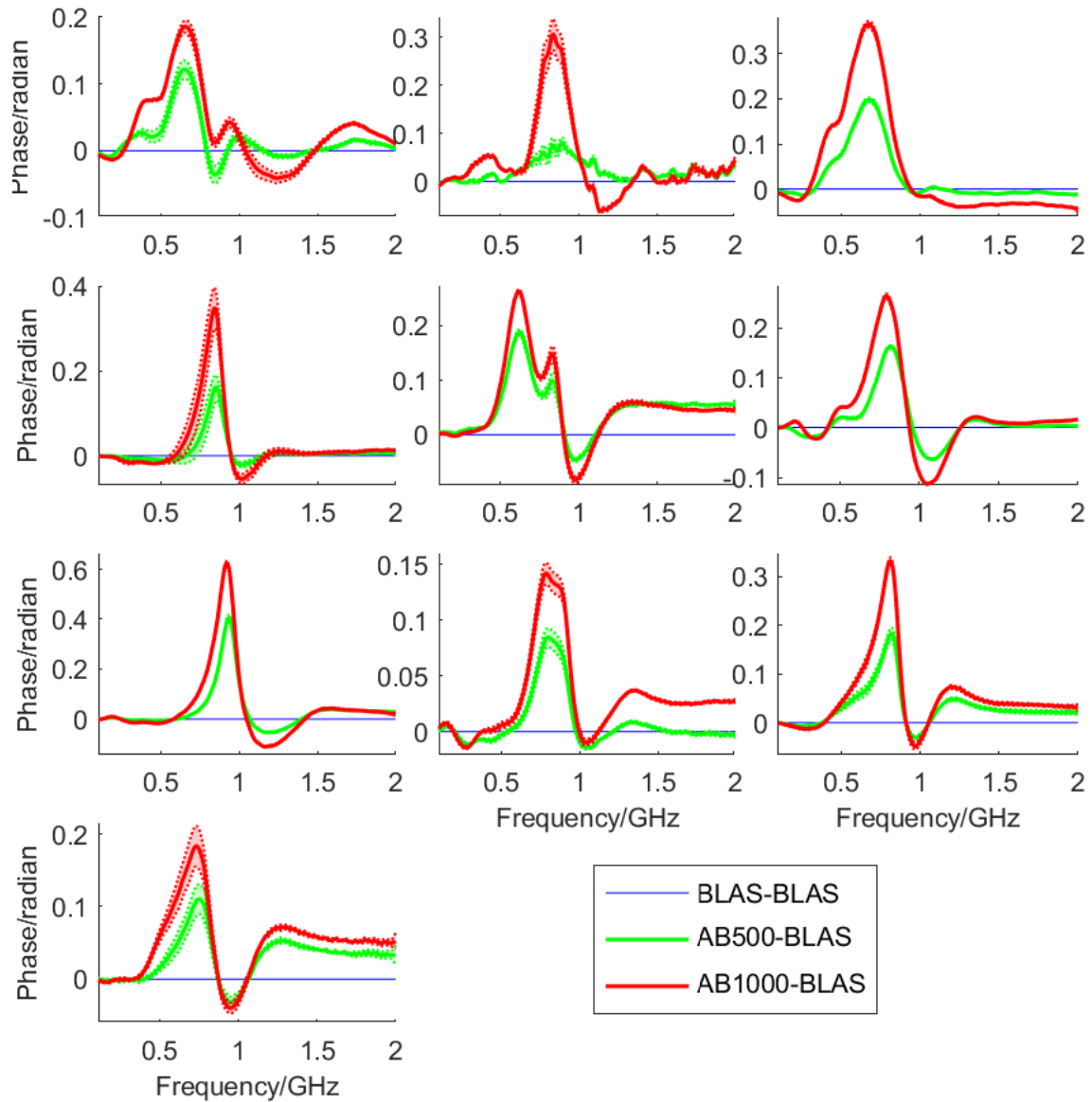
Figure A.9: The phase difference (between the baseline and hemoperitoneum) of 10 pigs for coefficient combination S_{77+88}. The shaded areas are the standard deviation of 10 repeated measurements.

A.2   Thorax data
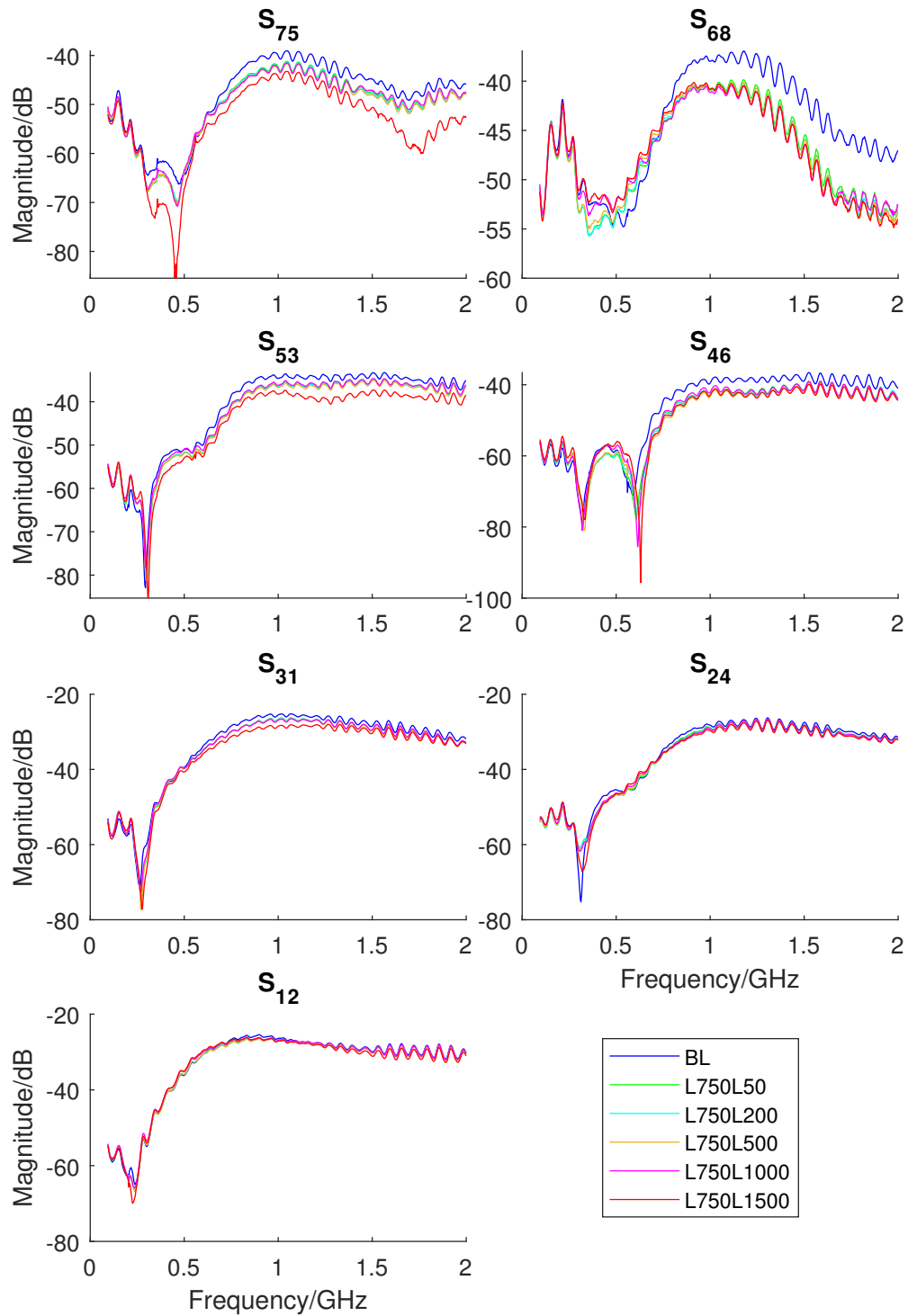
Figure A.10: The raw magnitude of some transmission coefficients of pig 1 in the polytrauma tests.
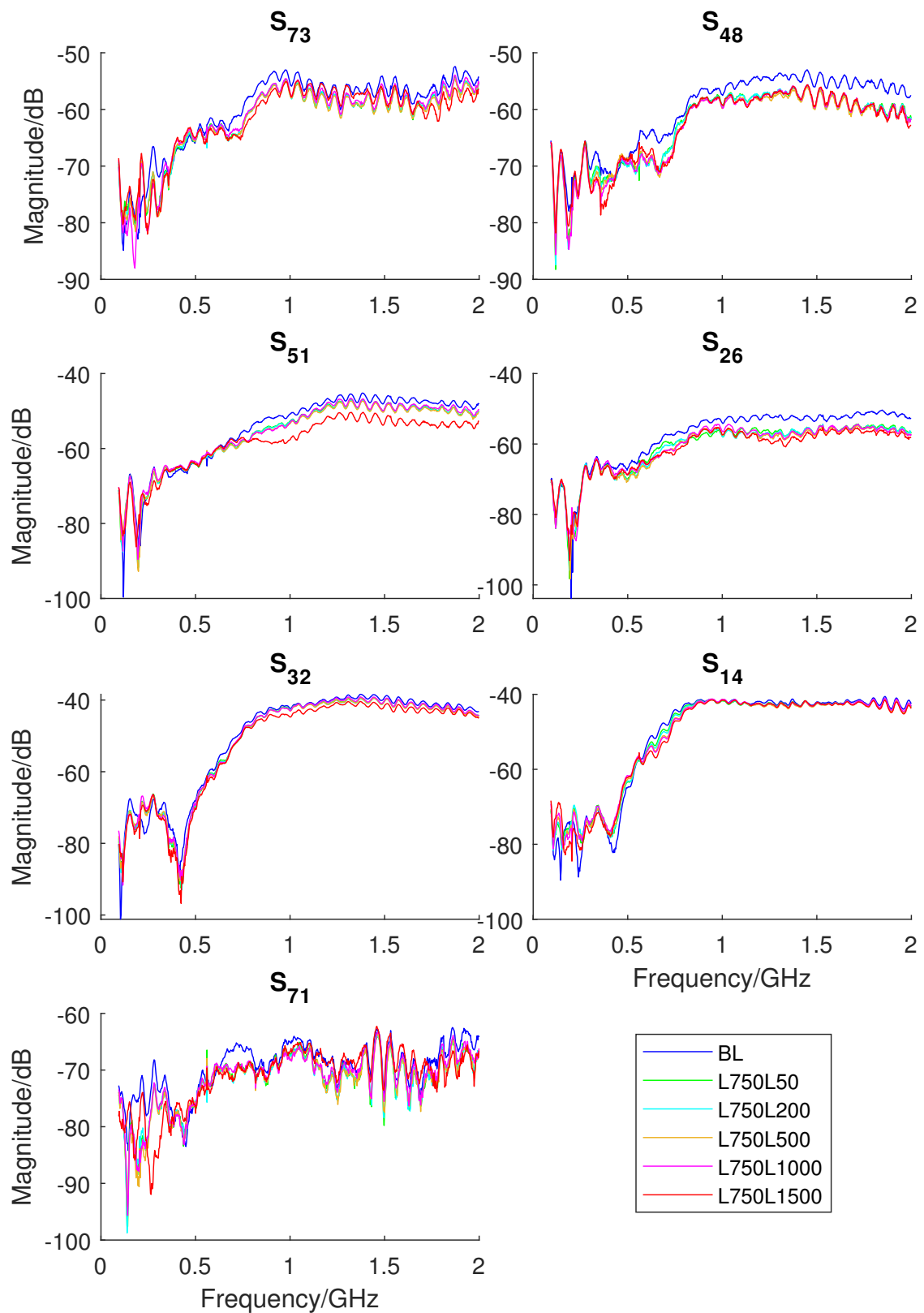
Figure A.11: The raw magnitude of some transmission coefficients of pig 1 in the polytrauma tests.
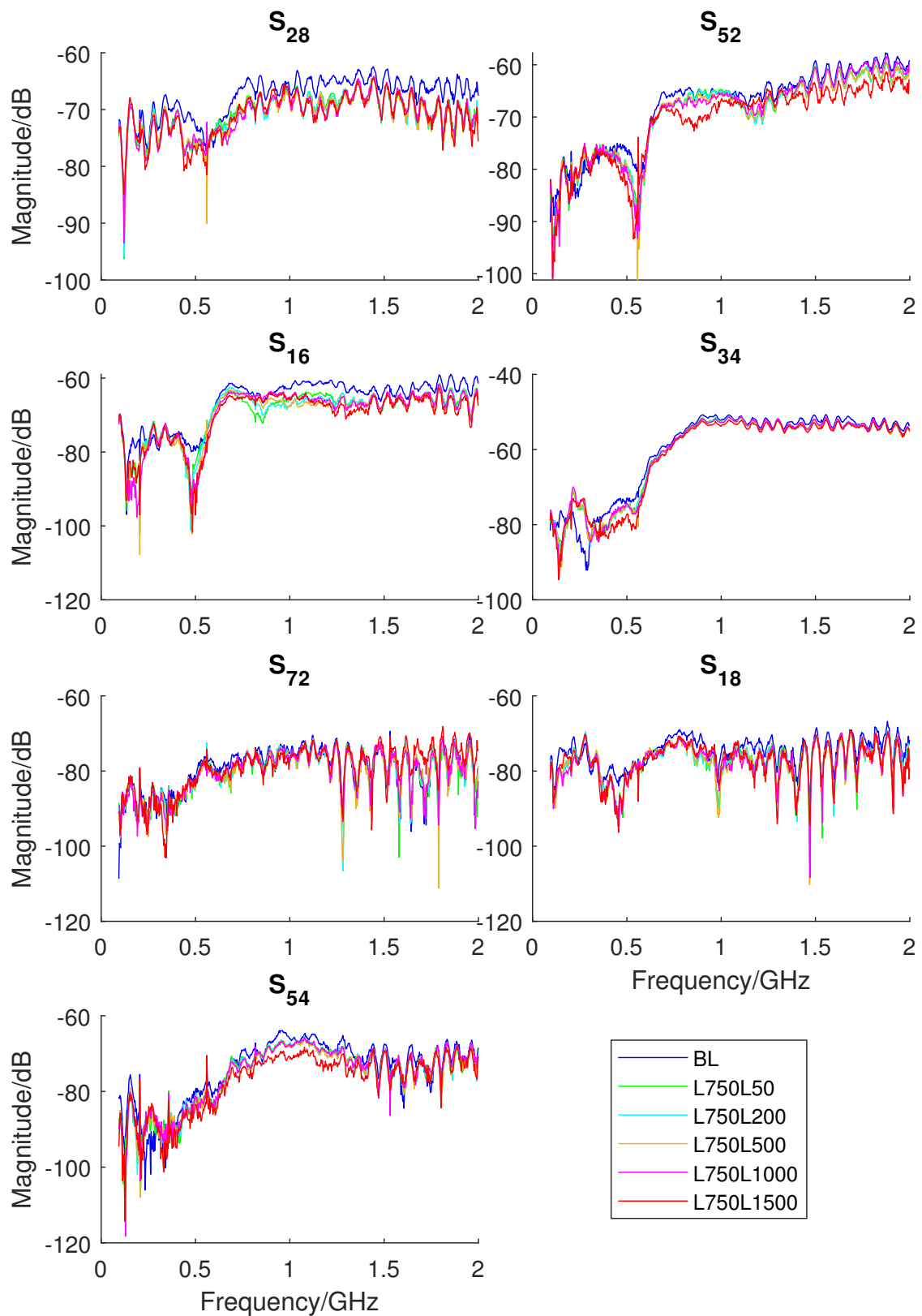
Figure A.12: The raw magnitude of some transmission coefficients of pig 1 in the polytrauma tests.
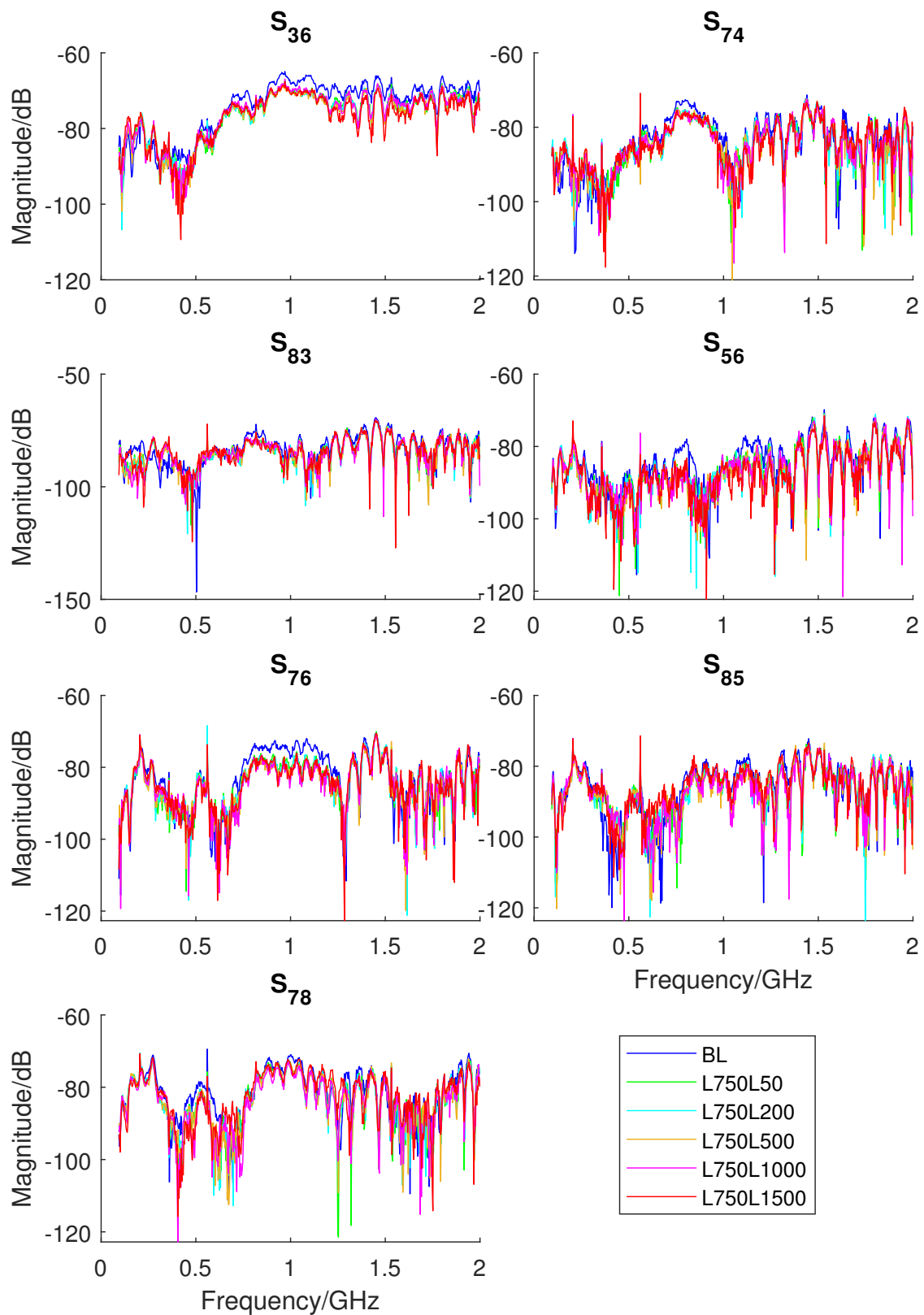
Figure A.13: The raw magnitude of some transmission coefficients of pig 1 in the polytrauma tests.
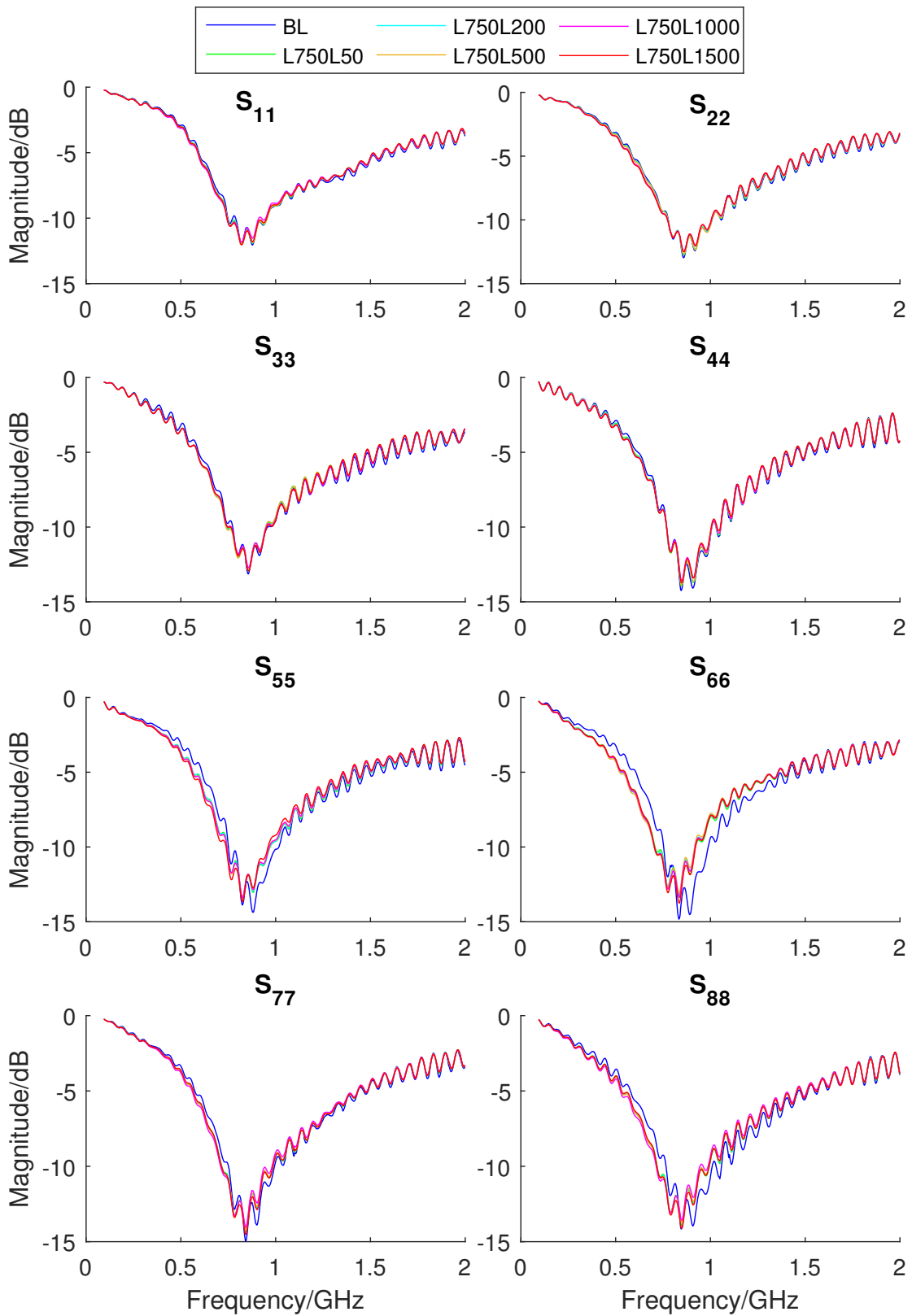
Figure A.14: The raw magnitude of all reflection coefficients of pig 1 in the polytrauma tests.
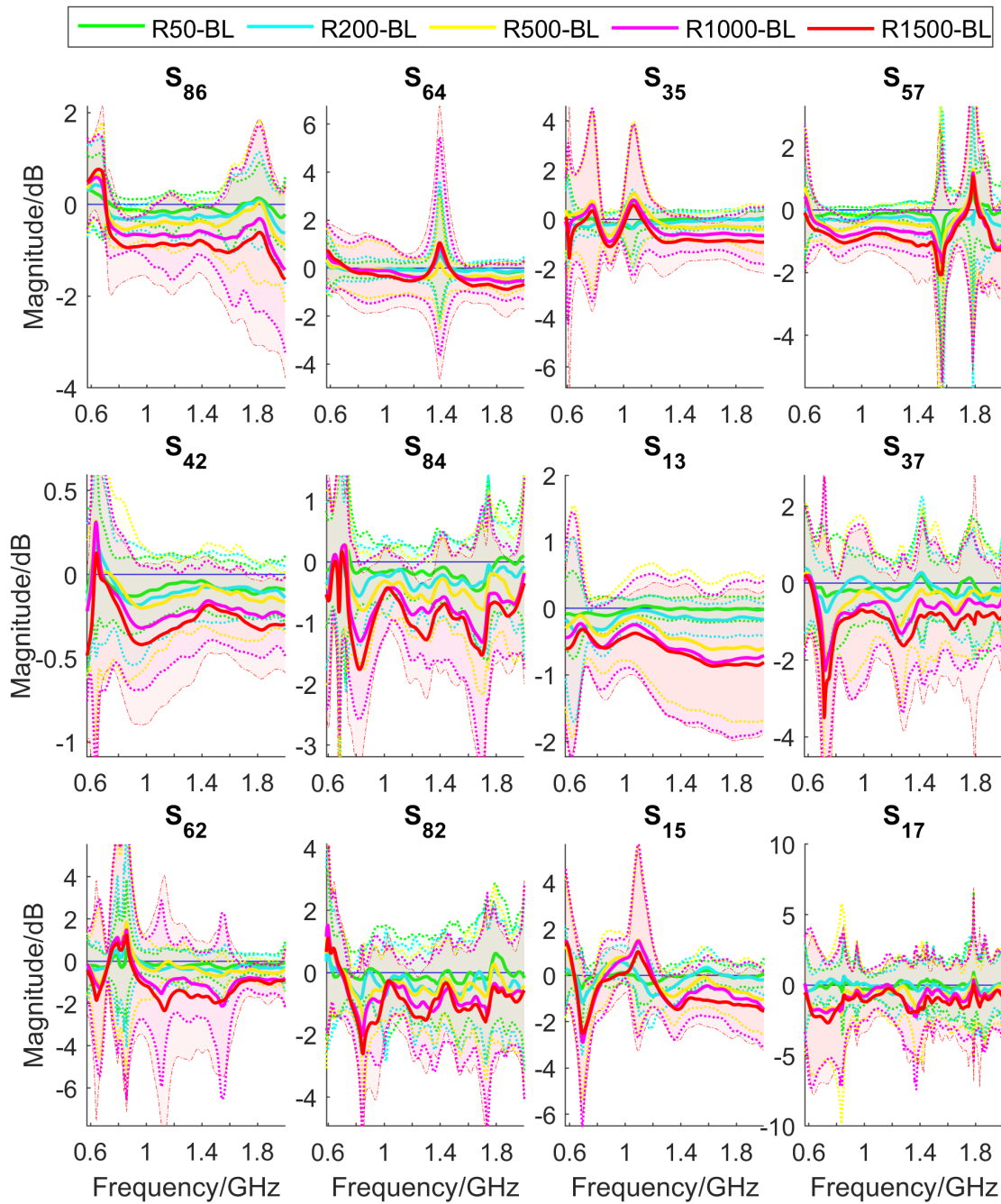
Figure A.15: The mean (solid line) and stand deviation (shaded area) of the difference in magnitude between the baseline and pneumothorax state for all examined transmission coefficients. The left and right coefficients are plotted on the left and right side respectively. Data below 0.6 GHz are not shown because there is not a common trend at these frequencies.
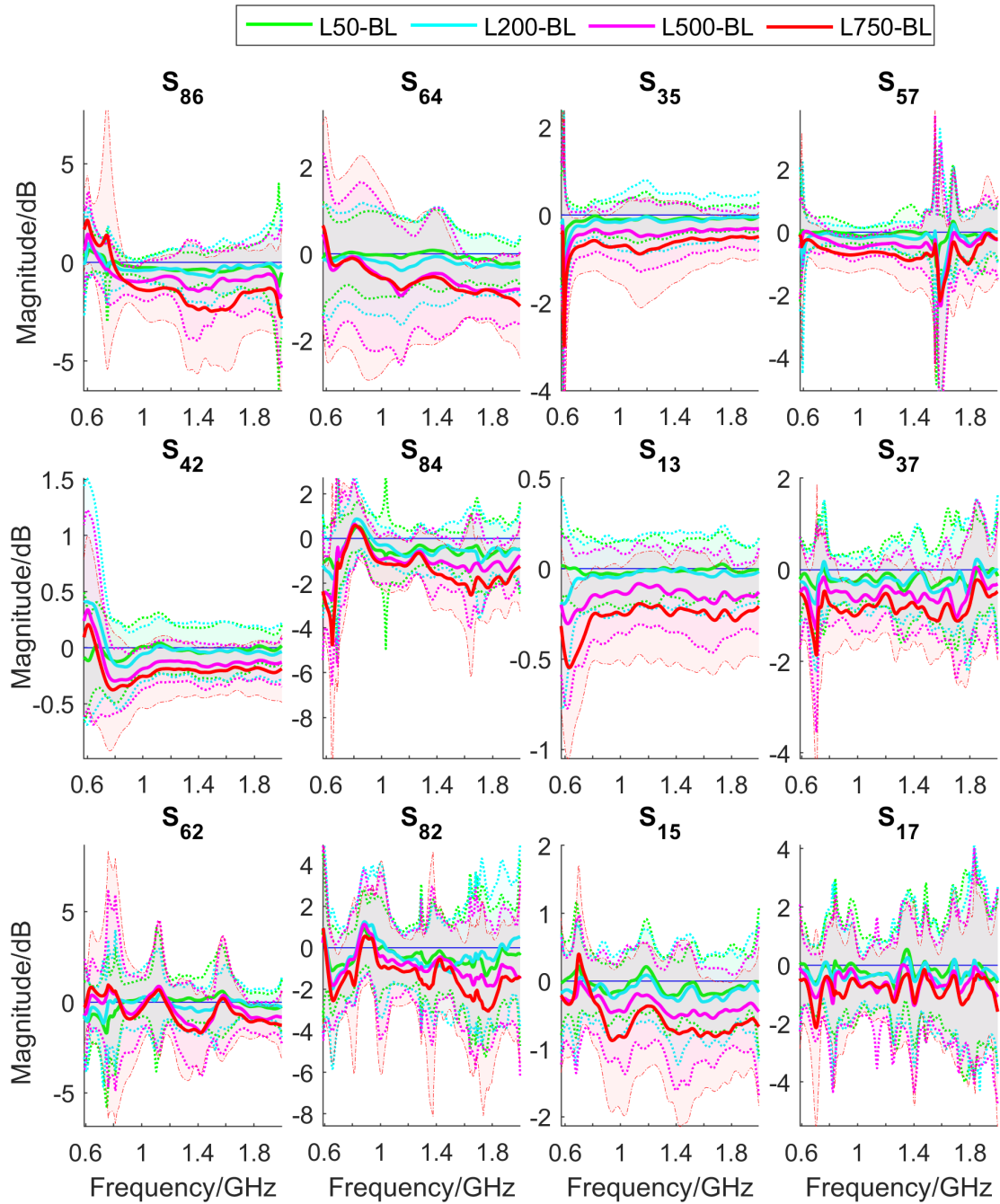
Figure A.16: The mean (solid line) and stand deviation (shaded area) of the difference in magnitude between the baseline and hemothorax state for all examined transmission coefficients. The left and right coefficients are plotted on the left and right side respectively. Data below 0.6 GHz are not shown because there is not a common trend at these frequencies.
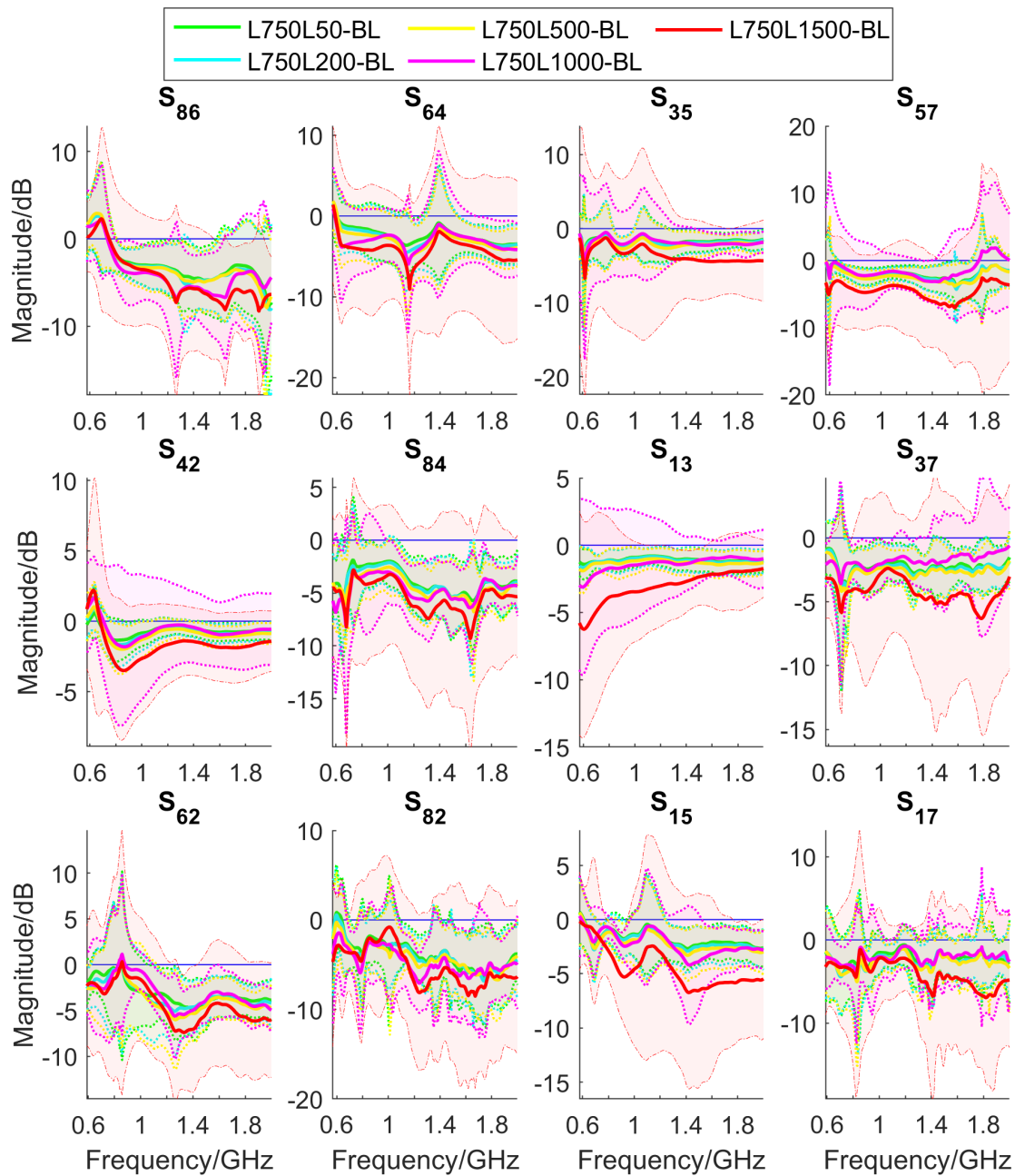
Figure A.17: The mean (solid line) and stand deviation (shaded area) of the difference in magnitude between the baseline and polytrauma state for all examined transmission coefficients. The left and right coefficients are plotted on the left and right side respectively. Data below 0.6 GHz are not shown because there is not a common trend at these frequencies.
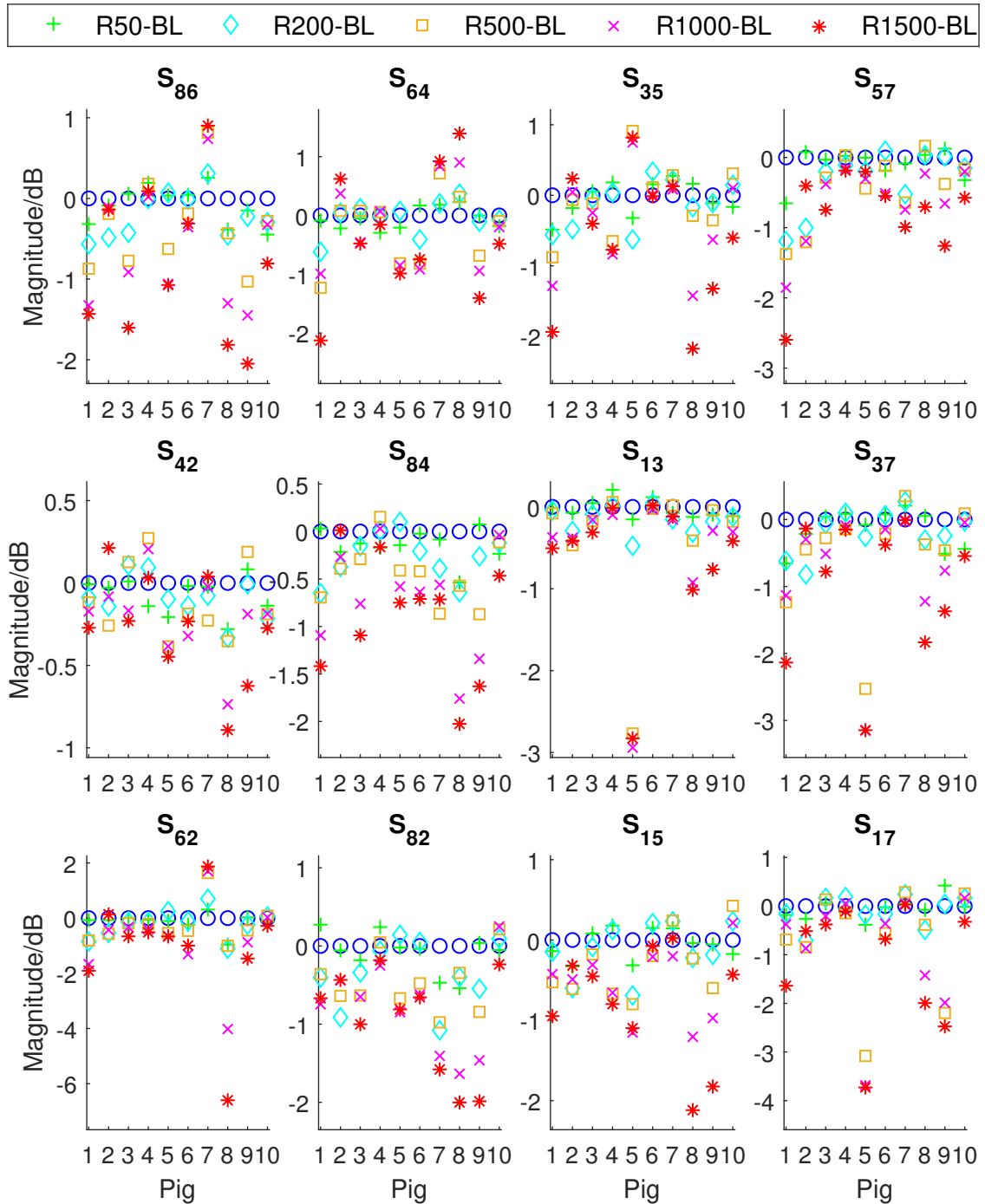
Figure A.18: The mean over the frequency range 0.6–2 GHz of the magnitude difference between the baseline and pneumothorax state for all examined transmission coefficients and pigs. The left and right coefficients are plotted on the left and right side respectively.
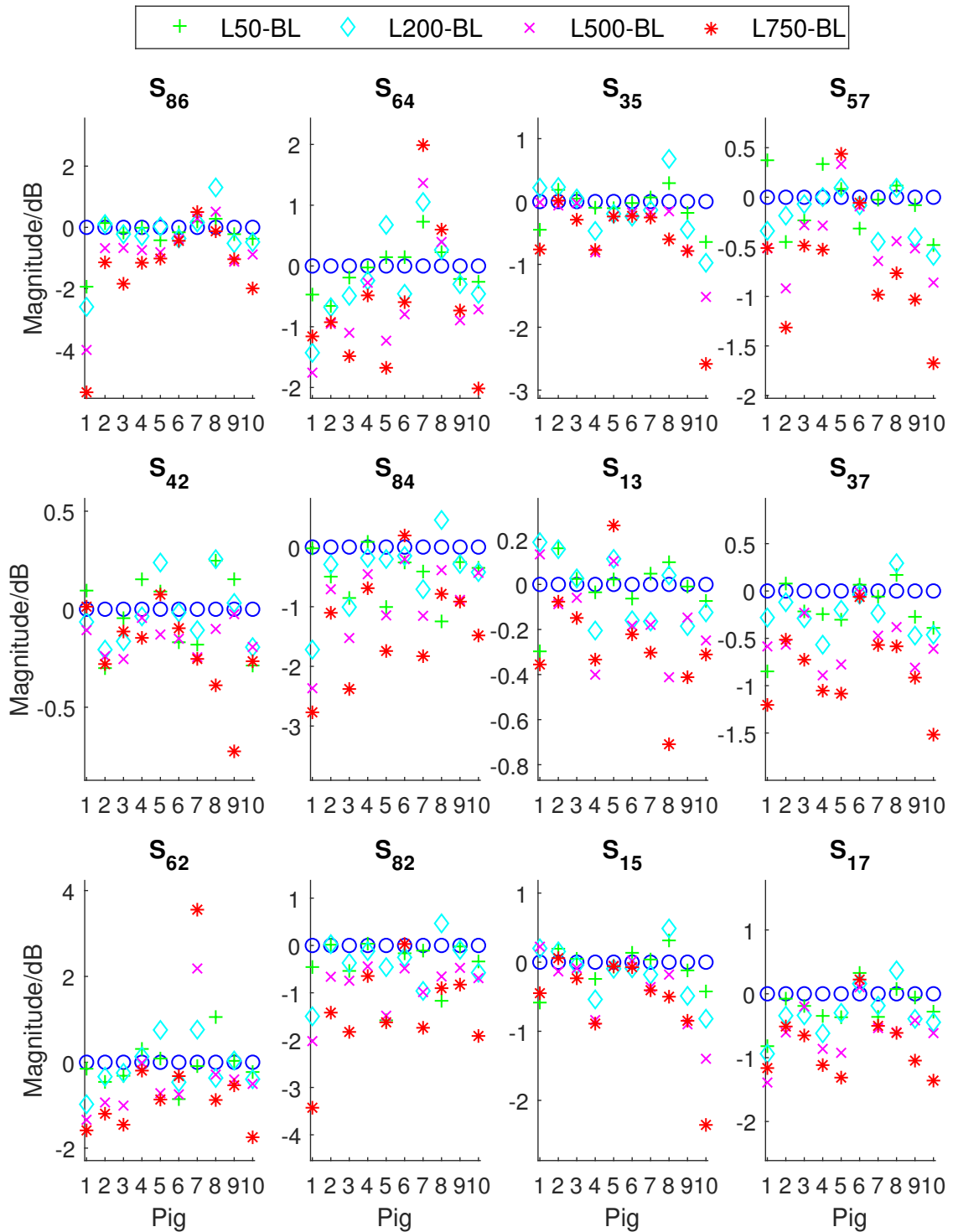
Figure A.19: The mean over the frequency range 0.6–2 GHz of the magnitude difference between the baseline and hemothorax state for all examined transmission coefficients and pigs. The left and right coefficients are plotted on the left and right side respectively.
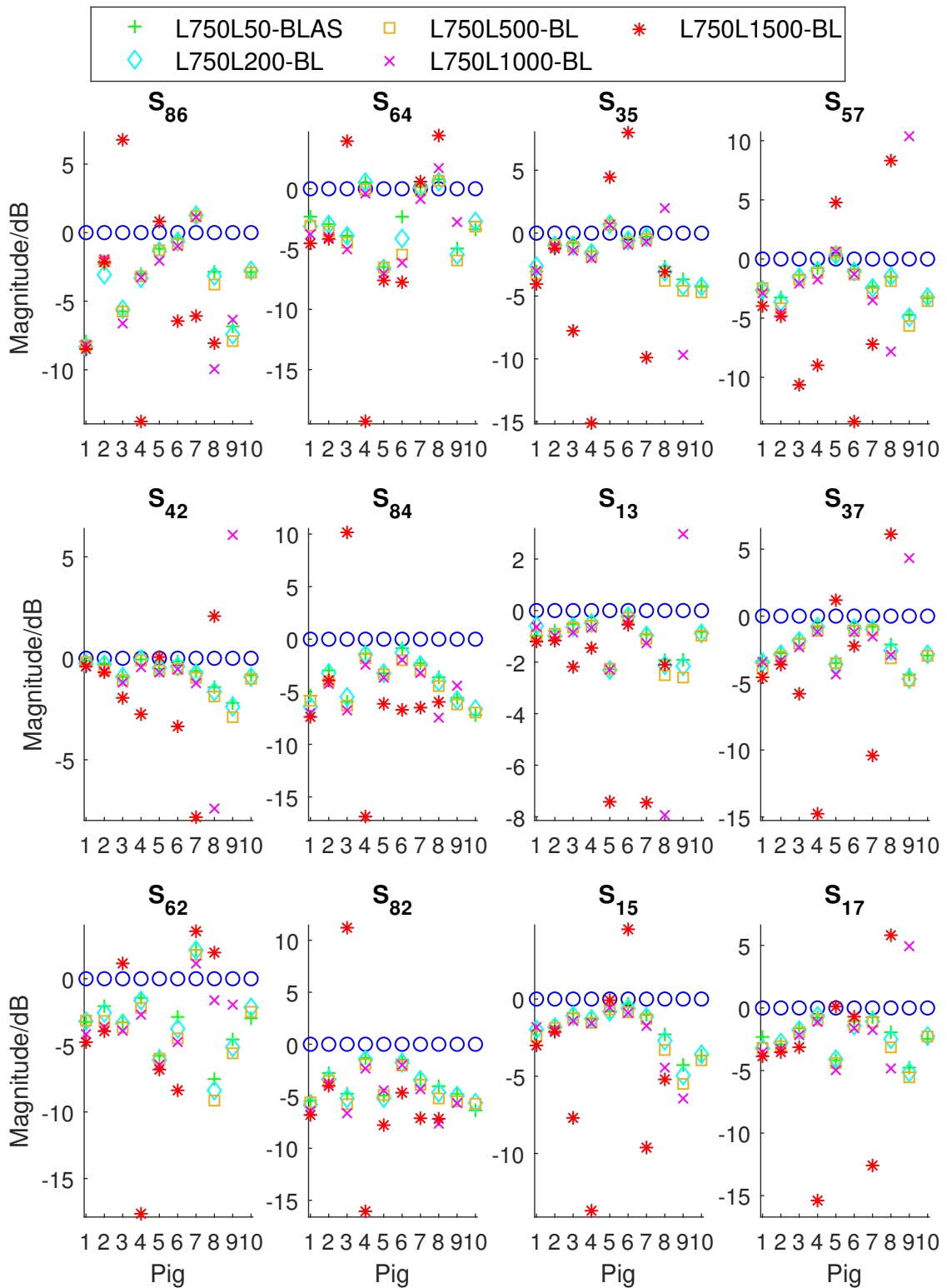
Figure A.20: The mean over the frequency range 0.6–2 GHz of the magnitude difference between the baseline and polytrauma for all examined transmission coefficients and pigs. The left and right coefficients are plotted on the left and right side respectively.
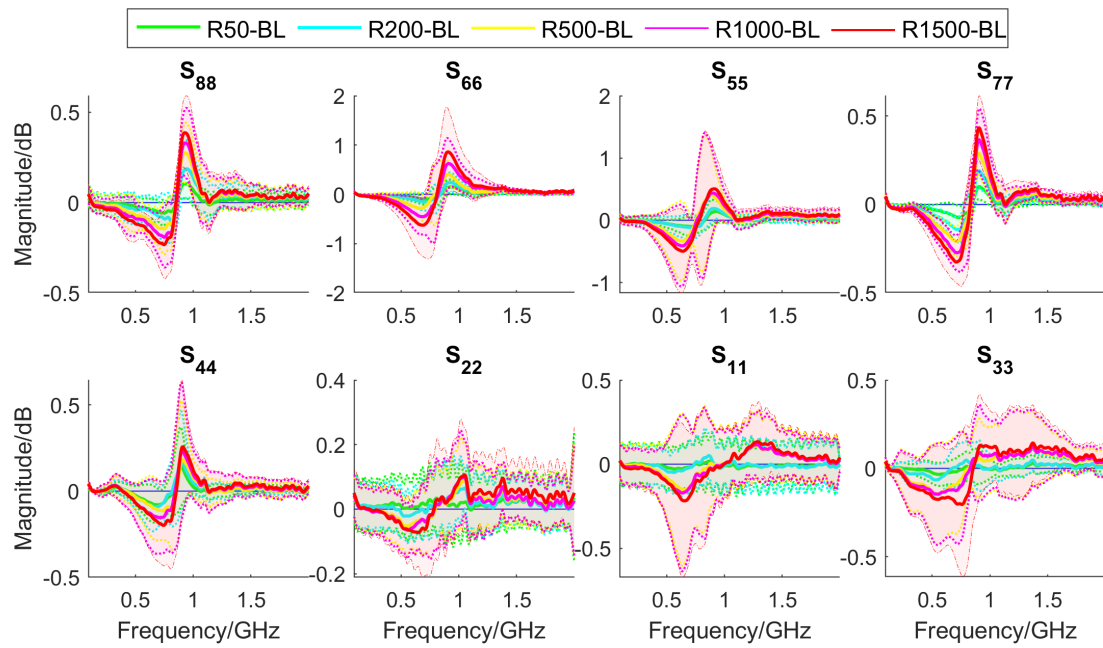
(a) Magnitude.
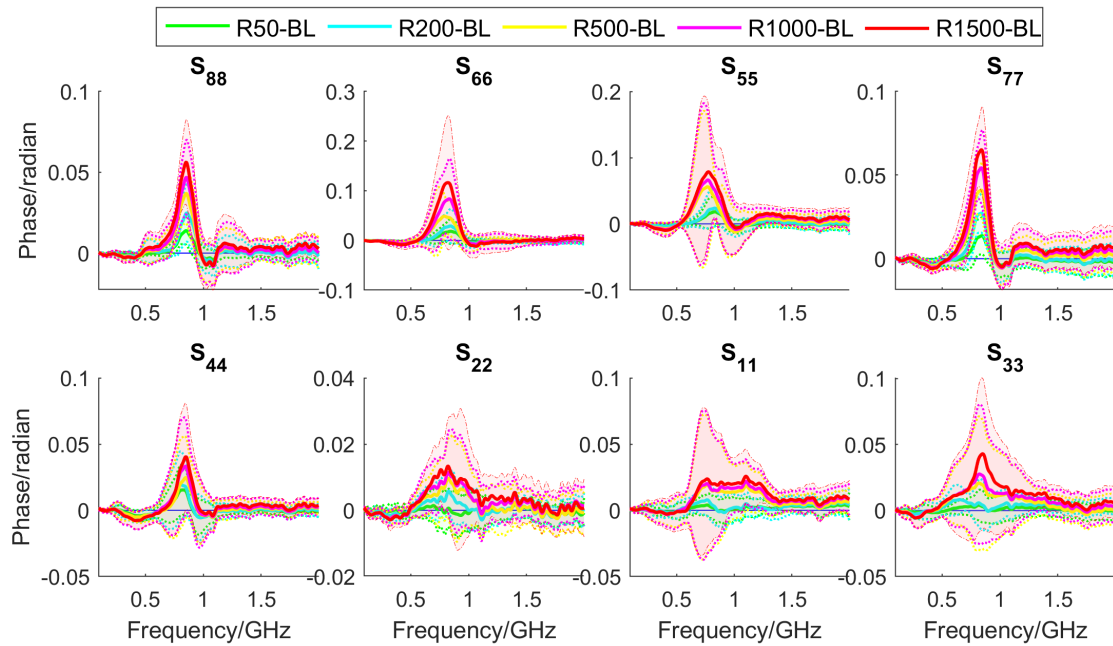
(b) Phase.

Figure A.21: The mean (solid line) and standard deviation (shaded area) of the difference between the baseline and pneumothorax in magnitude (A.21a) and phase (A.21b).
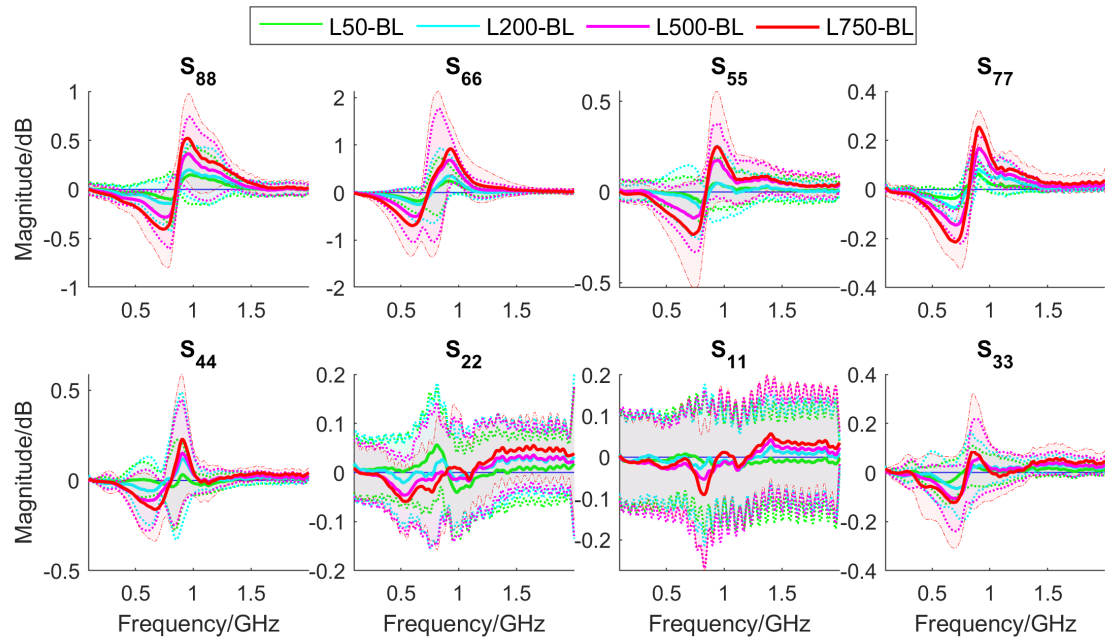
(a) Magnitude.
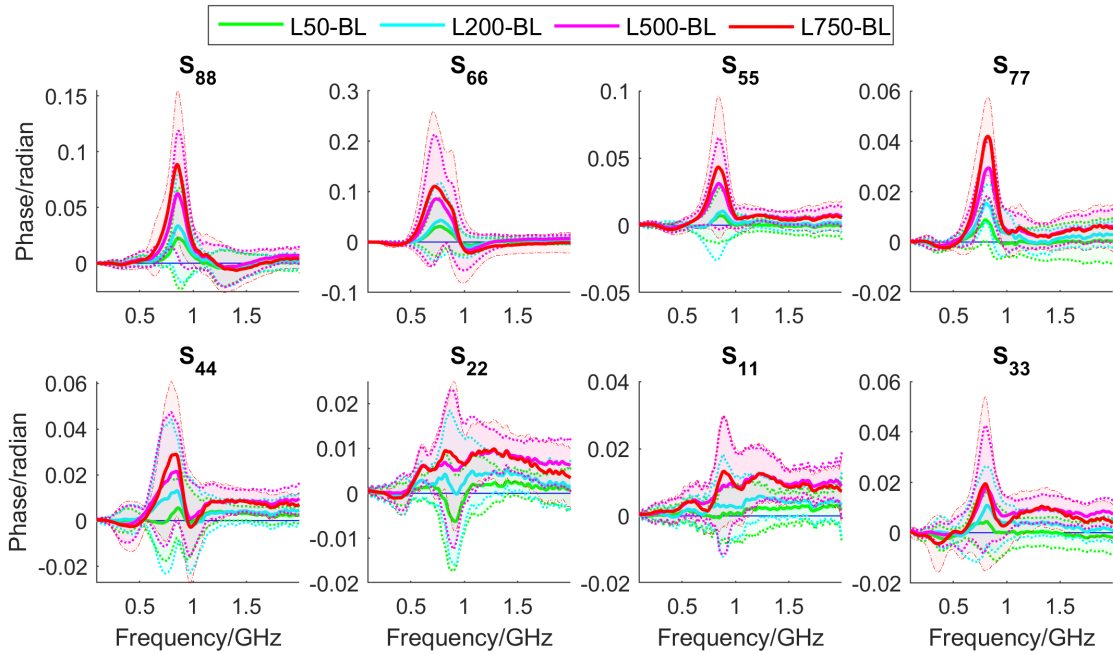
(b) Phase.

Figure A.22: The mean (solid line) and standard deviation (shaded area) of the different between the baseline and hemothorax in magnitude (A.22a) and phase (A.22b).
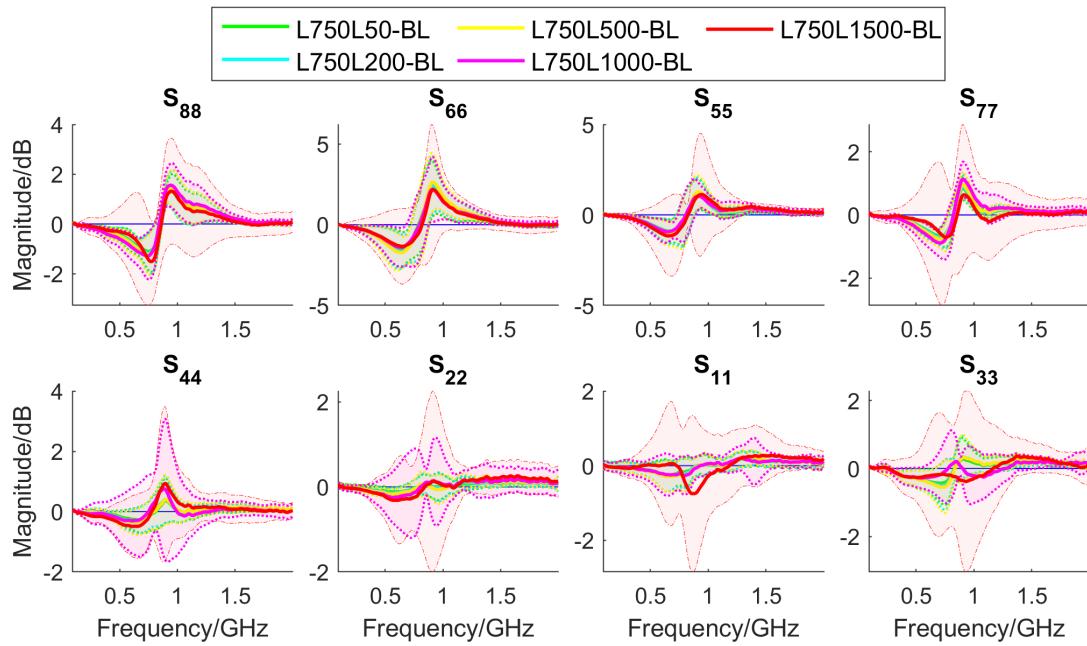
(a) Magnitude.
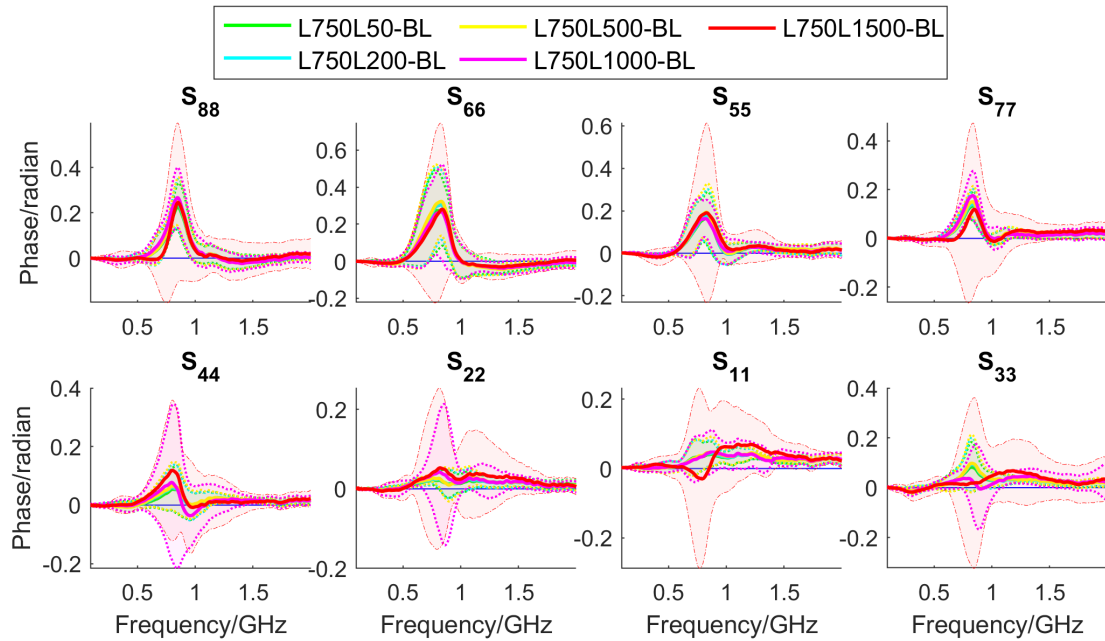
(b) Phase.

Figure A.23: The mean (solid line) and standard deviation (shaded area) of the different between the baseline and polytrauma in magnitude (A.23a) and phase (A.23b).

B

Statistic test

(a) Hemoperitoneum.

(b) Pneumothorax.

(c) Hemothorax.

(d) Polytrauma.
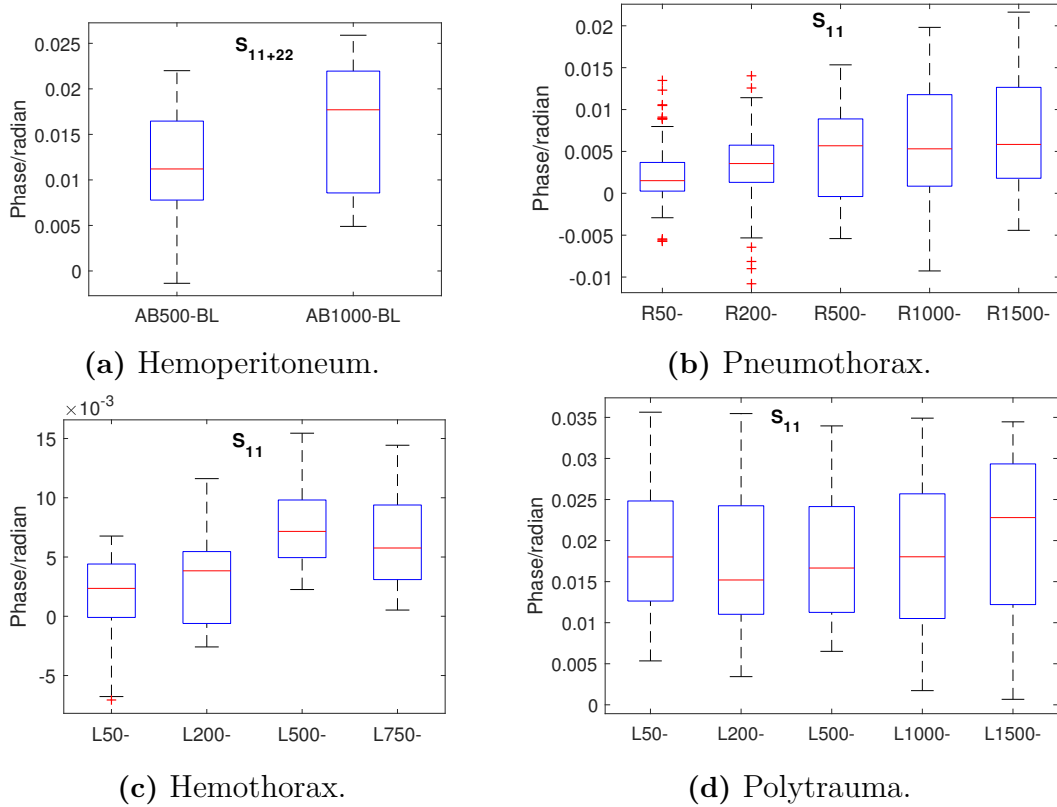
Figure B.1: The phase mean (the red line) and range of the difference in phase between the baseline and three types of trauma. The "-" symbol at the end of some x-axis labels indicates the subtraction of baseline. It is noted that for the combination of two trauma types, the symbol L750 (represents hemothorax) is skipped for clarity.

(a) Hemoperitoneum.

(b) Pneumothorax.

(c) Hemothorax.

(d) Polytrauma.
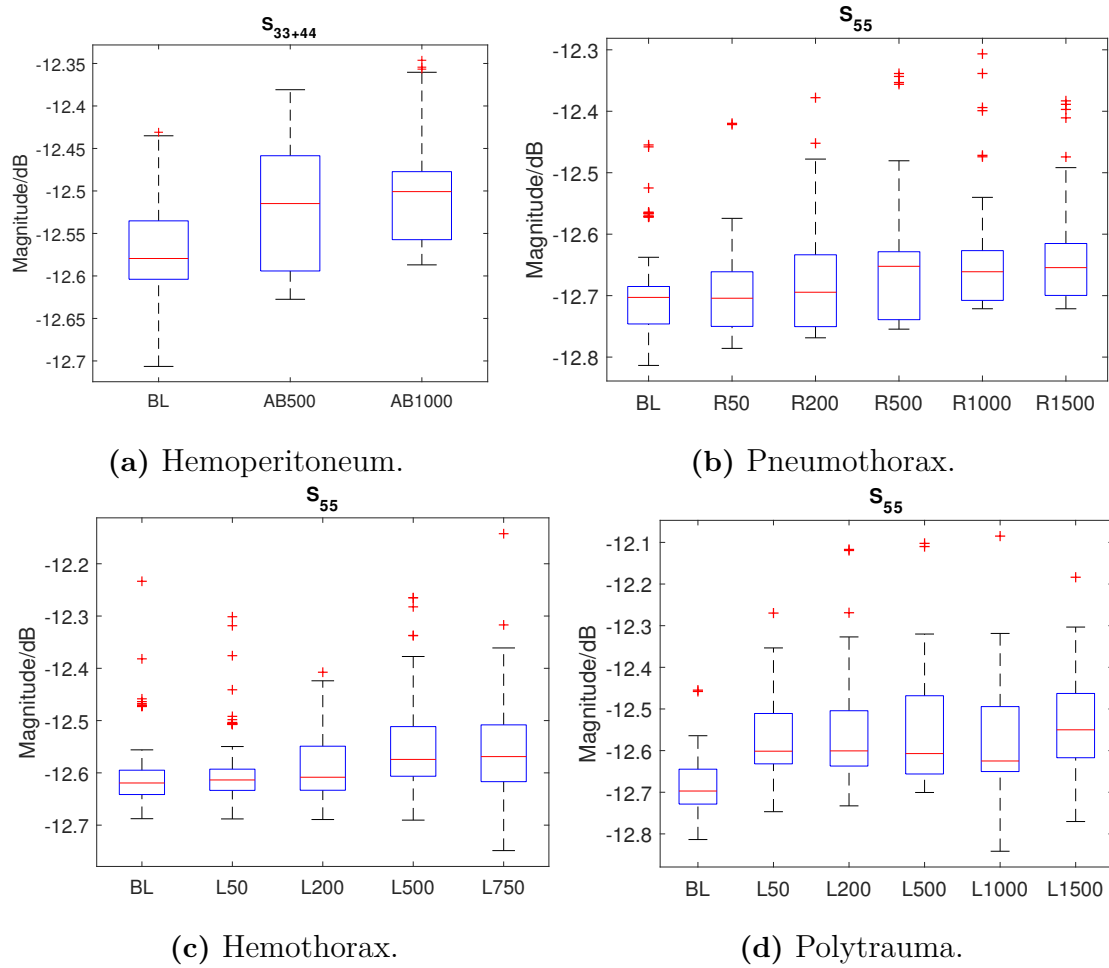
Figure B.2: The magnitude mean (the red line) and range of the baseline and four types of trauma for some coefficient magnitudes.

(a) Hemoperitoneum.

(b) Pneumothorax.

(c) Hemothorax.

(d) Combination.
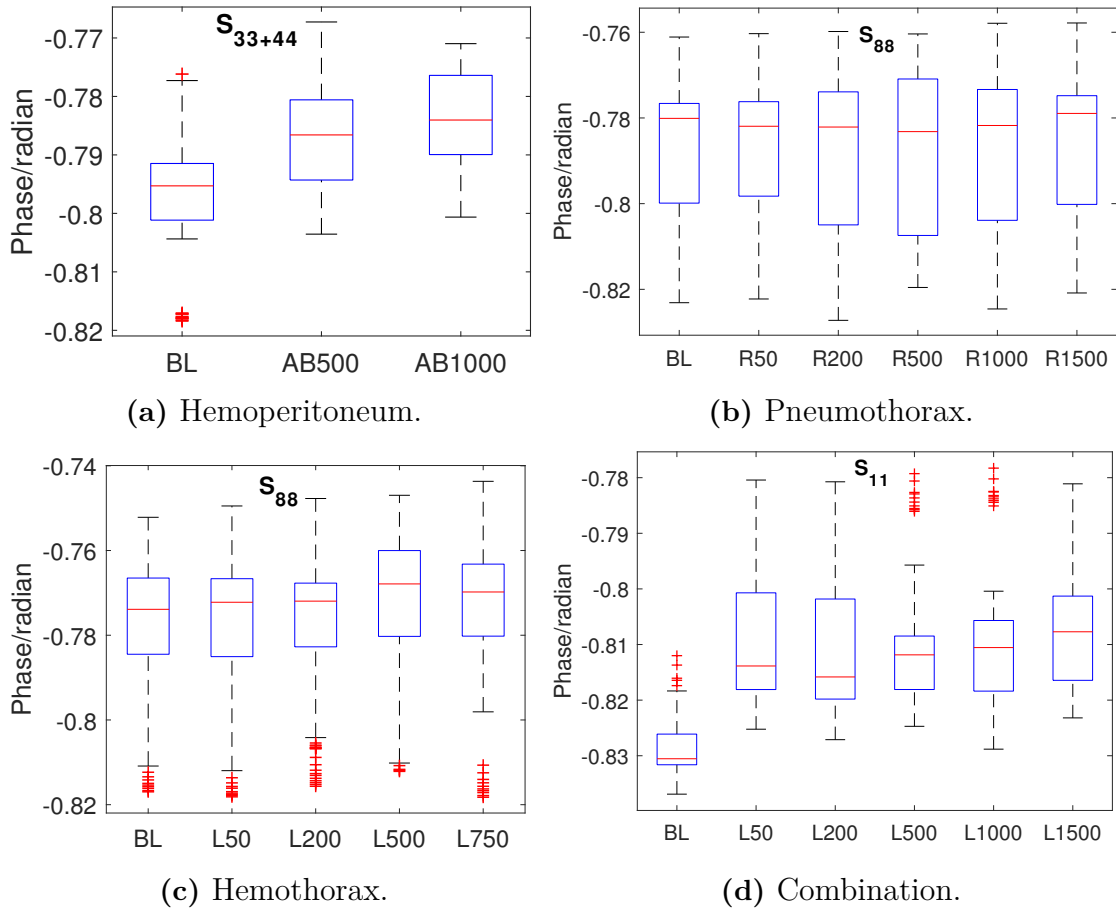
Figure B.3: The phase mean (the red line) and range of the baseline and four types of trauma for some reflection coefficients.